



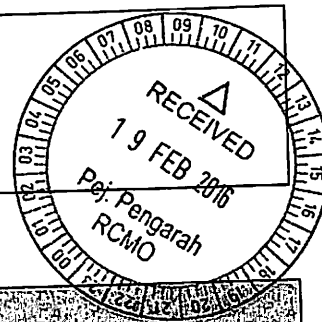
Laporan Akhir Projek Penyelidikan Jangka Pendek

**Cold Spray Synthesized Hydroxyapatite-
Magnesium Bioimplants Physico-
Chemical Behaviour, Adherence and
Environmental Compatibility**

by

**Prof. Dr. Zuhailawati Hussain
Dr. Sivakumar Ramakrishnan
Prof. Ahmad Fauzi Mohd Noor
Assoc. Prof. Dr. Afiah Abdul Rahim
Dr. Siti Noor Fazliah Mohd Noor**

2014



Please email a softcopy of this report to rcmo@usm.my

A PROJECT DETAILS	
i	<p>Title of Research:</p> <p>Cold Spray Synthesized Hydroxyapatite-Magnesium Bioimplants Physico-Chemical Behaviour, Adherence And Environmental Compatibility</p>
ii	<p>Account Number: 1001/PBahan/ 811224</p>
iii	<p>Name of Research Leader: PROF (DR) ZUHAILAWATI BINTI HUSSAIN</p>
iv	<p>Name of Co-Researcher:</p> <ol style="list-style-type: none"> 1. Dr. Sivakumar Ramakrishnan 2. Prof. Ahmad Fauzi Mohd Noor 3. Assoc. Prof. Dr. Afiah Abdul Rahim 4. Dr. Siti Noor Fazliah Mohd Noor
v	<p>Duration of this research:</p> <ol style="list-style-type: none"> a) Start Date : 15 Dec 2012 b) Completion Date : 14 Dec 2014 c) Duration : 2 Years 6 months d) Revised Date (if any) : none
B ABSTRACT OF RESEARCH	
<p><i>(An abstract of between 100 and 200 words must be prepared in Bahasa Malaysia and in English. This abstract will be included in the Report of the Research and Innovation Section at a later date as a means of presenting the project findings of the researcher/s to the University and the community at large)</i></p> <p>ABSTRAK</p> <p>Proses semburan sejuk yang mudah dan telah diubahsuai digunakan untuk menyalut serbuk hidroksiapatit ke atas substrat magnesium tulen yang dipanaskan kepada 350°C atau 550°C dan dihaluskan permukaan samada 240 atau 2000 gred kekasaran dengan jarak 20 mm atau 40 mm. Prosedur ini diulang</p>	

lima dan sepuluh kali. Satu reka bentuk faktorial pecahan (2^{4-1}) telah digunakan untuk menjelaskan faktor-faktor proses yang memberi kesan kepada ketebalan, kekuatan dan modulus elastik sampel. Analisis kaedah tindihan digunakan untuk menentukan nilai domain yang optimum. Kemudian, kaedah kecuraman digunakan untuk mengesah dan memindahkan nilai domain yang optimum. Sifat mekanik yang maksimum telah diperolehi pada jarak 30mm, 926.4 gred kekasaran permukaan permukaan dan 456°C suhu pemanasan substrat yang menghasilkan salutan optimum dengan ketebalan 49.77 μ m, 462.61 MPa nanohardness dan 45.69 GPa modulus elastik. Lapisan hidroksiapatit tidak menunjukkan perubahan fasa pada suhu 550°C. Daya mikroskop atom menunjukkan topografi lapisan seragam dan imbasan mikroskop elektron menunjukkan ikatan yang baik antara lapisan bersalut dan substrat. Kajian biodegradasi mencadangkan bahawa lapisan apatit tulang yang terbentuk di atas permukaan lapisan pada 1140 minit boleh menggalakkan ikatan tulang dengan tisu hidup dan meningkatkan jangka hayat lapisan. Kajian kehilangan berat menunjukkan bioaktiviti bagi sampel bersalut lebih baik berbanding dengan sampel tidak bersalut. Ujian lekatan mendedahkan bahawa pengurangan kekuatan ikatan datang dari pembubaran lapisan kimia yang berterusan. Pada 1140 minit rendaman, kekuatan ikatan adalah 40 MPa. Ujian percepatan kakisan menunjukkan bahawa lapisan hidroksiapatit melindungi dan mencegah daripada hakisan dalam persekitaran mengakis.

ABSTRACT

A simple and modified cold spray process was developed in which hydroxyapatite powder was coated onto pure magnesium substrates preheated to 350°C or 550°C and ground to either 240 grit or 2000 grit surface roughness, with standoff distances of 20 mm or 40 mm. The procedure was repeated five and ten times. A fractional factorial design (2^{4-1}) was applied to elucidate the process factors that significantly affected the thickness, nanohardness and elastic modulus of the coating sample. The overlaid method analysis was employed to determine trade off optimal values from multiple responses which is thickness, nanohardness and elastic modulus of the coating. Then, steepest method was used to reconfirm and relocate the optimal domain. The maximum mechanical properties of the coating were determined at 30mm standoff distance, 926.4 grit surface roughness and 456°C substrate heating temperature which accommodate the optimum coating of 49.77 μ m thickness, 462.61 MPa nanohardness and 45.69 GPa elastic modulus. The hydroxyapatite coatings did not show any phase changes at 550°C. Atomic force microscopy revealed a uniform coating topography and scanning electron microscopy revealed good bonding between the coated layers and the substrates. The biodegradable study suggested that the bone-like apatite layer formed on the surface of the coatings at 1140 minutes may promote the bone bonding with living tissues and increase the longevity of coatings. The mass loss experiment concluded that coated sample shows a better bioactivity compare to uncoated sample. The adhesion test revealed that reduction of bond strength comes mostly from the continuation of chemical dissolution of coatings. At 1140 minutes of immersion, the bond strength was 40 Mpa which satisfied the requirement for bioimplant application. The accelerated corrosion test concluded that the HAP coating remarkably protect and prevent from the corrosion in the corrosive environment.

C- BUDGET & EXPENDITURE

i **Total Approved Budget** : RM 196, 000

Yearly Budget Distributed

Year 1 : RM 121, 500

Year 2 : RM 74, 500

Year 3 : RM

Total Expenditure : RM 193,635.97

Balance : RM 2,364.03

Percentage of Amount Spent (%) : 98.7%

Please attach final account statement (eStatement) to indicate the project expenditure

ii **Equipment Purchased Under Vot 35000**

No.	Name of Equipment	Amount (RM)	Location	Status
1	Cold Spray Unit	39,520.00	PPK Bahan & Sumber Mineral	Dibeli

Please attach the Asset/Inventory Return Form (Borang Penyerahan Aset/Inventori) – Appendix 1

D RESEARCH ACHIEVEMENTS

i **Project Objectives (as stated/approved in the project proposal)**

No.	Project Objectives	Achievement
1	Completion of design of experiment and characterization of materials	Mac 2013
2	Completion of deposition of HAP coating on magnesium substrates using different conditions and statistical analysis	December 2013
3	Completion of interfacial and bonding mechanism	Mac 2014
4	Completion of In vitro degradation and biocompatibility studies	June 2015

II Research Output

a) Publications in ISI Web of Science/Scopus

No.	Publication (authors,title,journal,year,volume,pages,etc.)	Status of Publication (published/accepted/ under review)
1.	Abdullah C.W. Noorakma, Hussain Zuhailawati, V. Aishvarya, B. K. Dhindaw, Hydroxyapatite-Coated Magnesium-Based Biodegradable Alloy: Cold Spray Deposition and Simulated Body Fluid Studies, Journal of Materials Engineering and Performance: Volume 22, Issue 10 (2013), Page 2997-3004 Impact Factor: 0.998	Published
2.	Emee Marina Salleh, Sivakumar Ramakrishnan, Zuhailawati Hussain, Characterization of Binary Mg-Mn alloy Synthesized Through Mechanical Alloying: Effect of Milling Speed, Advanced Materials, Advanced Materials Research Vol. 1087 (2015) pp 479-483 Scopus	Published
3.	Md Razi Hasniyati, Hussain Zuhailawati, Sivakumar Ramakrishnan, Brij Kumar Dhindaw and Siti Noor Fazliah Mohd Noor, Cold spray Deposition of Hydroxyapatite Powder onto Magnesium Substrate for Biomaterial Application, Journal of Surface Engineering, DOI: http://dx.doi.org/10.1179/1743294415Y.0000000068 Impact Factor: 1.197	Accepted
4.	Emee Marina Salleh, Hussain Zuhailawati, Sivakumar Ramakrishnan and Mohamed Abdel-Hady Gepreel, A Statistical Prediction of Density and Hardness of Biodegradable Mechanically Alloyed Mg-Zn Alloy using Fractional Factorial Design, Journal of Alloys and Compounds 644 (2015) 476-484 Impact Factor: 2.999	Published
5.	Md Razi Hasniyati, Hussain Zuhailawati, Sivakumar Ramakrishnan and Brij Kumar Dhindaw, Optimization of Multiple Responses using Overlaid Contour Plot and Steepest Methods Analysis on Hydroxyapatite Coated Magnesium via Cold Spray Deposition, Surface and Coating Technology, 280 (2015) 250-255 Impact factor: 1.998	Published
6	Emee Marina Salleh, Sivakumar Ramakrishnan, and Zuhailawati Hussain, Design of experiment (DOE) study of biodegradable magnesium alloy synthesized by mechanical alloying using fractional factorial design, Proceedings of the 3 rd International Conference on Mathematical Sciences, AIP Conference Proceedings 1602, 1196-1201 (2014); doi: 10.1063/1.4882636, Scopus	Published
7	Md Razi Hasniyati, Hussain Zuhailawati, Sivakumar Ramakrishnan, Brij Kumar Dhindaw and Siti Noor Fazliah Mohd Noor,	Published

Design of Experiment (DOE) Study of Hydroxyapatite-Coated Magnesium by Cold Spray Deposition,
Materials Science Forum Vol 819 (2015) pp 341-346
 Scopus

b) Publications in Other Journals

No.	Publication (authors, title, journal, year, volume, pages, etc.)	Status of Publication (published/accepted/ under review)

c) Other Publications

(book, chapters in book, monograph, magazine, etc.)

No.	Publication (authors, title, journal, year, volume, pages, etc.)	Status of Publication (published/accepted/ under review)

d) Conference Proceeding

No.	Conference (conference name, date, place)	Title of Abstract/Article	Level (International/National)
1	3rd International Conference on Mathematical Sciences (ICMS3), Putra World Trade Centre, Kuala Lumpur, 17 – 19 December 2013	Design of Experiment (DOE) Study of Biodegradable Magnesium Alloy Synthesized by Mechanical Alloying Using Fractional Factorial Design	International
2	International Conference on Functional Materials & Metallurgy (IcoFM2014), Flamingo Hotel, Penang, 17-18 Sept 2014	Design of Experiment (DOE) Study of Hydroxyapatite-coated Magnesium by cold spray deposition	International
3	2nd Advanced Materials Conference (AMC) 2014, 25-24 November 2014, Langkawi	Development of Binary Mg-Ti alloy synthesized using mechanical alloying	National
4	International Conference on Recent Advances in Materials and Environment (RAMM) & 2nd International of Postgraduate Conference on Materials, Mineral and Polymer (MAMIP), Penang, Malaysia, 4-6 August 2015	A Statistical Prediction of Multiple Responses using Overlaid Contour Plot on Hydroxyapatite Coated Magnesium via Cold Spray Deposition	International

Please attach a full copy of the publication/proceeding listed above

iii Other Research Output/Impact From This Project
(patent, products, awards, copyright, external grant, networking, etc.)

Low cost and non-toxic Mg-Zn alloy that biocompatible to human bone has been discovered using powder metallurgy route. Results proposed that this new Mg alloy is much more superior than pure Mg in terms of mechanical strength.

E HUMAN CAPITAL DEVELOPMENT

a) Graduated Human Capital

Student	Nationality (No.)		Name
	National	International	
PhD	2		1. Hasniyati Md Razi (waiting for viva) 2. Emee Marina Salleh (waiting for viva) 2.
MSc	1		1. Che Wan Noorakma Abdullah 2.
Undergraduate			1. 2.

b) On-going Human Capital

Student	Nationality (No.)		Name
	National	International	
PhD	2		
MSc	1		1. Masyitah Mt Yusof 2.
Undergraduate			1. 2.

c) Others Human Capital

Student	Nationality (No.)		Name
	National	International	
Post Doctoral Fellow			1. 2.
Research Officer			1. 2.
Research Assistant			1. 2.
Others (.....)			1. 2.

F COMPREHENSIVE TECHNICAL REPORT

Applicants are required to prepare a comprehensive technical report explaining the project. The following format should be used (this report must be attached separately):

- Introduction
- Objectives
- Methods
- Results

- Discussion
- Conclusion and Suggestion
- Acknowledgements
- References

G PROBLEMS/CONSTRAINTS/CHALLENGES IF ANY

(Please provide issues arising from the project and how they were resolved)

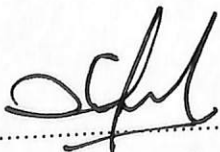
Problem to purchase magnesium plate as its is controlled item. We bought using credit card through Alibaba web. We also encounter during corrosion of sample in biofluid liquid – solution and methodology of testing due to infamiliar testing and apparatus

H RECOMMENDATION

(Please provide recommendations that can be used to improve the delivery of information, grant management, guidelines and policy, etc.)

We managed to solved the problem mentioned in G through good partner and sharing idea with collaborator in IPPT.

Project Leader's Signature:

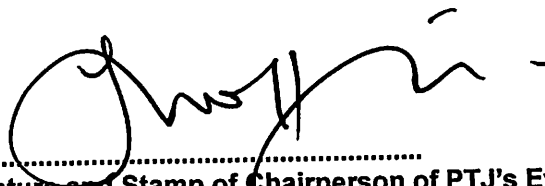


Name : Prof. Zuhailawati Hussein

Date : 16. 2. 16

COMMENTS IF ANY/ENDORSEMENT BY PTJ'S RESEARCH COMMITTEE

Good research achievement. The researchers have completed the research with excellent results. 2 PhD and 1 msc ~~graduates~~ graduates have been produced. The team has published 7 papers (ISI and Scopus).



Signature and Stamp of Chairperson of PTJ's Evaluation Committee

Name :

Date :

PROF. MADYA DR. KHAIRUNISAK ABDUL RAZAK
Timbalan Dekan
Penyelidikan, Siswazah dan Jaringan
Pusat Peng. Kej. Bahan & Sumber Mineral
Kampus Kejuruteraan
Universiti Sains Malaysia

Signature and Stamp of Dean/ Director of PTJ



USM UNIVERSITI
SAINS
MALAYSIA

BORANG PENYERAHAN ASET / INVENTORI

A. BUTIR PENYELIDIK

1. NAMA PENYELIDIK : PROF. (DR) ZUHAILAWATI Bt. HUSSAIN
 2. NO STAF : AE 50260
 3. PTJ : PPK BSM
 4. KOD PROJEK : 1001/PBAHAN / 811224
 5. TARIKH TAMAT PENYELIDIKAN : 14 JUNE 2015

B. MAKLUMAT ASET / INVENTORI

BIL	KETERANGAN ASET	NO HARTA	NO. SIRI	HARGA (RM)
1	COLD SPRAY CABINET	AK00007500	-	13,160.00
2	COLD SPRAY GUN QT-E7/H	AK00007501	1324	11,760.00
3	COLD SPRAY GUN QT-E2000-7/H	AK00007502	1399	14,600.00

C. PERAKUAN PENYERAHAN

Saya dengan ini menyerahkan aset/ inventori seperti butiran B di atas kepada pihak Universiti:

(Prof. Zuhailawati
Hussain)

Tarikh: 15.12.2016

D. PERAKUAN PENERIMAAN

Saya telah memeriksa dan menyemak setiap alatan dan didapati :

- Lengkap
 Rosak
 Hilang : Nyatakan.....
 Lain-lain : Nyatakan

Diperakukan Oleh :

Mohd. Sayuti Azeman
Pencapaian Junitera
P.P. Kejuruteraan Bahan & Sumber Mineral
USM Kampus Kejuruteraan

Tandatangan
Pegawai Aset PTJ

Nama : MOTHO SAYUT BIN AZEMAN
Tarikh : 11 / 2 / 2016

*Nota : Sesalanan borang yang telah lengkap perlulah dikemukakan kepada Unit Pengurusan Harta, Jabatan Bendahari dan Pejabat RCMO untuk tujuan rekod.



UNIVERSITI SAINS MALAYSIA

JABATAN BENDAHARI

PENYATA PERBELANJAAN SEHINGGA 2 DISEMBER 2015

Projek :

No. Akaun : 1001.PBAHAN.811224.

Vot	Nama Vot	Peruntukan Projek	Perbelanjaan Terkumpul Sehingga Thn Lalu	Baki Peruntukan Tahun Lalu	Peruntukan Thn Semasa	Jumlah Peruntukan Thn Semasa	Tanggung Semasa	Bayaran Thn Semasa	Jum Belanja Thn Semasa	Baki Projek
111	GAJI	28,812.12	0.00	28,812.12	0.00	28,812.12	0.00	28,679.52	28,679.52	132.60
221	PERJALANAN DAN SARA HIDUP	9,422.00	0.00	9,422.00	0.00	9,422.00	0.00	0.00	0.00	9,422.00
224	SEWAAN	1,958.00	0.00	1,958.00	0.00	1,958.00	0.00	245.00	245.00	1,713.00
226	BEKALAN BAHAN MENTAH	7,000.00	0.00	7,000.00	0.00	7,000.00	0.00	1,351.00	1,351.00	5,649.00
227	BEKALAN DAN BAHAN LAIN	-12,876.70	0.00	-12,876.70	0.00	-12,876.70	0.00	3,716.37	3,716.37	-16,593.07
228	PENYELENGGARAN & PEMBAIKAN KECIL	-3,000.00	0.00	-3,000.00	0.00	-3,000.00	0.00	1,580.00	1,580.00	-4,580.00
229	PERKHIDMATAN IKTISAS & HOSPITALITI	9,830.50	0.00	9,830.50	0.00	9,830.50	0.00	3,330.00	3,330.00	6,500.50
335	HARTA MODAL	120.00	0.00	120.00	0.00	120.00	0.00	0.00	0.00	120.00
	Jumlah	41,265.92	0.00	41,265.92	0.00	41,265.92	0.00	38,901.89	38,901.89	2,364.03

Penyata ini adalah cetakan komputer tiada tandatangan diperlukan

Penyata ini adalah dianggap tepat jika tiada maklumbalas dalam tempoh masa 14 hari dari tarikh penyata

ABSTRACT

A simple and modified cold spray process was developed in which hydroxyapatite powder was coated onto pure magnesium substrates preheated to 350°C or 550°C and ground to either 240 grit or 2000 grit surface roughness, with standoff distances of 20 mm or 40 mm. The procedure was repeated five and ten times. A fractional factorial design (2^{4-1}) was applied to elucidate the process factors that significantly affected the thickness, nanohardness and elastic modulus of the coating sample. The overlaid method analysis was employed to determine trade off optimal values from multiple responses which is thickness, nanohardness and elastic modulus of the coating. Then, steepest method was used to reconfirm and relocate the optimal domain. The maximum mechanical properties of the coating were determined at 30mm standoff distance, 926.4 grit surface roughness and 456°C substrate heating temperature which accommodate the optimum coating of 49.77 μ m thickness, 462.61 MPa nanohardness and 45.69 GPa elastic modulus. The hydroxyapatite coatings did not show any phase changes at 550°C. Atomic force microscopy revealed a uniform coating topography and scanning electron microscopy revealed good bonding between the coated layers and the substrates. The biodegradable study suggested that the bone-like apatite layer formed on the surface of the coatings at 1140 minutes may promote the bone bonding with living tissues and increase the longevity of coatings. The mass loss experiment concluded that coated sample shows a better bioactivity compare to uncoated sample. The adhesion test revealed that reduction of bond strength comes mostly from the continuation of chemical dissolution of coatings. At 1140 minutes of immersion, the bond strength was 40 Mpa which satisfied the requirement for bioimplant application. The accelerated corrosion test concluded that the HAP coating remarkably protect and prevent from the corrosion in the corrosive environment.

1. Introduction

Magnesium (Mg) stands out as a potential candidate for temporary implants in biomedical applications due to its light weight, as well as its elastic modulus and compressive yield strength that are compatible with those of natural bone [1]. The density of Mg is 1.738 g cm^{-3} , which is only slightly less than that of natural bone ($1.8\text{--}2.1 \text{ g cm}^{-3}$), while the elastic modulus of pure Mg is 45 GPa, as compared to human bone (40–57 GPa). The use of pure Mg in bio implants has been seriously considered [2]. Magnesium participates in human metabolic reactions and is therefore non-toxic. It is biocompatible and biodegradable in human body fluid, thus eliminating the need for a second operation to remove a temporary implant. Use of Mg alloys is generally not advisable because most alloying elements can be toxic to the human body (except for Ca alloys, for example). Furthermore, preparation of these alloys adds to the cost of the implant without giving any distinct advantages. As the main limitation of the use of Mg in medical applications is its extremely rapid degradation rate due to corrosion, its surface must be coated with materials of high corrosion resistance. One coating material with potential to retard the biodegradation rate of Mg in human body fluid is hydroxyapatite (HAP; $[\text{Ca}_{10}(\text{PO}_4)_6\text{OH}_2]$), whose primary component consists of the same ions that are responsible for the construction of the mineral part of bone and teeth. It is bioactive with bone-bonding ability, thus making it suitable for clinical use as bone spacers and fillers. The absence of cytotoxic effects makes HAP biocompatible with both hard and soft tissues [3].

To coat HAP powder onto highly degradable Mg substrates, any processing technique that melts the Mg substrate or accelerates the dissolution of Mg in fluid must be avoided. Thus, this work proposes a cold spray technique as a method that is suitable for coating HAP onto Mg substrates. This technique is also known as cold gas-dynamic spraying, kinetic spraying, high-velocity powder deposition or supersonic powder deposition [4]. In principle, deformable metallic particles (or other feedstock powders) are introduced into a high-velocity, gas-dynamic stream and directed onto a substrate surface where they impact and form a coating [5]. Cold spray technology overcomes the shortcomings of thermal spraying, which involves melting and solidification of the coating [6] as well as those of the dipping technique, notably the dissolution of Mg. Cold spraying has been reported to produce coatings of proper density and adhesion with substrates such as Cu, Al, Fe, Ti, Zn, Ni and Mg alloys [7-11]. However, to date, there have been few reports dealing with the cold spraying of HAP powder to form a coating layer on a pure Mg substrate.

To determine the conditions that produce high-quality HAP coating on a Mg substrate, a trial and error method is not a good option. Several factors influence the properties of the coating prepared by the cold spray technique, so evaluation of the effects of individual factors is time-consuming, and the process of determining the factors that would give optimum results is difficult and erratic. Instead, the design of experiment (DOE) statistical approach, in which a mathematical model is developed using experimental runs, can be used, as it is a powerful and efficient approach for solving challenging quality problems [12]. In practice, DOE has been used successfully in several industrial applications for optimising manufacturing processes. For example, DOE has been applied to optimise the plasma spray process of yttria-stabilised zirconia coatings [13]. Of the available DOE methods, a fractional factorial design is a variation of the basic factorial design in which only a subset of the run is used. These fractional factorial designs are among the most widely used types of designs for product and process designs and for process improvements.

On the other hand, multiple response optimization methodology is a collection of mathematical and statistical techniques for designing experiments, building models, evaluating the effects caused by factors, and searching for optimum conditions for the modeling and analysis of multiple response optimization problems. The multiple responses of interest are influenced by several variables. The aim is to optimize these responses [14]. Frequently, the overlaid method analysis is employed to determine the tradeoff optimal values from multiple regressive equations. If the mean of the center points exceeds the mean of factorial points, the optimum would be near or with the experimental design space. If the mean of the center points was less than the mean of the factorial points, then the optimum would be outside the experimental design space and the method of the steepest analysis should be applied. The steepest ascent method analysis is a procedure for moving sequentially in the direction of the maximum increase in the response. If the minimization is desired, then the technique is called the method of steepest descent [15].

This work proposes a novel approach of adapting the cold spray technique to coat HAP onto Mg substrate at low temperature. The work evaluates the effects of several cold spraying process variables (standoff distance between nozzle spray and substrate, surface roughness of the substrate, substrate temperature, and number of sprays) on the properties of the HAP coating on the heated Mg substrate. The results chosen for optimisation comprised only physical properties: coating thickness, hardness and modulus of the coating. Fractional factorial design, which reduces the

number of experimental runs to half of that required by conventional full factorial design, is utilised to reduce the time and cost of the experimental work. The optimised coating is then characterised using atomic force microscopy (AFM) and scanning electron microscopy (SEM) studies. Moreover, as far as the authors are concerned, most of published reports are limited to the effects of the process parameters on a single response. Thus, the aim of this work is to highlight the use of overlaid contour plots and the steepest methods to analyze multiple responses of thickness, nanohardness, and the elastic modulus of the coating. Then, the trade-off optimal values of the responses were derived.

Despite the encouraging incentives from the design of experiment as an alternative to typical experiment design for enhance the mechanical properties of HAP coating on Mg substrate there are still great challenges to overcome. Since the coated samples were meant for load bearing application where time bound healing should start before the whole implant dissolves. Thus, the aim of this study is to find the bioactivity and biodegradation rate when the coating sample subjected to the physiological medium like in the simulated body fluid (SBF). This work also focused on the accelerated corrosion test to investigate the protectiveness of HAP coating in the 3.5wt% NaCl solution towards immersion time intervals as Mg is generally known to degrade in the aqueous environment.

2. Objectives

The main objectives of this research work are:

1. To investigate the thickness, nanohardness and elastic modulus of HAP coated pure Mg developed using modified cold spraying technique.
2. To identify significant factors of cold spraying process factors including their interaction of the HAP coating properties using fractional factorial design.
3. To suggest optimized cold spray parameters through the use of overlaid contour plots and the steepest methods for multiple responses of thickness, nanohardness and elastic modulus of the coating.

4. To investigate compatibilities of HAP coated on pure Mg substrate in term of biodegradation in biofluids.
5. To investigate the corrosion properties of HAP coated onto pure Mg substrate in 3.5wt% NaCl solution.

3. Methods

3.1 Sample preparation

Pure Mg plate provided by Xi'an Yuechen Metal Products, China was cut into 15 mm x 15 mm x 5 mm. Before the cold spray process, the samples were pre-treated as follows: (1) the specimen surfaces were serially ground with either 240 grit or 2000 grit SiC papers and (2) the specimens were cleaned ultrasonically in acetone for 5 min. For HAP, $\text{Ca}_{10}(\text{PO}_4)_6\text{OH}_2$ powder (Sigma-Aldrich, Malaysia) was used as the feedstock for the cold spray process. The average HAP powder size used in this experiment was 5 μm . The pure Mg substrate was placed inside a furnace, where it was preheated to a temperature of either 350°C or 550°C for 1 hour, and then the HAP powder was cold-sprayed onto the substrate. The particles were accelerated through a standard de Laval type of nozzle with rectangular exit cross-section (aperture of 4mm x 6mm and throat diameter of 1mm). The nozzle was positioned at either 20 mm or 40 mm from the preheated substrate with the spray angle between the nozzle and substrate maintained at 90°. The air pressure was 1MPa and the air temperature was maintained at room temperature. The procedure was repeated either five or ten times. Each spray procedure takes around 10 to 15 min to be completed. The particle velocity obtained from this procedure was 14.5 m/s.

3.2 DOE

DOE was carried out using Minitab 16 (Minitab Inc, USA). RSM was used with fractional factorial design to obtain a mathematical correlation between standoff distance, surface roughness, substrate heating temperature and number of sprays of HAP coated onto pure Mg substrates, to yield the highly desirable mechanical properties (thickness, nanohardness and elastic modulus) of the samples.

This present work used a 2^{4-1} fractional factorial design to identify factors that significantly influence the mechanical properties of the coated samples, so that insignificant factors could be eliminated. In this way, the thickness, nanohardness and elastic modulus of the coatings were selected as the response variables to represent the mechanical properties and soundness of the HAP coatings. To avoid too wide a range in the screening tests, the range of factors used was designated as +1(high) or -1(low), as given in Table 1. The levels of the factors were chosen based on preliminary experiments. A minimum standoff distance of 20 mm was required for convenient location of the nozzle with respect to the sample in the furnace. Beyond a 60 mm standoff distance, the stream of particles tended to flare. An upper boundary of substrate temperature was chosen that was well below the melting point of Mg. A lower boundary of substrate temperature was chosen so that a reasonable thickness of coating could be obtained. Surface roughness levels were varied from near-smooth (2000 grit) to rough (240 grit). In the present work, a 2^{4-1} fractional factorial design was formulated for four factors with two replications, leading to a total of 16 sets of samples.

Table 1: Levels of factors for screening

Variable	Notation	Units	Level	
			-	+
Standoff Distance	A	mm	20	60
Surface Roughness	B	grid	240	2000
Substrate Heating Temperature	C	°C	350	550
Number of Sprays	D	...	5	10

Analysis of variance (ANOVA) was used to determine the adequacy of the factorial model. Then, optimisation experiments were performed to determine the best settings and define the nature of curvature of the response curves.

3.3 Multi Regression Equation Modeling using Fractional Factorial Design

A 2^{4-1} fractional factorial design with two replications was used to pick factors that influenced the mechanical properties of the coating sample significantly and any insignificant ones were eliminated to obtain a smaller and more manageable set of factors. This DOE design was carried out

using Minitab 16 (Minitab Inc. USA). To avoid too wide a range in the screening tests, the range of factors used was designated as +1(high) or -1(low), as given in Table 1. The levels of the factors were chosen based on preliminary experiments. Analysis of variance (ANOVA) was used to determine the adequacy of the factorial model. Then, optimization experiments were performed to determine the best settings and define the nature of curvature of the response curves. Lastly, the experiments were performed along the steepest ascent and descent paths until the response did not increase or decrease any more to find the optimal value for the responses.

3.4 Biodegradable study using SBF solution

The biodegradable study of HAP coated onto magnesium was evaluated in the simulated body fluid (SBF) for 0 min, 10 min, 30 min, 60 min (1 hr), 120 min (2 hr), 240 min (4 hr) and 1140 min (24 hr) before they were taken out for testing and analysis.

The test sample for this study was coated Mg substrate with HAP powder and uncoated Mg substrate represented as the control sample to check the biodegradation effect of SBF on the pure Mg substrate. Both samples were immersed in SBF which were kept up at 37°C as normal human body temperature and subjected to a gentle shaking movement using Incubator Shaker, IKA KS 4000i Control, China.

After different periods of immersion, the coatings were removed from the fluid, gently rinsed in ethanol and dried overnight without heating. The solutions were then filtered out and kept for ICPOES analysis. After the samples had been completely dried, they were analysed by SEM and EDX analysis.

3.5 Accelerated test of degradation in 3.5wt % NaCl solution

Immersion testing was performed for observing the degradation behaviour of optimised HAP coated on Mg and the uncoated sample to investigate the protective effect of the coating. In the accelerated test of degradation, the high concentration of 3.5wt% NaCl solution was used to compare the degradation rate before and after coating. The accelerated solution was prepared by dissolving 35g of NaCl in 1000ml of distilled water. The test sample for this experiment was coated Mg substrate with HAP powder and pure Mg substrate as an experimental control. Both samples were soaked in

the 3.5wt% NaCl solution for 1, 4, 10, 14 days before they were taken out, delicately washed with ethanol and dried at room temperature before testing and analysis.

3.6 Characterisation of HAP powder coated onto Mg substrate

3.6.1 Elemental composition by X-ray fluorescence (XRF)

Semi quantitative analysis of pure magnesium substrate was performed by X-ray Fluorescence Spectroscopy (XRF) using RIX 3000 XRF spectrometer by Rigaku. The XRF spectrometer equipped with rhodium (Rh) X-ray tube, 4 kW generator and interface to PC with RIX for Windows software. The sample was ground and polish before testing. The sample was then exposed to the primary X-ray beam for elemental analysis.

3.6.2 Particle size analysis (PSA)

The particle size distribution of hydroxyapatite powder was determined using laser diffraction particle size analyzer Mastersizer E (Malvern Instruments Ltd., United Kingdom). Calgon was used as the dispersion medium. The particle size and volume distribution was generated directly from the Malvern Mastersizer Version 2.15 software. The particle size distribution of hydroxyapatite powder was expressed by span value. Span is defined as $(d_{90}-d_{10})/d_{50}$, where d_{10} , d_{50} , d_{90} value represent the 10th, 50th and 90th of cumulative volume passing, respectively. The geometric mean diameter, meanwhile, was described by the volume moment diameter (VMD).

3.6.3 Phases identification by X-Ray diffraction (XRD)

X-ray diffraction (XRD; Bruker AXS D8, USA) analysis, performed to identify phases in the HAP coating deposited by the cold spray technique, was conducted through a range of Bragg angles (2θ) of 20°–80° using CuK α radiation ($\lambda = 0.15406$ nm). The voltage was set to 40 kV, with a current of 40 mA. The scan angle range was from 0° to 70° with 0.034° scan steps. The diffractograms obtained were then analysed using X'PertHighScorePlus (XHP) software (PAN Analytical Version 2.2e) to determine and identify the types of phases existed as the sintering temperature increased.

3.6.4 Atomic force microscopy (AFM)

The atomic force microscopy (AFM) was utilized to image the structure at atomic level on the HAP coating. The atomic force microscope provided three-dimensional images of the samples and surface profiles of the coatings. The model of AFM used in this analysis was NanoNavi SII, Japan. The mode of AFM operation during this test was non-contact model.

3.6.5 Elemental composition, phase identification and morphology conditions by scanning electron microscopy (SEM) and energy dispersive X-ray analyser (EDX)

The surface morphology was examined with the aid of a field emission scanning electron microscope (FESEM-Zeiss Supra 35VP-24-58) equipped with Energy dispersive X-ray (EDX). Sample were first thin coated with gold palladium (AuPd) and were observed and imaged at a working distance of 10 mm, with 15-kV accelerating voltage and the semi-quantitative elemental compositions on selected spot images were analyzed using EDX. BSE (back-scattered electron) image was utilized for distinguishing different phases while energy dispersive X-rays (EDX) provide semi-quantitative chemical composition by peak height ratio relative to the standard.

3.6.6 Determine hardness and elastic modulus using nanoindentation test

Nanoindentation test can reveal mechanical properties within the HAP coating in term of nanohardness and elastic modulus. In contrast with conventional microhardness, that the latter is not able to give the elastic modulus measurement. This is because of the fact that measurements are made after the load has been removed from the sample. The nanoindentation testing with an appropriate instrument is one of the simplest ways to measure the mechanical properties of materials. In this study, nanoindentation was performed using a NanoTest instrument (Micro Materials Ltd.Wrexham, UK). This instrument was found suitable to measure the thin film coating. It is performed by deforming the material and measuring the indentation made.

3.6.7 Determination of Mg, Ca and P by inductively couple plasma optical emission spectroscopy (ICPOES)

Inductively coupled plasma optical emission spectroscopy (ICPOES) was used to analyse three ions concentrations of the sample which are Mg, Ca and P. The original concentration of SBF

solution was determined before in vitro test. After the sample had reached its respective immersion time, the sample was taken out from the SBF solution and the analysed by ICPOES. For determination of ion concentration in SBF solution after certain immersion period, all samples solution was filtered through a syringe filter. The filtrates were dilute for 20 times, sealed in the vials, labelled and stored at 4°C.

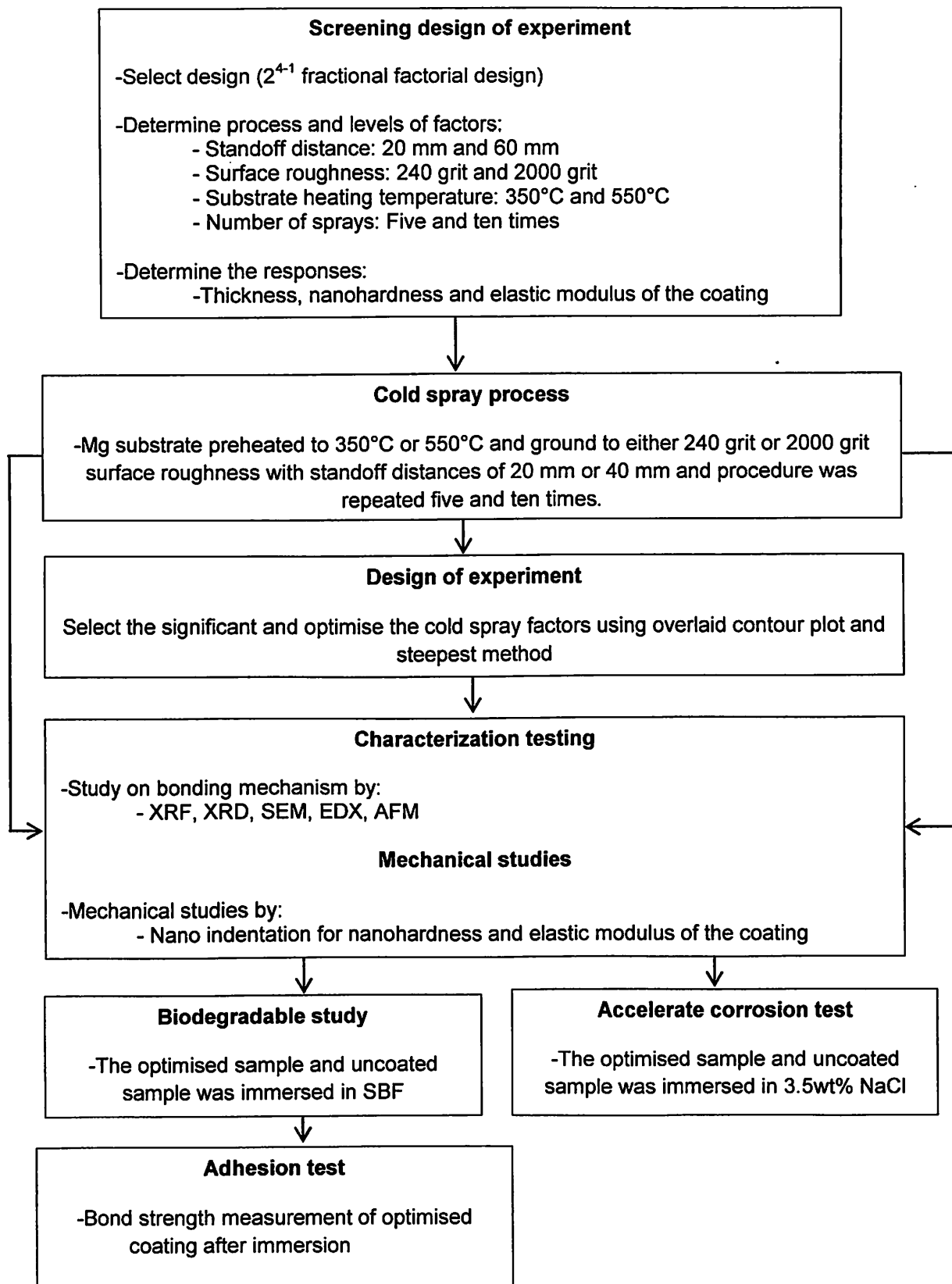


Figure 1: Flow chart for all the procedures involved

4. Results and Discussion

4.1 Phase studies

Figure 1 shows XRD patterns of the HAP and pure Mg with the HAP coating. The XRD pattern of the coating demonstrates the presence of HAP. The XRD patterns in Figure 1 indicate that the cold spray process does not affect the pure HAP phase, even at a substrate pre-heated temperature of 550°C. As the coating is thin (10–50 μm), peaks of pure Mg are seen in the XRD pattern due to the high penetration of the X-ray radiation beneath the coating, which reveals the presence of the substrate metal.

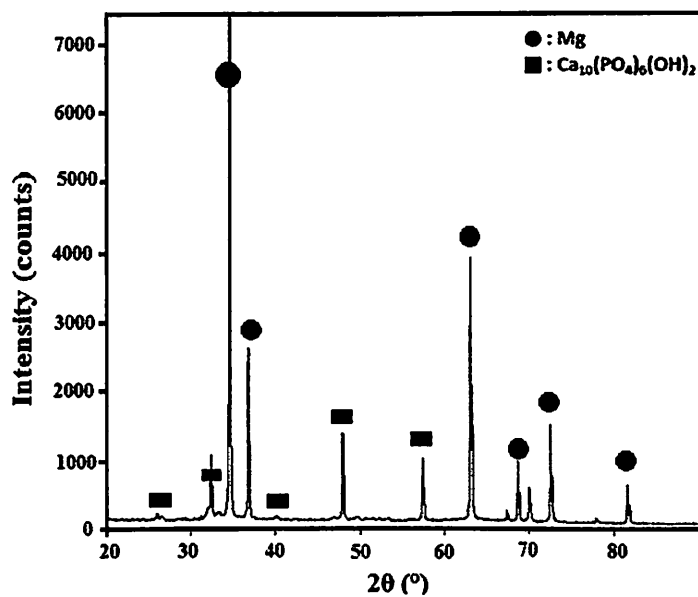


Figure 2: X-ray diffraction spectrums for pure Mg and HAP at 550°C

3.2. Screening factors

The properties of the cold spray coatings depend on the parameters used in the spraying process. Establishing relationships between the properties and the processing parameters is important for producing coatings with the desired characteristics. The results of the screening stages of the two-level fractional factorial experimental design are presented in Table 2.

Table 2: Experimental design and measured responses

Run No	Variables in coded levels				Actual responses		
	Standoff Distance (A)	Surface Roughness (B)	Substrate Heating Temperature (C)	Number of Sprays (D)	Thickness of Coating/ μm (Y1)	Nanohardness/MPa (Y2)	Elastic Modulus/G Pa (Y3)
1	+	+	+	+	21.96	69.49	13.96
2	-	+	-	+	18.73	47.58	16.81
3	-	+	-	+	18.19	39.12	15.26
4	+	+	-	-	13.03	36.82	9.09
5	+	-	+	-	23.56	67.23	13.80
6	+	-	+	-	24.43	73.60	19.30
7	+	+	+	+	21.84	67.72	14.70
8	+	-	-	+	20.31	64.07	13.69
9	-	+	+	-	32.63	156.87	23.46
10	+	+	-	-	17.48	35.01	11.08
11	-	-	+	+	44.90	429.02	43.06
12	+	-	-	+	21.48	65.61	16.32
13	-	-	+	+	39.08	323.71	36.33
14	-	-	-	-	35.09	197.65	30.73
15	-	-	-	-	38.97	223.71	26.33
16	-	+	+	-	25.58	156.87	23.46

3.2.1. ANOVA

To gain a better understanding of the role of individual and combined process parameters, data are analysed statistically to relate the response variables to the independent process parameters. After the effects are estimated, the factors affecting the mechanical properties of the coating are determined by performing ANOVA.

Table 3: ANOVA for thickness, nanohardness and elastic modulus

Source	p-value (Prob>F)		
	Thickness	Nanohardness	Elastic Modulus
A	0.0002	<0.0001	<0.0001
B	0.0004	<0.0001	<0.0001
C	0.0044	0.0002	<0.0001
D	0.9682	0.9771	0.1169
AB	0.0061	<0.0001	0.0003
AC	0.2757	0.0068	0.0071
AD	0.3660	0.5785	0.5711

A half-normal plot and ANOVA were generated using the 2^{4-1} fractional factorial design in the screening experiment, as shown in Figure 2 and in Table 3. Figure 2 (a) shows that the factors A, B, C and the interaction AB are positioned away from the straight line, indicating that variables A, B, C and interaction AB are significant model terms. This finding is also supported by ANOVA, as shown in Table 3 for thickness, which gives a p-value of the individual factors A, B, C and of the combined factor AB as <0.005. Figures 2 (b) and (c) demonstrate that the factors A, B, C and the interactions AB and AC are significant model terms.

Half Normal Plot of the Standardized Effects

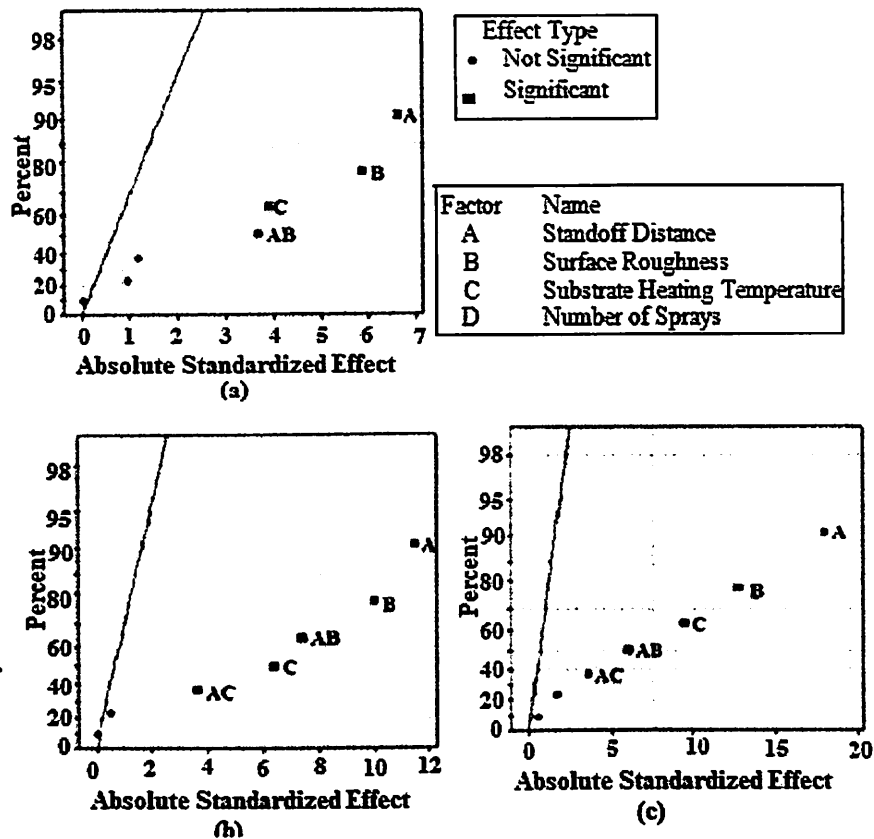


Figure 2: Half Normal Plot

The ANOVA for both responses shows that these factors are significant with p-values <0.05. From the response results, an approximate polynomial relationship between variables and responses can be determined and expressed as the following mathematical equations:

$$Y1 = 26.38 - 5.87*A - 5.20*B + 3.47*C + 0.036*D + 3.27*AB - 1.04*AC + 0.85*AD \quad (1)$$

$$Y2 = 155.83 - 84.29*A - 73.49*B + 46.96*C + 0.22*D + 54.21*AB - 26.58*AC - 4.25*AD \quad (2)$$

$$Y3 = 23.23 - 8.02*A - 5.67*B + 4.24*C - 0.78*D + 2.66*AB - 1.60*AC + 0.26*AD \quad (3)$$

Factors with positive coefficients shown that the factors have to be increased and those with negative coefficients have to be lowered for maximise the responses.

Overlaid Analysis for Multiple Regression

Response contour plots were generated from the model equations (Eq(s). 1, 2, and 3) obtained in the regression analysis. Figure 3 shows the analysis of the contour plots for thickness ,

which revealed that high thickness ($> 40 \mu\text{m}$) was obtained at any one of the following combinations: (a) standoff distance 20–25mm, surface roughness < 500 grit, substrate heating temperature 350°C ; (b) standoff distance 20–30mm, substrate heating temperature $440\text{--}550^\circ\text{C}$, surface roughness 240grit; and (c) surface roughness 350–700grit, substrate heating temperature $440\text{--}550^\circ\text{C}$, standoff distance 20 mm .

The analysis of the contour plots for nanohardness revealed that high nanohardness ($> 400\text{MPa}$) was obtained at any one of the following combinations: (a) standoff distance 20–35 mm, surface roughness 20–900 grit, substrate heating temperature 350°C ; (b) standoff distance 20–30mm, substrate heating temperature $490\text{--}550^\circ\text{C}$, surface roughness 240 grit; and (c) surface roughness 350–600grit, substrate heating temperature $490\text{--}550^\circ\text{C}$, standoff distance 20 mm. Meanwhile, for elastic modulus revealed that high elastic modulus ($> 40\text{MPa}$) was obtained at any one of the following combinations: (a) standoff distance 20–30 mm, surface roughness 20–600 grit, substrate heating temperature 350°C ; (b) standoff distance 20–30mm, substrate heating temperature $450\text{--}550^\circ\text{C}$, surface roughness 240 grit; and (c) surface roughness 350–800 grit, substrate heating temperature $460\text{--}550^\circ\text{C}$, standoff distance. Apart from these combinations, which were based on low values of the hold variables when the other two factors were varied, other combinations based on high and low values of the variables, can be arrived at.

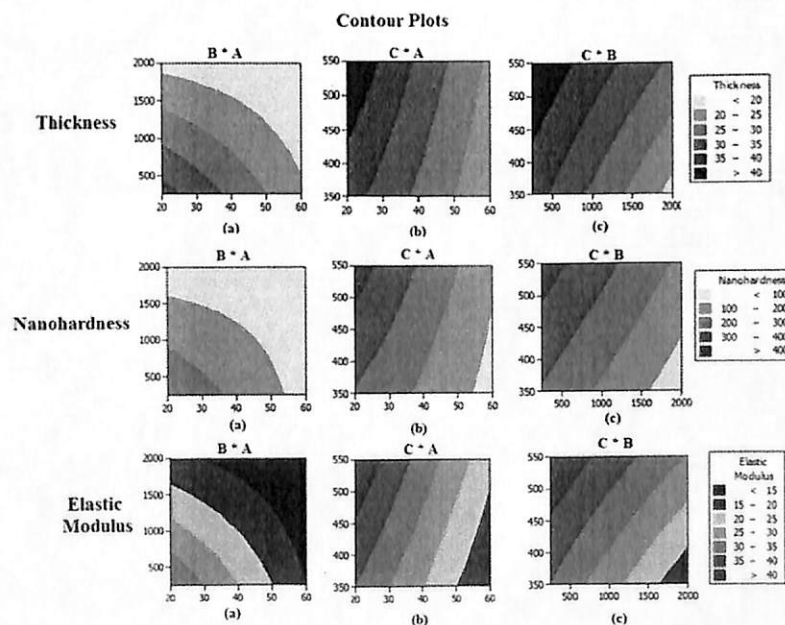


Figure 3: Analysis of contour plot

The coating thickness, nanohardness, and elastic modulus were overlaid using Eq(s). 1, 2, and 3 and the contour plot to find the feasible region (shown as the white region) having the desired properties (Figure 4). For overlaying, substrate heating temperature and surface roughness were chosen as variables keeping the values of standoff distance constant at low point (Fig. 4(a)). The desired values of all these properties could be obtained at any given combination within the optimized region. Two more feasible regions were obtained (Fig. 4(b), 4(c)). On random check the difference between the calculated and experimental values was found to be less than 3%.

Overlaid Contour Plot of Thickness, Nanohardness and Elastic Modulus

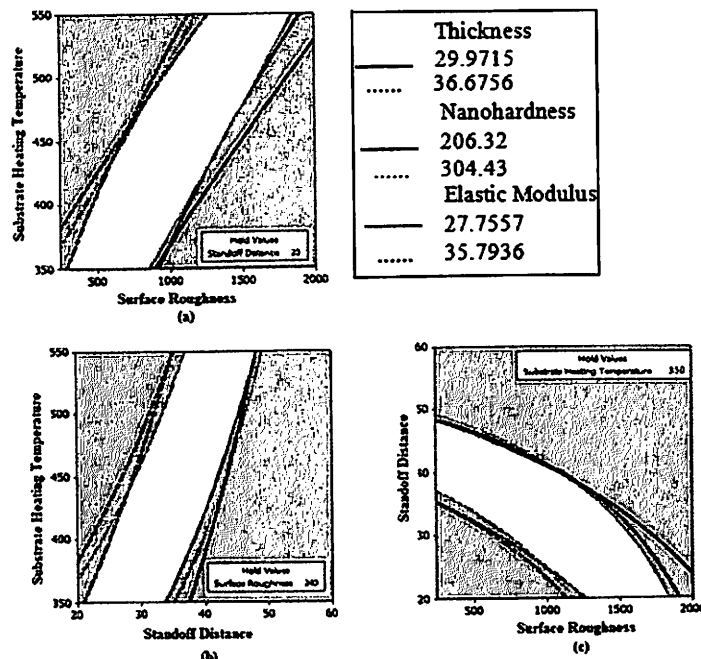


Figure 4: Overlaid contour plot

Steepest Method Analysis

To further optimize the process based on the regression equations (Eq(s). 1–3); experiments were conducted as proposed by the steepest method. The regression coefficient of standoff Distance (X_1) in Eq. 4 was chosen as a standard because its coefficient is higher among the other coefficients in Eq(s). 3, 4, and 5. Based on Table 1 and Eq. 4, X_i is noted by Δ_i , and the change in x_i be noted by δ_i . The coded variables are obtained by the following formula:

$$X_i = \frac{X_i - \bar{x}_i}{s_i} \text{ (Eq. 4)}$$

Where \bar{x}_i (respectively s_i) is the mean (respectively the standard deviation) of the two levels of x_i . Thus,

$$x_i + \delta_i = \frac{(x_i + \Delta_i) - \bar{x}_i}{s_i} \text{ (Eq. 5)}$$

$$\text{Then } \delta_i = \frac{\Delta_i}{s_i}$$

To the change in X_1 , $\Delta_1 = 10$ corresponds the change in x_1 , $\delta_2 = 10/20 = 0.5$ units.

In the relation $\frac{x_1}{b_1} = \frac{x_2}{b_2} = \frac{x_3}{b_3}$, we can substitute δ_i to x_i :

$$\frac{\delta_1}{b_1} = \frac{\delta_2}{b_2}, \text{ thus for } X_1, \frac{0.5}{4.21} = \frac{\delta_2}{1.8835} \text{ and } \delta_1 = 0.22, \text{ so } \Delta_2 = 0.22 * 880 = 193.6 \text{ grit}$$

$$\text{For } X_3, \frac{0.5}{4.21} = \frac{\delta_3}{0.470}$$

And $\delta_3 = 0.06$, so $\Delta_3 = 0.06 * 100 = 6^\circ\text{C}$

Table 3 shows the results of steepest method experiment. According to Table 3, the increase in response is observed through the 4th step; however, all steps beyond this point result in a decrease in all responses. Therefore, the factors at run 4 were selected as the new optimal solution.

Table 3: Points along the path of steepest ascent and decent and observed thickness of the nanohardness and elastic modulus of the sample at the points

Run No		Standoff Distance X_1	Surface Roughness X_2	Substrate Heating Temperature X_3	Thickness, (μm)	Nanohardness, MPa	Elastic Modulus, GPa
	Base	40	1120	450			
1	Base - $3\Delta_i$	70	1700.8	432	5.92	31.86	9.28
2	Base - $2\Delta_i$	60	1507.2	438	18.04	40.4	9.96
3	Base - Δ_i	50	1313.6	444	35.38	51.31	11.21
	Δ_i	-10	-193.6	+6			
4	Base + Δ_i	30	926.4	456	49.77	462.61	45.69
5	Base + $2\Delta_i$	20	732.8	462	47.23	422.50	42.96
6	Base + $3\Delta_i$	10	539.2	468	45.08	419.85	42.57

Optimisation of factors

Figure 5 provides an optimal solution for the input variable combinations and an optimisation plot. The response optimiser in Minitab suggests the following combination of input variable settings as jointly optimising three responses: thickness (Y1) as 46.26 μm , nanohardness (Y2) as 436.46 MPa and elastic modulus (Y3) as 43.89 GPa. It also provides the trade-off values of standoff distance as 22.7 mm, surface roughness as 649.2 grit and substrate heating temperature as 495.27°C. These parameters accommodate the optimum requirements of the cold spray process. In Figure 3, all the responses are treated as equally important, and therefore the default value 1.0 is given for $d=1$.

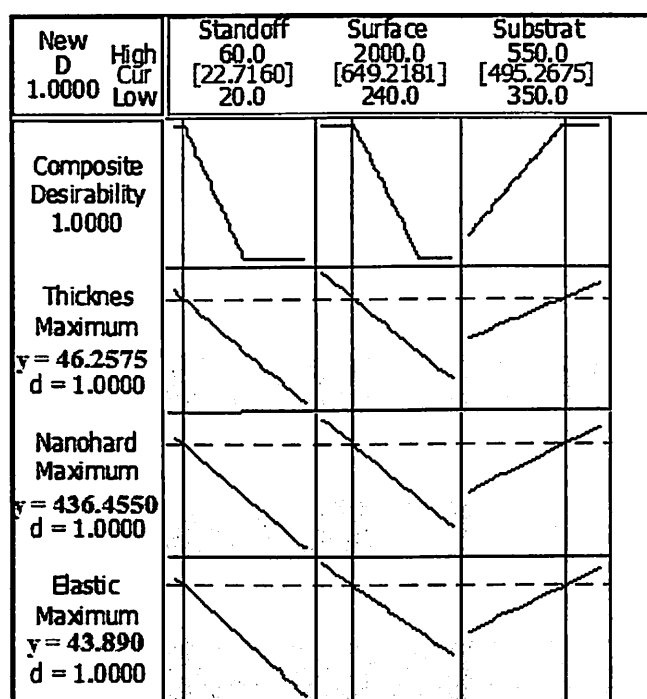


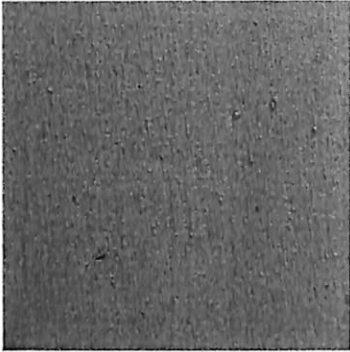
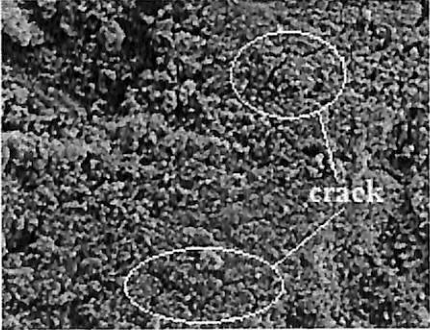
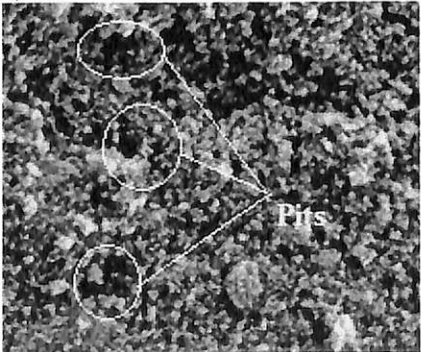
Figure 5: Optimisation of factors

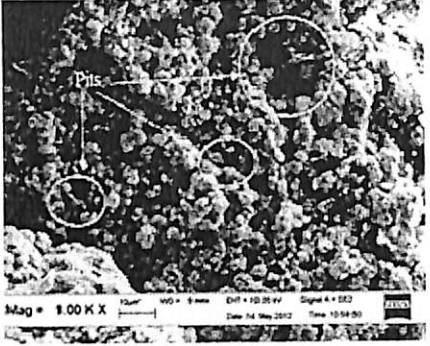
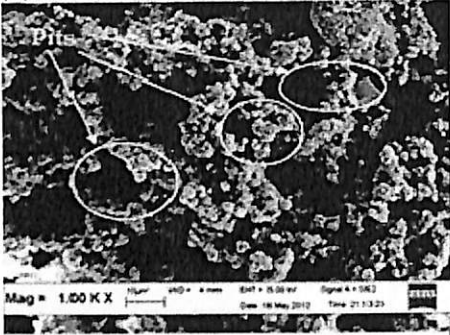
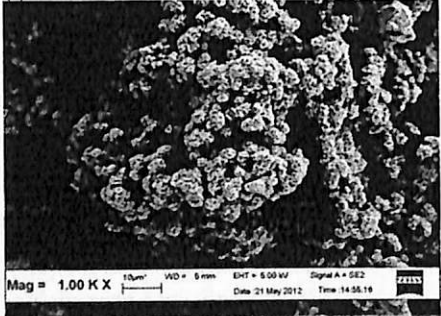
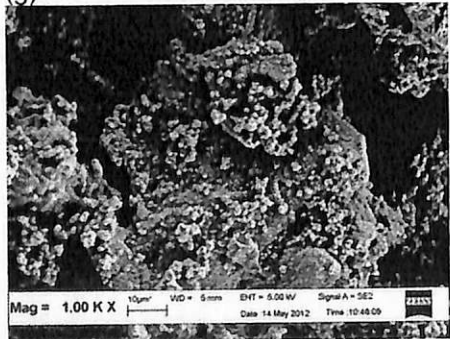
Characterization and biodegradable assessment in simulated body fluid (SBF)

Biodegradable assessment was performed to evaluate the bioactivity of the coating and the protection capacity of the coating to the Mg substrate. The coated and uncoated samples were immersed in SBF for 0 min, 10 min, 30 min, 60 min (1hr), 120 min (2hr), 240 min (4hr) and 1440 min (24hr) at 37°C. Table 4 shows the SEM micrograph, microanalysis of the substrate and ICP analysis after immersion of uncoated samples at different time period in the SBF solution. At 0 min immersion, the SEM microanalysis showed that the uncoated sample contain 100wt% of Mg indicating that there

is no other element present within the Mg only sample as shown in Table 4(a). Tiny cracks were visible after 10 min immersion in SBF solution with tiny pits formation which grew deeper with prolonged immersion period towards the end of experiment. The uncoated sample showed significant corrosive behaviour in the SBF as expected. SEM microanalysis showed the presence of other elements such as O, P, Ca in varying proportions besides Mg on the surface. Layers of corrosion product were clearly visible covering the entire surface. An electrochemical reaction mechanism occurred as the Mg was a reactive metal with ease of degradability in aqueous solution.

Table 4: SEM micrograph, microanalysis of substrate and ICP analysis of SBF solution after immersion of uncoated samples at different time period

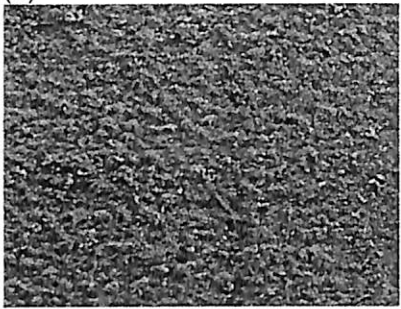
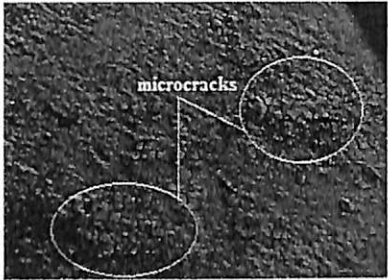
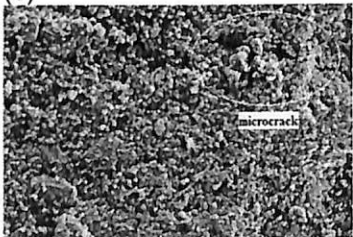
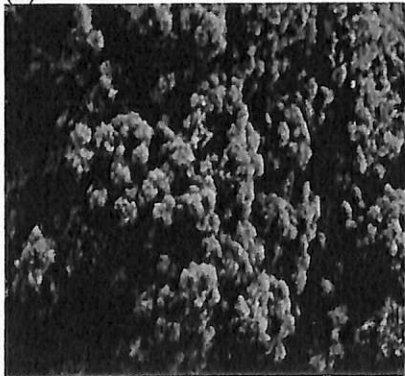
Time (min)	SEM micrograph	SEM microanalysis	ICP analysis																							
0	(a) 	<table border="1"> <thead> <tr> <th>Element</th> <th>Wt%</th> <th>At%</th> </tr> </thead> <tbody> <tr> <td>MgK</td> <td>100.00</td> <td>100.00</td> </tr> </tbody> </table>	Element	Wt%	At%	MgK	100.00	100.00	<table border="1"> <thead> <tr> <th>Ion</th> <th>Conc. (mg/mL)</th> </tr> </thead> <tbody> <tr> <td>Mg</td> <td>0.00</td> </tr> <tr> <td>P</td> <td>19.26</td> </tr> <tr> <td>Ca</td> <td>0.02</td> </tr> </tbody> </table>	Ion	Conc. (mg/mL)	Mg	0.00	P	19.26	Ca	0.02									
Element	Wt%	At%																								
MgK	100.00	100.00																								
Ion	Conc. (mg/mL)																									
Mg	0.00																									
P	19.26																									
Ca	0.02																									
10	(b) 	<table border="1"> <thead> <tr> <th>Element</th> <th>Wt%</th> <th>At%</th> </tr> </thead> <tbody> <tr> <td>O K</td> <td>46.40</td> <td>56.88</td> </tr> <tr> <td>MgK</td> <td>52.94</td> <td>42.70</td> </tr> <tr> <td>P K</td> <td>00.66</td> <td>00.42</td> </tr> <tr> <td>CaK</td> <td>00.00</td> <td>00.00</td> </tr> </tbody> </table>	Element	Wt%	At%	O K	46.40	56.88	MgK	52.94	42.70	P K	00.66	00.42	CaK	00.00	00.00	<table border="1"> <thead> <tr> <th>Ion</th> <th>Conc. (mg/mL)</th> </tr> </thead> <tbody> <tr> <td>Mg</td> <td>1.01</td> </tr> <tr> <td>P</td> <td>14.74</td> </tr> <tr> <td>Ca</td> <td>0.41</td> </tr> </tbody> </table>	Ion	Conc. (mg/mL)	Mg	1.01	P	14.74	Ca	0.41
Element	Wt%	At%																								
O K	46.40	56.88																								
MgK	52.94	42.70																								
P K	00.66	00.42																								
CaK	00.00	00.00																								
Ion	Conc. (mg/mL)																									
Mg	1.01																									
P	14.74																									
Ca	0.41																									
30	(c) 	<table border="1"> <thead> <tr> <th>Element</th> <th>Wt%</th> <th>At%</th> </tr> </thead> <tbody> <tr> <td>O K</td> <td>45.52</td> <td>56.13</td> </tr> <tr> <td>MgK</td> <td>52.59</td> <td>42.67</td> </tr> <tr> <td>P K</td> <td>01.89</td> <td>01.20</td> </tr> <tr> <td>CaK</td> <td>00.42</td> <td>00.20</td> </tr> </tbody> </table>	Element	Wt%	At%	O K	45.52	56.13	MgK	52.59	42.67	P K	01.89	01.20	CaK	00.42	00.20	<table border="1"> <thead> <tr> <th>Ion</th> <th>Conc. (mg/mL)</th> </tr> </thead> <tbody> <tr> <td>Mg</td> <td>2.57</td> </tr> <tr> <td>P</td> <td>12.72</td> </tr> <tr> <td>Ca</td> <td>0.67</td> </tr> </tbody> </table>	Ion	Conc. (mg/mL)	Mg	2.57	P	12.72	Ca	0.67
Element	Wt%	At%																								
O K	45.52	56.13																								
MgK	52.59	42.67																								
P K	01.89	01.20																								
CaK	00.42	00.20																								
Ion	Conc. (mg/mL)																									
Mg	2.57																									
P	12.72																									
Ca	0.67																									

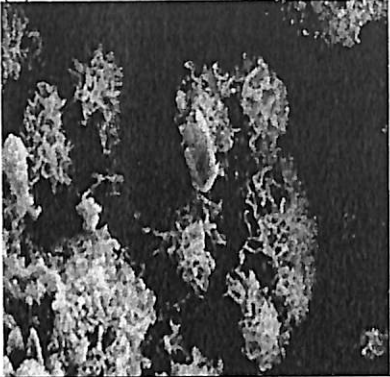
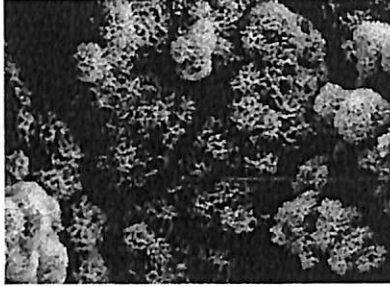

Time (min)	SEM micrograph	SEM microanalysis	ICP analysis																							
60	(d) 	<table border="1"> <thead> <tr> <th>Element</th> <th>Wt%</th> <th>At%</th> </tr> </thead> <tbody> <tr> <td><i>O K</i></td> <td>36.76</td> <td>47.16</td> </tr> <tr> <td><i>MgK</i></td> <td>61.28</td> <td>51.74</td> </tr> <tr> <td><i>P K</i></td> <td>00.68</td> <td>00.45</td> </tr> <tr> <td><i>CaK</i></td> <td>01.28</td> <td>00.66</td> </tr> </tbody> </table>	Element	Wt%	At%	<i>O K</i>	36.76	47.16	<i>MgK</i>	61.28	51.74	<i>P K</i>	00.68	00.45	<i>CaK</i>	01.28	00.66	<table border="1"> <thead> <tr> <th>Ion</th> <th>Conc. (mg/mL)</th> </tr> </thead> <tbody> <tr> <td>Mg</td> <td>5.45</td> </tr> <tr> <td>P</td> <td>15.17</td> </tr> <tr> <td>Ca</td> <td>0.49</td> </tr> </tbody> </table>	Ion	Conc. (mg/mL)	Mg	5.45	P	15.17	Ca	0.49
Element	Wt%	At%																								
<i>O K</i>	36.76	47.16																								
<i>MgK</i>	61.28	51.74																								
<i>P K</i>	00.68	00.45																								
<i>CaK</i>	01.28	00.66																								
Ion	Conc. (mg/mL)																									
Mg	5.45																									
P	15.17																									
Ca	0.49																									
120	(e) 	<table border="1"> <thead> <tr> <th>Element</th> <th>Wt%</th> <th>At%</th> </tr> </thead> <tbody> <tr> <td><i>O K</i></td> <td>42.75</td> <td>53.68</td> </tr> <tr> <td><i>MgK</i></td> <td>51.00</td> <td>42.72</td> </tr> <tr> <td><i>P K</i></td> <td>03.72</td> <td>02.41</td> </tr> <tr> <td><i>CaK</i></td> <td>00.95</td> <td>00.48</td> </tr> </tbody> </table>	Element	Wt%	At%	<i>O K</i>	42.75	53.68	<i>MgK</i>	51.00	42.72	<i>P K</i>	03.72	02.41	<i>CaK</i>	00.95	00.48	<table border="1"> <thead> <tr> <th>Ion</th> <th>Conc. (mg/mL)</th> </tr> </thead> <tbody> <tr> <td>Mg</td> <td>9.57</td> </tr> <tr> <td>P</td> <td>14.95</td> </tr> <tr> <td>Ca</td> <td>0.63</td> </tr> </tbody> </table>	Ion	Conc. (mg/mL)	Mg	9.57	P	14.95	Ca	0.63
Element	Wt%	At%																								
<i>O K</i>	42.75	53.68																								
<i>MgK</i>	51.00	42.72																								
<i>P K</i>	03.72	02.41																								
<i>CaK</i>	00.95	00.48																								
Ion	Conc. (mg/mL)																									
Mg	9.57																									
P	14.95																									
Ca	0.63																									
240	(f) 	<table border="1"> <thead> <tr> <th>Element</th> <th>Wt%</th> <th>At%</th> </tr> </thead> <tbody> <tr> <td><i>O K</i></td> <td>42.54</td> <td>52.89</td> </tr> <tr> <td><i>MgK</i></td> <td>51.24</td> <td>43.12</td> </tr> <tr> <td><i>P K</i></td> <td>05.78</td> <td>04.94</td> </tr> <tr> <td><i>CaK</i></td> <td>04.32</td> <td>03.73</td> </tr> </tbody> </table>	Element	Wt%	At%	<i>O K</i>	42.54	52.89	<i>MgK</i>	51.24	43.12	<i>P K</i>	05.78	04.94	<i>CaK</i>	04.32	03.73	<table border="1"> <thead> <tr> <th>Ion</th> <th>Conc. (mg/mL)</th> </tr> </thead> <tbody> <tr> <td>Mg</td> <td>15.18</td> </tr> <tr> <td>P</td> <td>14.34</td> </tr> <tr> <td>Ca</td> <td>0.71</td> </tr> </tbody> </table>	Ion	Conc. (mg/mL)	Mg	15.18	P	14.34	Ca	0.71
Element	Wt%	At%																								
<i>O K</i>	42.54	52.89																								
<i>MgK</i>	51.24	43.12																								
<i>P K</i>	05.78	04.94																								
<i>CaK</i>	04.32	03.73																								
Ion	Conc. (mg/mL)																									
Mg	15.18																									
P	14.34																									
Ca	0.71																									
1140	(g) 	<table border="1"> <thead> <tr> <th>Element</th> <th>Wt%</th> <th>At%</th> </tr> </thead> <tbody> <tr> <td><i>O K</i></td> <td>30.54</td> <td>27.89</td> </tr> <tr> <td><i>MgK</i></td> <td>60.36</td> <td>56.12</td> </tr> <tr> <td><i>P K</i></td> <td>05.78</td> <td>04.94</td> </tr> <tr> <td><i>CaK</i></td> <td>04.32</td> <td>03.73</td> </tr> </tbody> </table>	Element	Wt%	At%	<i>O K</i>	30.54	27.89	<i>MgK</i>	60.36	56.12	<i>P K</i>	05.78	04.94	<i>CaK</i>	04.32	03.73	<table border="1"> <thead> <tr> <th>Ion</th> <th>Conc. (mg/mL)</th> </tr> </thead> <tbody> <tr> <td>Mg</td> <td>15.75</td> </tr> <tr> <td>P</td> <td>3.51</td> </tr> <tr> <td>Ca</td> <td>0.56</td> </tr> </tbody> </table>	Ion	Conc. (mg/mL)	Mg	15.75	P	3.51	Ca	0.56
Element	Wt%	At%																								
<i>O K</i>	30.54	27.89																								
<i>MgK</i>	60.36	56.12																								
<i>P K</i>	05.78	04.94																								
<i>CaK</i>	04.32	03.73																								
Ion	Conc. (mg/mL)																									
Mg	15.75																									
P	3.51																									
Ca	0.56																									

The surface morphologies, chemical composition and ICP analysis of HAP coated on Mg substrate after soaking in SBF for different period is shown in Table 5. At 0 min immersion, the HAP layer is well distributed on the coated sample as shown in Table 5(a). The microanalysis results

showed the presence of O, P and Ca element on the sample surface indicating that the O, P and Ca may originate from the existing HAP layer coated on the Mg. The ICP-OES showed that the O, P and Ca concentration present within the SBF is lower than that observed from the microanalysis results.

Table 5: SEM micrograph, microanalysis of substrate and ICP analysis of SBF solution after immersion of coated samples for different time period

Time (min)	SEM micrograph	SEM microanalysis	ICP analysis																							
0	(a) 	<table border="1"> <thead> <tr> <th>Element</th> <th>Wt%</th> <th>At%</th> </tr> </thead> <tbody> <tr> <td><i>O K</i></td> <td>30.86</td> <td>31.01</td> </tr> <tr> <td><i>MgK</i></td> <td>00.50</td> <td>00.42</td> </tr> <tr> <td><i>P K</i></td> <td>24.97</td> <td>20.95</td> </tr> <tr> <td><i>CaK</i></td> <td>44.12</td> <td>37.73</td> </tr> </tbody> </table>	Element	Wt%	At%	<i>O K</i>	30.86	31.01	<i>MgK</i>	00.50	00.42	<i>P K</i>	24.97	20.95	<i>CaK</i>	44.12	37.73	<table border="1"> <thead> <tr> <th>Ion</th> <th>Conc.(mg/m L)</th> </tr> </thead> <tbody> <tr> <td>Mg</td> <td>0.00</td> </tr> <tr> <td>P</td> <td>19.26</td> </tr> <tr> <td>Ca</td> <td>0.02</td> </tr> </tbody> </table>	Ion	Conc.(mg/m L)	Mg	0.00	P	19.26	Ca	0.02
Element	Wt%	At%																								
<i>O K</i>	30.86	31.01																								
<i>MgK</i>	00.50	00.42																								
<i>P K</i>	24.97	20.95																								
<i>CaK</i>	44.12	37.73																								
Ion	Conc.(mg/m L)																									
Mg	0.00																									
P	19.26																									
Ca	0.02																									
10	(b) 	<table border="1"> <thead> <tr> <th>Element</th> <th>Wt%</th> <th>At%</th> </tr> </thead> <tbody> <tr> <td><i>O K</i></td> <td>31.66</td> <td>31.01</td> </tr> <tr> <td><i>MgK</i></td> <td>01.78</td> <td>01.09</td> </tr> <tr> <td><i>P K</i></td> <td>23.97</td> <td>19.95</td> </tr> <tr> <td><i>CaK</i></td> <td>43.12</td> <td>27.73</td> </tr> </tbody> </table>	Element	Wt%	At%	<i>O K</i>	31.66	31.01	<i>MgK</i>	01.78	01.09	<i>P K</i>	23.97	19.95	<i>CaK</i>	43.12	27.73	<table border="1"> <thead> <tr> <th>Ion</th> <th>Conc.(mg/ L)</th> </tr> </thead> <tbody> <tr> <td>Mg</td> <td>1.63</td> </tr> <tr> <td>P</td> <td>13.74</td> </tr> <tr> <td>Ca</td> <td>0.91</td> </tr> </tbody> </table>	Ion	Conc.(mg/ L)	Mg	1.63	P	13.74	Ca	0.91
Element	Wt%	At%																								
<i>O K</i>	31.66	31.01																								
<i>MgK</i>	01.78	01.09																								
<i>P K</i>	23.97	19.95																								
<i>CaK</i>	43.12	27.73																								
Ion	Conc.(mg/ L)																									
Mg	1.63																									
P	13.74																									
Ca	0.91																									
30	(c) 	<table border="1"> <thead> <tr> <th>Element</th> <th>Wt%</th> <th>At%</th> </tr> </thead> <tbody> <tr> <td><i>O K</i></td> <td>38.65</td> <td>49.18</td> </tr> <tr> <td><i>MgK</i></td> <td>02.12</td> <td>01.79</td> </tr> <tr> <td><i>P K</i></td> <td>22.45</td> <td>21.72</td> </tr> <tr> <td><i>CaK</i></td> <td>42.00</td> <td>37.58</td> </tr> </tbody> </table>	Element	Wt%	At%	<i>O K</i>	38.65	49.18	<i>MgK</i>	02.12	01.79	<i>P K</i>	22.45	21.72	<i>CaK</i>	42.00	37.58	<table border="1"> <thead> <tr> <th>Ion</th> <th>Conc.(mg/ L)</th> </tr> </thead> <tbody> <tr> <td>Mg</td> <td>4.47</td> </tr> <tr> <td>P</td> <td>15.79</td> </tr> <tr> <td>Ca</td> <td>0.89</td> </tr> </tbody> </table>	Ion	Conc.(mg/ L)	Mg	4.47	P	15.79	Ca	0.89
Element	Wt%	At%																								
<i>O K</i>	38.65	49.18																								
<i>MgK</i>	02.12	01.79																								
<i>P K</i>	22.45	21.72																								
<i>CaK</i>	42.00	37.58																								
Ion	Conc.(mg/ L)																									
Mg	4.47																									
P	15.79																									
Ca	0.89																									
60	(d) 	<table border="1"> <thead> <tr> <th>Element</th> <th>Wt%</th> <th>At%</th> </tr> </thead> <tbody> <tr> <td><i>O K</i></td> <td>40.25</td> <td>39.13</td> </tr> <tr> <td><i>MgK</i></td> <td>04.57</td> <td>03.16</td> </tr> <tr> <td><i>P K</i></td> <td>02.59</td> <td>02.11</td> </tr> <tr> <td><i>CaK</i></td> <td>40.21</td> <td>35.19</td> </tr> </tbody> </table>	Element	Wt%	At%	<i>O K</i>	40.25	39.13	<i>MgK</i>	04.57	03.16	<i>P K</i>	02.59	02.11	<i>CaK</i>	40.21	35.19	<table border="1"> <thead> <tr> <th>Ion</th> <th>Conc.(mg/ L)</th> </tr> </thead> <tbody> <tr> <td>Mg</td> <td>5.15</td> </tr> <tr> <td>P</td> <td>12.13</td> </tr> <tr> <td>Ca</td> <td>0.78</td> </tr> </tbody> </table>	Ion	Conc.(mg/ L)	Mg	5.15	P	12.13	Ca	0.78
Element	Wt%	At%																								
<i>O K</i>	40.25	39.13																								
<i>MgK</i>	04.57	03.16																								
<i>P K</i>	02.59	02.11																								
<i>CaK</i>	40.21	35.19																								
Ion	Conc.(mg/ L)																									
Mg	5.15																									
P	12.13																									
Ca	0.78																									

Time (min)	SEM micrograph	SEM microanalysis	ICP analysis																							
120	(e) 	<table border="1"> <thead> <tr> <th>Element</th> <th>Wt%</th> <th>At%</th> </tr> </thead> <tbody> <tr> <td><i>O K</i></td> <td>30.15</td> <td>48.01</td> </tr> <tr> <td><i>MgK</i></td> <td>08.00</td> <td>08.39</td> </tr> <tr> <td><i>P K</i></td> <td>02.95</td> <td>01.88</td> </tr> <tr> <td><i>CaK</i></td> <td>38.89</td> <td>24.72</td> </tr> </tbody> </table>	Element	Wt%	At%	<i>O K</i>	30.15	48.01	<i>MgK</i>	08.00	08.39	<i>P K</i>	02.95	01.88	<i>CaK</i>	38.89	24.72	<table border="1"> <thead> <tr> <th>Ion</th> <th>Conc.(mg/m L)</th> </tr> </thead> <tbody> <tr> <td>Mg</td> <td>8.48</td> </tr> <tr> <td>P</td> <td>12.98</td> </tr> <tr> <td>Ca</td> <td>0.70</td> </tr> </tbody> </table>	Ion	Conc.(mg/m L)	Mg	8.48	P	12.98	Ca	0.70
Element	Wt%	At%																								
<i>O K</i>	30.15	48.01																								
<i>MgK</i>	08.00	08.39																								
<i>P K</i>	02.95	01.88																								
<i>CaK</i>	38.89	24.72																								
Ion	Conc.(mg/m L)																									
Mg	8.48																									
P	12.98																									
Ca	0.70																									
240	(f) 	<table border="1"> <thead> <tr> <th>Element</th> <th>Wt%</th> <th>At%</th> </tr> </thead> <tbody> <tr> <td><i>O K</i></td> <td>38.45</td> <td>36.51</td> </tr> <tr> <td><i>MgK</i></td> <td>08.00</td> <td>08.39</td> </tr> <tr> <td><i>P K</i></td> <td>05.36</td> <td>05.00</td> </tr> <tr> <td><i>CaK</i></td> <td>48.02</td> <td>44.36</td> </tr> </tbody> </table>	Element	Wt%	At%	<i>O K</i>	38.45	36.51	<i>MgK</i>	08.00	08.39	<i>P K</i>	05.36	05.00	<i>CaK</i>	48.02	44.36	<table border="1"> <thead> <tr> <th>Ion</th> <th>Conc.(mg/m L)</th> </tr> </thead> <tbody> <tr> <td>Mg</td> <td>16.37</td> </tr> <tr> <td>P</td> <td>17.05</td> </tr> <tr> <td>Ca</td> <td>0.79</td> </tr> </tbody> </table>	Ion	Conc.(mg/m L)	Mg	16.37	P	17.05	Ca	0.79
Element	Wt%	At%																								
<i>O K</i>	38.45	36.51																								
<i>MgK</i>	08.00	08.39																								
<i>P K</i>	05.36	05.00																								
<i>CaK</i>	48.02	44.36																								
Ion	Conc.(mg/m L)																									
Mg	16.37																									
P	17.05																									
Ca	0.79																									
1440	(g) 	<table border="1"> <thead> <tr> <th>Element</th> <th>Wt%</th> <th>At%</th> </tr> </thead> <tbody> <tr> <td><i>O K</i></td> <td>30.52</td> <td>27.45</td> </tr> <tr> <td><i>MgK</i></td> <td>07.52</td> <td>07.41</td> </tr> <tr> <td><i>P K</i></td> <td>10.23</td> <td>15.26</td> </tr> <tr> <td><i>CaK</i></td> <td>50.26</td> <td>47.20</td> </tr> </tbody> </table>	Element	Wt%	At%	<i>O K</i>	30.52	27.45	<i>MgK</i>	07.52	07.41	<i>P K</i>	10.23	15.26	<i>CaK</i>	50.26	47.20	<table border="1"> <thead> <tr> <th>Ion</th> <th>Conc.(mg/m L)</th> </tr> </thead> <tbody> <tr> <td>Mg</td> <td>14.64</td> </tr> <tr> <td>P</td> <td>3.87</td> </tr> <tr> <td>Ca</td> <td>0.57</td> </tr> </tbody> </table>	Ion	Conc.(mg/m L)	Mg	14.64	P	3.87	Ca	0.57
Element	Wt%	At%																								
<i>O K</i>	30.52	27.45																								
<i>MgK</i>	07.52	07.41																								
<i>P K</i>	10.23	15.26																								
<i>CaK</i>	50.26	47.20																								
Ion	Conc.(mg/m L)																									
Mg	14.64																									
P	3.87																									
Ca	0.57																									

Mass Loss as a measure of biocorrosion

Mass loss experiments are among the simplest in-vitro methods for investigating the corrosion process of HAP coated Mg. Results obtained from mass loss tests are typically accurate, assuming that issues involved in the removal of the corrosion layer are minimized. Additionally, a substantial degree of corrosion is necessary for precise measurement of the mass change, which requires multiple replicates in order to provide confidence in mass loss results. Table 6 shows the specific mass loss for the uncoated and coated sample after immersion in SBF solution for various time periods.

Table 6: Specific mass loss for uncoated and coated sample after immersion in SBF solution for various time periods.

Time, min	Specific Mass Loss, %	
	Uncoated sample	Coated Sample
0	0	0
10	0.26	-0.09
30	0.30	-0.12
60	0.45	-0.27
120	0.47	-0.38
240	0.48	-0.38
1140	0.50	-0.45

Figure 6 shows the specific mass loss of specimens immersed in SBF for uncoated and coated sample.

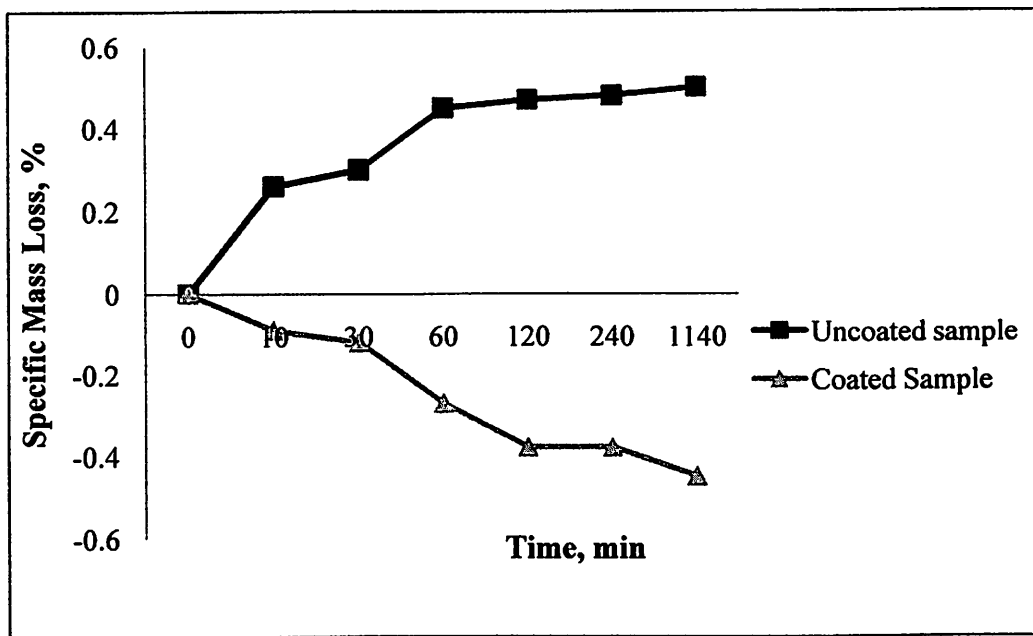


Figure 6: Specific mass loss of specimens immersed in SBF for uncoated and coated sample

There was a drastic mass loss of Mg substrate without coating in the first 10 min resulting from high Cl^- concentration in SBF causing the Mg substrate to corrode at a fast rate (Figure 6). The corrosion rate tends to slow-down after 60 min immersion which may be due to the Ca-P-Mg deposition on Mg substrate that inhibits further corrosion.

Adhesion Test for HAP coated on Mg substrate

Following soaking in SBF, the bond strength of HAP coated on Mg substrate may degrade through chemical dissolution. Adhesion of the composite coating with the magnesium substrate is one

of the most important properties for the *in vivo* implantation. The interlamellar microstructure of the coating will be weakened and the bonding at the HAP coating and the substrate will decrease. The bond strength data measured from the adhesion tests are shown in Table 7.

Table 7: Bond strength data for HAP coated on Mg substrate for various immersion period

Time, min	Bond Strength (MPa)
0	75
10	70
30	68
60	67
120	55
240	48
1140	40

Based on Table 7, average bond strength of 75 MPa is reached for the coating without soaking. Following soaking in SBF, the bond strength of the coatings decreases. The bond strength decreased about 6.67% following 10 min immersion. Continuous immersion into SBF up to 30 min resulted in further reduction with a total of 9.33% reduction than the original strength. Upon reaching 60 min immersion and up to 1140 min, the bond strength reductions tend to stabilize. The continued chemical dissolution of the coatings may have contributed to the reduction of the bond strength between the HAP-Mg interface through weakening of the lamella formed between the coating and the substrate surface. Higher dissolution rate of the coating may enhance decaying of the bonding at the interface of coating and substrate.

Accelerated corrosion test

The accelerated corrosion test in a 3.5wt% NaCl solution was performed for uncoated and coated Mg substrate with HAP in order to examine the corrosion behaviour for both samples. Both samples were immersing in this solution for 1, 4, 10 and 21 days. According to the SEM micrograph and EDX results in Table 8, the dissolution reaction took place as soon as the control sample was immersed in the NaCl solution. The surface morphology obtained showed scattered tiny pits on the surface. The EDX analysis showed the existence of Mg and O as the main elements of the compound formed indicating that the $Mg(OH)_2$ was formed.

Magnesium hydroxide accumulated on the Mg surface and act as a corrosion protection layer. However, since the 3.5 wt% NaCl solutions contain high chloride concentration, this promotes corrosion.

Table 8: SEM micrograph and microanalysis of substrate after immersion of uncoated samples for different periods

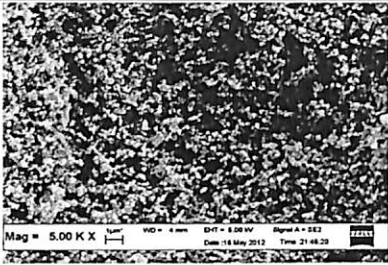
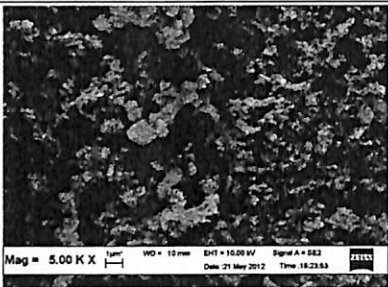
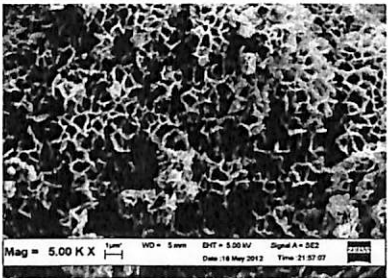
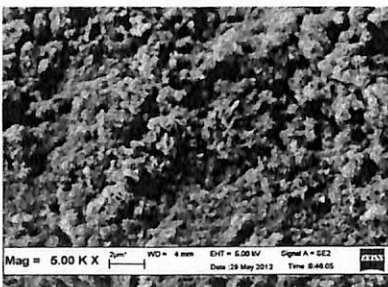
Day	SEM micrograph	SEM microanalysis															
1		<table border="1"> <thead> <tr> <th>Element</th> <th>Wt%</th> <th>At%</th> </tr> </thead> <tbody> <tr> <td><i>O K</i></td> <td>47.86</td> <td>58.22</td> </tr> <tr> <td><i>NaK</i></td> <td>02.49</td> <td>02.11</td> </tr> <tr> <td><i>MgK</i></td> <td>49.31</td> <td>39.48</td> </tr> <tr> <td><i>ClK</i></td> <td>00.34</td> <td>00.19</td> </tr> </tbody> </table>	Element	Wt%	At%	<i>O K</i>	47.86	58.22	<i>NaK</i>	02.49	02.11	<i>MgK</i>	49.31	39.48	<i>ClK</i>	00.34	00.19
Element	Wt%	At%															
<i>O K</i>	47.86	58.22															
<i>NaK</i>	02.49	02.11															
<i>MgK</i>	49.31	39.48															
<i>ClK</i>	00.34	00.19															
4		<table border="1"> <thead> <tr> <th>Element</th> <th>Wt%</th> <th>At%</th> </tr> </thead> <tbody> <tr> <td><i>O K</i></td> <td>44.48</td> <td>54.97</td> </tr> <tr> <td><i>NaK</i></td> <td>01.75</td> <td>01.51</td> </tr> <tr> <td><i>MgK</i></td> <td>52.94</td> <td>43.06</td> </tr> <tr> <td><i>ClK</i></td> <td>00.83</td> <td>00.46</td> </tr> </tbody> </table>	Element	Wt%	At%	<i>O K</i>	44.48	54.97	<i>NaK</i>	01.75	01.51	<i>MgK</i>	52.94	43.06	<i>ClK</i>	00.83	00.46
Element	Wt%	At%															
<i>O K</i>	44.48	54.97															
<i>NaK</i>	01.75	01.51															
<i>MgK</i>	52.94	43.06															
<i>ClK</i>	00.83	00.46															
10		<table border="1"> <thead> <tr> <th>Element</th> <th>Wt%</th> <th>At%</th> </tr> </thead> <tbody> <tr> <td><i>O K</i></td> <td>47.50</td> <td>57.96</td> </tr> <tr> <td><i>NaK</i></td> <td>00.88</td> <td>00.75</td> </tr> <tr> <td><i>MgK</i></td> <td>50.99</td> <td>40.94</td> </tr> <tr> <td><i>ClK</i></td> <td>00.63</td> <td>00.35</td> </tr> </tbody> </table>	Element	Wt%	At%	<i>O K</i>	47.50	57.96	<i>NaK</i>	00.88	00.75	<i>MgK</i>	50.99	40.94	<i>ClK</i>	00.63	00.35
Element	Wt%	At%															
<i>O K</i>	47.50	57.96															
<i>NaK</i>	00.88	00.75															
<i>MgK</i>	50.99	40.94															
<i>ClK</i>	00.63	00.35															
21		<table border="1"> <thead> <tr> <th>Element</th> <th>Wt%</th> <th>At%</th> </tr> </thead> <tbody> <tr> <td><i>O K</i></td> <td>45.62</td> <td>56.13</td> </tr> <tr> <td><i>NaK</i></td> <td>03.16</td> <td>02.71</td> </tr> <tr> <td><i>MgK</i></td> <td>50.04</td> <td>40.51</td> </tr> <tr> <td><i>ClK</i></td> <td>01.18</td> <td>00.66</td> </tr> </tbody> </table>	Element	Wt%	At%	<i>O K</i>	45.62	56.13	<i>NaK</i>	03.16	02.71	<i>MgK</i>	50.04	40.51	<i>ClK</i>	01.18	00.66
Element	Wt%	At%															
<i>O K</i>	45.62	56.13															
<i>NaK</i>	03.16	02.71															
<i>MgK</i>	50.04	40.51															
<i>ClK</i>	01.18	00.66															

At day 10 with increasing immersion period, similar phenomenon was observed. Many pores had formed on the coated Mg surface. The EDX analysis showed minor changes in the weight percentage of all elements indicating that a stable film was created on the sample surface. At the final stage of immersion, the film started to dissociate into thin flakes and peeled off from the sample surface. As shown in SEM micrograph, the surface degradation occurred gradually and finally leading to complete failure of the film.

Table 9 represented the HAP coated samples degradation progress. Based on the observation of surface morphologies and the elemental compositions, it is shown that HAP coating remarkably prevented the substrate corrosion under a severe environment for example the 3.5 wt% NaCl solutions. At day one immersion, the HAP coating is still present and covering the Mg surface. The surface morphology appeared similar to the original appearance of the coatings prior to immersion in SBF as shown by the elemental composition of Ca, P and O elements detected on the surface. As the immersion period increased from 1 to 4 days, the HAP coating began to degrade in a slow manner. The EDX analysis unveiled a decreased in the weight percentages of Ca and P up to 50% from the original weight. The loss of initial HAP protective layer exposed the coated Mg substrate to the corrosive environment. Consequently, the HAP-coated Mg started to degrade via the electrochemical reactions. The possible degradation products of the reaction were magnesium hydroxide and hydrogen gas (Witte et al., 2008).

The magnesium hydroxide accumulated on the underlying Mg substrate as a corrosion protection layer. At day 10, the surface morphology revealed whitish corrosion products covering the coated Mg sample. The concentration of Ca and P elements decreased significantly while the weight percentages of Mg and O were further increased. Increased immersion period also indicated that a higher surface area was exposed to the corrosive environment. As the immersion period lengthen, the adhesiveness of HAP coating became weakened resulting in higher volume of HAP to dissolve into the solution. Less visible changes were observed for the sample surface morphology after 10 days immersion which appear similar as those observed at day 4 (Table 9).

Table 9: SEM micrograph and microanalysis of substrate after immersion of coated samples for different time period

Day	SEM micrograph	SEM microanalysis																					
1		<table border="1"> <thead> <tr> <th>Element</th> <th>Wt%</th> <th>At%</th> </tr> </thead> <tbody> <tr> <td><i>O K</i></td> <td>34.50</td> <td>53.97</td> </tr> <tr> <td><i>NaK</i></td> <td>01.20</td> <td>01.31</td> </tr> <tr> <td><i>MgK</i></td> <td>00.98</td> <td>01.01</td> </tr> <tr> <td><i>P K</i></td> <td>22.47</td> <td>18.16</td> </tr> <tr> <td><i>ClK</i></td> <td>00.62</td> <td>00.44</td> </tr> <tr> <td><i>CaK</i></td> <td>40.24</td> <td>25.13</td> </tr> </tbody> </table>	Element	Wt%	At%	<i>O K</i>	34.50	53.97	<i>NaK</i>	01.20	01.31	<i>MgK</i>	00.98	01.01	<i>P K</i>	22.47	18.16	<i>ClK</i>	00.62	00.44	<i>CaK</i>	40.24	25.13
Element	Wt%	At%																					
<i>O K</i>	34.50	53.97																					
<i>NaK</i>	01.20	01.31																					
<i>MgK</i>	00.98	01.01																					
<i>P K</i>	22.47	18.16																					
<i>ClK</i>	00.62	00.44																					
<i>CaK</i>	40.24	25.13																					
4		<table border="1"> <thead> <tr> <th>Element</th> <th>Wt%</th> <th>At%</th> </tr> </thead> <tbody> <tr> <td><i>O K</i></td> <td>40.01</td> <td>54.46</td> </tr> <tr> <td><i>NaK</i></td> <td>00.44</td> <td>00.42</td> </tr> <tr> <td><i>MgK</i></td> <td>31.51</td> <td>28.23</td> </tr> <tr> <td><i>P K</i></td> <td>08.10</td> <td>05.70</td> </tr> <tr> <td><i>ClK</i></td> <td>05.13</td> <td>03.15</td> </tr> <tr> <td><i>CaK</i></td> <td>14.81</td> <td>08.05</td> </tr> </tbody> </table>	Element	Wt%	At%	<i>O K</i>	40.01	54.46	<i>NaK</i>	00.44	00.42	<i>MgK</i>	31.51	28.23	<i>P K</i>	08.10	05.70	<i>ClK</i>	05.13	03.15	<i>CaK</i>	14.81	08.05
Element	Wt%	At%																					
<i>O K</i>	40.01	54.46																					
<i>NaK</i>	00.44	00.42																					
<i>MgK</i>	31.51	28.23																					
<i>P K</i>	08.10	05.70																					
<i>ClK</i>	05.13	03.15																					
<i>CaK</i>	14.81	08.05																					
10		<table border="1"> <thead> <tr> <th>Element</th> <th>Wt%</th> <th>At%</th> </tr> </thead> <tbody> <tr> <td><i>O K</i></td> <td>45.02</td> <td>55.76</td> </tr> <tr> <td><i>NaK</i></td> <td>01.05</td> <td>00.90</td> </tr> <tr> <td><i>MgK</i></td> <td>50.73</td> <td>41.35</td> </tr> <tr> <td><i>P K</i></td> <td>02.59</td> <td>01.65</td> </tr> <tr> <td><i>ClK</i></td> <td>00.61</td> <td>00.34</td> </tr> <tr> <td><i>CaK</i></td> <td>00.00</td> <td>00.00</td> </tr> </tbody> </table>	Element	Wt%	At%	<i>O K</i>	45.02	55.76	<i>NaK</i>	01.05	00.90	<i>MgK</i>	50.73	41.35	<i>P K</i>	02.59	01.65	<i>ClK</i>	00.61	00.34	<i>CaK</i>	00.00	00.00
Element	Wt%	At%																					
<i>O K</i>	45.02	55.76																					
<i>NaK</i>	01.05	00.90																					
<i>MgK</i>	50.73	41.35																					
<i>P K</i>	02.59	01.65																					
<i>ClK</i>	00.61	00.34																					
<i>CaK</i>	00.00	00.00																					
21		<table border="1"> <thead> <tr> <th>Element</th> <th>Wt%</th> <th>At%</th> </tr> </thead> <tbody> <tr> <td><i>O K</i></td> <td>43.87</td> <td>55.30</td> </tr> <tr> <td><i>NaK</i></td> <td>00.52</td> <td>00.46</td> </tr> <tr> <td><i>MgK</i></td> <td>48.17</td> <td>39.96</td> </tr> <tr> <td><i>P K</i></td> <td>00.93</td> <td>00.61</td> </tr> <tr> <td><i>ClK</i></td> <td>06.17</td> <td>03.51</td> </tr> <tr> <td><i>CaK</i></td> <td>00.32</td> <td>00.16</td> </tr> </tbody> </table>	Element	Wt%	At%	<i>O K</i>	43.87	55.30	<i>NaK</i>	00.52	00.46	<i>MgK</i>	48.17	39.96	<i>P K</i>	00.93	00.61	<i>ClK</i>	06.17	03.51	<i>CaK</i>	00.32	00.16
Element	Wt%	At%																					
<i>O K</i>	43.87	55.30																					
<i>NaK</i>	00.52	00.46																					
<i>MgK</i>	48.17	39.96																					
<i>P K</i>	00.93	00.61																					
<i>ClK</i>	06.17	03.51																					
<i>CaK</i>	00.32	00.16																					

As the immersion time increased up to 21 days, more and more Cl^- are adsorbed on the film layer covering the surface which destroyed the dynamic balance at this period. The magnesium hydroxide began to transform into a highly soluble magnesium chloride. The possible reaction was $\text{Mg}(\text{OH})_2 + 2\text{Cl}^- \rightarrow \text{MgCl}_2 + 2\text{OH}^-$. Based on the surface morphologies and chemical analysis of both

samples, it can be concluded that the HAP coating remarkably protected and prevented the corrosion from taking place within the corrosive environment.

5. Conclusion and suggestions

The research work described in this study is about the coating of HAP powder on the Mg substrate by a low temperature processing method. In this study, HAP powder was sprayed using simple modified spray at room temperature whereby the pressurized air was utilized. There was no heated gas required in this modified technique. Thickness, nanohardness and elastic modulus of HAP coated pure Mg was determined using this modified cold spraying technique. Four factors (standoff distance between the nozzle and substrate, substrate surface roughness, substrate heating temperature and number of sprays) were investigated to determine the significant factors including their interaction in influencing the thickness, nanohardness and elastic modulus of the coating. The experimental results were examined by the ANOVA.

Based on ANOVA, standoff distance, substrate surface roughness and substrate heating temperature were determined as significant factors for all the responses while number of sprays was determined as insignificant. The response contour plots were generated to visualize how a response varied with changes in the factors. Based on the response contour plots, it was revealed that high thickness ($>40\ \mu\text{m}$) was obtained when standoff distance is at 20-25 mm, surface roughness at 240-700 grit and substrate heating temperature at 350-550°C. High nanohardness ($>400\ \text{MPa}$) obtained when standoff distance is at 20-35 mm, surface roughness at 240-900 grit and substrate heating temperature at 350-550°C and high elastic modulus ($>40\ \text{GPa}$) was obtained at 20-30 mm for standoff distance, 240-800 grit for surface roughness and 350-550°C for substrate heating temperature.

The response contour plots of these responses were overlaid to find the feasible region. Then the optimal solution was determined by maximizing the composite desirability. All the responses were treated equally and the default value 1.0 was given for $d = 1$. The response optimizer in Minitab 16 suggested the potential combination of the input variable settings that jointly optimize three responses the thickness (Y1) as 46 μm , nanohardness (Y2) as 437 MPa and elastic modulus (Y3) as 44 GPa and provided the trade-off values of standoff distance as 22.7 mm, surface roughness as 649.2 grit, and substrate heating temperature as 495°C parameters that can relatively accommodate the optimum requirement of the cold spray process.

To further optimize the process, experiments were conducted as proposed by the steepest method. Based on steepest method, the optimum responses (thickness- 49.77 μm , nanohardness- 462.61 MPa and elastic modulus- 45.69 MPa) was observed at 30mm standoff distance, 926.4 grit of surface roughness and 456°C substrate heating temperature. This optimum sample was taken for biodegradable study in SBF solution and accelerated corrosion test.

The biodegradable study for uncoated and coated sample was performed for 0 min, 10 min, 30 min, 60 min (1hr), 120 min (2hr), 240 min (4hr) and 1440 min (24hr) at 37°C in SBF solution. The uncoated sample after 1140 min of immersion indicates the presence of O, Mg, Ca and P on the surface of the corroded Mg. The presence of O and Mg was consistent with a corrosion product of Mg(OH)_2 while the Ca and P are thought to be associated with the SBF. For coated sample, after 1440 min of immersion, the coating surface is completely covered by a dune-like layer along the whole surface of the coating. Microcracks of tortoise-shell character appeared on the newly formed layer, similar to the cracks formed naturally on a dry mud deposit. Therefore, the results suggested that the bone-like apatite layer formed on the surface of the coatings may promote the bone bonding with living tissues and increase the longevity of coatings during implanting in vivo.

Adhesion of the coating was measured after the immersion in SBF. There is only slight variation in bond strength after 60 min of immersion. The reduction of bond strength comes mostly from the continuation of chemical dissolution of coatings, which weakens the bonding of the lamella in the coating and the bonding of the interface between coating and substrate. Fast dissolution of the coating resulted in more bonding decay at the interface of coating and substrate. However, after 1140 min of immersion in SBF, the bond strength of the coating was 40 MPa which indicated that the sample still having the desired bond strength needed for bioimplant application (35 MPa).

The accelerated corrosion test in a 3.5wt% NaCl solution was performed for uncoated and coated Mg substrate with HAP to examine the corrosion behaviour for both samples at 1 day, 4 days, 10 days and 21 days. For uncoated sample, at the final stage of immersion, the film started to rupture and flake away. However, the coated sample showed that HAP coating remarkably prevented the substrate corrosion under a severe environment like NaCl solution. As the immersion time increased more Cl^- adsorbed on the film layer covering the surface to destroy the dynamic balance at this period. Based on the surface morphologies and chemical analysis of both sample, it is concluded that

the HAP coating remarkably protect and prevent the Mg substrate from the corrosion in the corrosive environment.

Suggestions

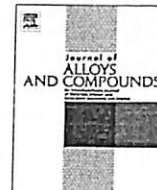
1. Other biomaterials such as zirconia can be used using the suggested optimization design. Moreover, mixing the zirconia and HAP powder may give better results in biodegradable performance.
2. The mechanical characterization could be extended to include nano tribology and scratch tests.
3. The in vitro test can be carried out with different kind of solutions. Further in vitro studied of the HAP-coated Mg with cell lines can confirm this potential application.

Acknowledgements

The authors would like to thank UniversitiSains Malaysia (RU Grant No. 811224) for financial support and scholarship scheme (MyBrain15) of the Ministry of Higher Education, Malaysia. The use of the nanoindentation technology in the School of Mechanical Engineering, UniversitiSains Malaysia, is gratefully acknowledged.

References

1. V. K. Champagne: 'The cold spray materials deposition process: fundamentals and applications', 25–27; 2007, New York, Woodhead Publishing.
2. G. E. J. Poinern, S. Brundavanam and D. Fawcett: 'Biomedical magnesium alloys: a review of material properties, surface modifications and potential as a biodegradable orthopaedic implant', *Journal of Biomedical Engineering*, 2012, 6, 218–240.
3. A. Choudhuri, P. S. Mohanty and J. Karthikeyan: 'Bio-ceramic composite coatings by cold spray technology', Proc. Int. Conf. on 'Thermal Spray', Las Vegas, NV, USA, 2009, 391–396.
4. R. S. Lima, A. Kucuk, C. C. Berndt, J. Karthikeyan, C. M. Kay and J. Lindemann: 'Deposition efficiency, mechanical properties and coating roughness in cold-sprayed titanium', *Journal of Materials Science*, 2002, 21, 1687–1689.
5. C. Li and W. Li: 'Deposition characteristics of titanium coating in cold spraying', *Surface Coating Technology*, 2003, 167, 278–283.
6. H. K. Kang and S. B. Kang: 'Tungsten/copper composite deposits produced by a cold spray', *Scripta Materialia*, 2013, 49, 1169–1174.
7. H. Lee, S. Jung, S. Lee, Y. You and Y. Ko: 'Correlation between Al₂O₃ particles and interface of Al–Al₂O₃ coatings by cold spray', *Applied Surface Science*, 2005, 252, 1891–189.
8. T. Van Steenkiste: 'Kinetic sprayed rare earth iron alloy composite coatings', *Journal of Thermal Spray Technology*, 2006, 15, 501–506.
9. X. Zheng, M. Huang and C. Ding: 'Bond strength of plasma sprayed hydroxyapatite/Ti composite coatings', *Biomaterials*, 2000, 21, 841–849.
10. P. King, S. Zahiri and M. Jahedi: 'Rare earth/metal composite formation by cold spray', *Journal of Thermal Spray Technology*, 2007, 17, 221–227.
11. C. W. Abdullah, H. Zuhailawati, V. Aishvarya and B. K. Dhindaw: 'Hydroxyapatite-coated magnesium-based biodegradable alloy: cold spray deposition and simulated body fluid studies', *Journal of Materials Engineering and Performance*, 2013, 10, 2997–3004.
12. C. D. Montgomery: 'Design and analysis of experiments', 7th edn; 2009, Asia, John Wiley & Son.
13. J. F. Li, H. L. Liao, C. X. Ding and C. Coddet: 'Optimizing the plasma spray process parameters of yttria stabilized zirconia coatings using a uniform design of experiments', *Journal of Materials Processing Technology*, 2005, 160, 34–42.
- 14 L.F. Alvarez, Approximation model building for design optimization using the response surface methodology and genetic programming, PHD Dissertation (2000), University of Bradford.
- 15 R. Muthuvelayudham, T. Viruthagiri, Application of central composite design based response surface methodology in parameter optimization and on cellulose production using agricultural waste, World Academy of Science, Engineering and Technology. (2010) 890-897.



A statistical prediction of density and hardness of biodegradable mechanically alloyed Mg–Zn alloy using fractional factorial design



Emee Marina Salleh^a, Hussain Zuhailawati^{a,*}, Sivakumar Ramakrishnan^a,
Mohamed Abdel-Hady Gepreel^b

^a Biomaterials Niche Area, School of Materials and Mineral Resources Engineering, Engineering Campus, Universiti Sains Malaysia, 14300 Nibong Tebal, Penang, Malaysia

^b Department of Materials Science and Engineering, Egypt-Japan University of Science and Technology (E-JUST), P.O. Box 179, New Borg El-Arab City, 21934 Alexandria, Egypt

ARTICLE INFO

Article history:

Received 9 November 2014

Received in revised form 27 March 2015

Accepted 15 April 2015

Available online 1 May 2015

Keywords:

Mg–Zn alloys

Mechanical alloying

Hardness

Density

Fractional factorial design

ABSTRACT

This work aims to develop a statistical model that could be used to predict density and hardness properties of biodegradable mechanically alloyed magnesium–zinc alloy since both properties relies on densification of the powder during compaction and sintering. The effect of mechanical alloying parameters (i.e., milling time, milling speed, ball-to-powder weight ratio and percentage of zinc) and their interactions were investigated involving 4 numerical factors with 2 replicates, thus 16-run of two-level fractional factorial design. Results of analysis of variance (ANOVA), regression analysis and *R*-squared test indicated the good accuracy of the model. Density of sintered Mg–Zn alloy was between 1.80 and 1.99 g/cm³ which closed to density of human bone. Hardness of pure Mg increased from 27 HV to 54 HV to 94 HV with the addition of 3–10 wt% Zn.

© 2015 Elsevier B.V. All rights reserved.

1. Introduction

Nowadays, there is a growing interest in using biodegradable alloys in a number of critical medical applications. Mg alloys have a potential as biodegradable metallic implants since they can be gradually dissolved, absorbed, consumed or excreted in human body and then disappear after bone tissues heal that could avoid secondary operation for implant removal [1,2]. However, Mg implants demonstrate higher biological activity which could cause high degradation rate in human bio-environment [3,4]. Thus, alloying with other metal elements is the most effective tool to improve mechanical properties and corrosion resistance of Mg. There are only small numbers of elements that can be tolerated in human body and can also retard biodegradation of Mg alloys including calcium (Ca), zinc (Zn), manganese (Mn) and perhaps very small amount of low toxicity rare earth (RE) elements such as tantalum (Ta) and niobium (Nb) [5,6]. Gu et al. [7] has reported that addition of Zn mechanically improves the yield strength and ultimate tensile strength of Mg with improved corrosion resistance as Zn provides the lowest hydrogen evolution rate in comparison to Al, Ag, Si, Sn, Y and Zr alloying elements. Thus, addition of certain amount of Zn into pure Mg matrix beneficially improves its mechanical

properties, corrosion resistance without giving harsh effect to human body.

In this current work, binary Mg–Zn alloy was produced using mechanical alloying (MA) followed consolidation process by compaction and sintering. MA is a unique processing method that entirely involves a solid state process enables to produce alloy powders with a controlled fine microstructure which occurs by repeated fracturing and rewelding of the mixture of powder particles in a highly energetic ball mill [8,9]. By this technique, a number of defects that commonly generated from casting such as porosity and inclusions can be minimized. However, fabrication of mechanically alloyed Mg–Zn alloy needs detailed investigation as its properties definitely relies on densification of the alloy powder which later influences the properties of the alloy including density and hardness.

Frequently conventional research methodology via trial and error method is adopted to identify the significant or important which definitely involves high cost and time consuming since lots of experimental work need to be carried out. In order to reduce the number of experiment, design of experiment (DOE) method can be adopted [10]. In this work fractional factorial design (FFD) was used because this type of design is suitable for products and process design, process improvement and industrial/business experimentation. In addition, when certain high-order interactions are probably negligible, information on the main effects and low-order interactions may be obtained by running only a fraction

* Corresponding author. Tel.: +60 4 5995258; fax: +60 4 5941011.

E-mail address: zuhaila@usm.my (H. Zuhailawati).

of complete factorial design [11]. Hence, this paper report an attempt made to examine the interdependence of mechanically alloying process parameters and mathematical model to predict density and microhardness of Mg–Zn alloy using fractional factorial design, analysis of variance and regression analysis.

2. Experimental work

2.1. Materials preparation and characterization

A mixture of elemental magnesium powder (99.00% pure) and zinc powder (99.70% pure) was mechanically milled at room temperature using a high-energy Fritsch Pulverisette P-5 planetary mill under argon atmosphere. SEM micrographs of the starting Mg and Zn powders are shown in Fig. 1. Mg powders are irregular-shaped and Zn powders are mostly ellipsoidal, elongated particles. The average particle size of elemental Mg powder and Zn powder are 227.41 μm and 121.65 μm respectively as shown in Table 1. 20 mm-diameter stainless steel balls were used during mechanical milling. 3% n-heptane was added to the powder mixture prior to the milling process to prevent excessive cold welding of the elemental alloy powders. Then, the milled powders were uniaxially cold pressed under 400 MPa for 2 min at room temperature to produce 10-mm diameter of green Mg–Zn alloy pellets and sintered at 350 °C under argon flow at 5 °C/min for both heating and cooling rate for an hour in order to form solid bodies. Qualitative X-ray diffraction (XRD) analysis with angular scanning range $2\theta \leq 90^\circ$ was conducted to identify the presence of element and phases. The data attained using D8 Advance, Bruker AXS. Phase identification of stripping its $K_{\alpha 2}$ component is represented in form of diffractogram of intensity versus 2θ . APW software was used to analyze the present phase in all samples. Internal strain was determined by the Williamson–Hall method as shown in the following equation:

$$B_r \cos \theta = \frac{0.89\lambda}{(D)} + 2\eta \sin \theta \quad (1)$$

where B_r is line broadening, θ is Bragg's angle, λ is wavelength, D is crystallite size and η is internal strain. The instrumental broadening B_i was removed using Gaussian profile

$$B_r^2 = B^2 - B_i^2 \quad (2)$$

where B is the full width at half maximum.

Microstructure of the sintered Mg–Zn alloys was studied using optical microscope (OM). Density of the sintered alloys was measured by pycnometer density equipment according to Archimedes' principle. The samples were immersed in tap water which was placed on Sartorius electronic analytical balance with four decimals accuracy. Seven readings were taken from the sample. Relative density (TD%) was calculated according to:

$$\text{TD}\% = (\text{Actual Density}/\text{Density}_{\text{ROM}}) \times 100\% \quad (3)$$

$$\text{Density}_{\text{ROM}} = \rho_{\text{Mg}} V_{\text{Mg}} + \rho_{\text{Zn}} V_{\text{Zn}} \quad (4)$$

$$V_{\text{Mg}} + V_{\text{Zn}} = 1 \quad (5)$$

where ρ_{Mg} and ρ_{Zn} represent the density of Mg and Zn, respectively, whereas V_{Mg} and V_{Zn} represent the volume fraction of Mg and Zn, respectively, incorporated in the alloy material. The relative density is useful for comparing the measured sintered densities to the predicted rule-of-mixture densities. Microhardness test using Shimadzu tester was carried out by placing samples with the 100 mm² surface area under a diamond indenter. The test was performed under 500 gf of indentation load with 10 s of dwell time. Ten readings were taken from the same sample.

Table 1
Particle size distribution of magnesium and zinc powders.

Element	X10 (μm)	X50 (μm)	X90 (μm)
Magnesium	61.33	102.63	227.41
Zinc	27.60	65.81	121.65

2.2. Statistical design

Statistical design of experiments has been increasingly employed by engineers and researchers for screening out main effects and optimization matters. The ease of obtaining data over a wide range experimental region with a fair degree of accuracy makes it very attractive. This approach helps to understand better how the change in the levels of application of a group of parameters affects the response. A combination of the levels of the parameter, which leads to certain optimum response, can also be located through this approach [12]. The factorial design can cover the main and interaction effects of the parameters within the whole range of selected parameters. From the literature [8,13,14], several mechanical alloying factors that have a significant influence on the properties of mechanically alloyed soft metal powder were identified and they are milling time, milling speed, ball-to-powder weight ratio (BPR), the size of grinding media, grinding media materials, geometry of mill and milling temperature. However, in order to reduce the complexity of the milling parameters, this study focused only on the effect of milling time, milling speed (energy), BPR and effect of Zn addition on the Mg properties as well. Factors and levels evaluated in the experiments to be conducted are as listed in Table 2. The upper limits of milling time, milling speed, BPR and percentage of Zn were set at 10 h, 300 rpm, 15:1 and 10 wt% respectively according the previous preliminary study where the results were not reported in this work. The upper limits were set to avoid excessive cold welding of powder during milling that could hinder powder densification.

In this study, the experimental procedure was performed according to 2^{k-1} fractional factorial design, which is a series of experiments involving k factors, each of which has two levels ('low' – and 'high' +). It is our interest to highlight the usefulness of this new fractional factorial design method. Since our work involves 4 factors, fractional factorial of 2-level design was applied to minimize the number of experimental run without sacrificing its accuracy. So that the prediction of binary Mg–Zn alloy's properties would be economically obtained at a short period of time. Table 3 shows the complete experimental design and actual responses of the experiment used in this study. The actual responses, density and hardness were denoted by Y1 and Y2 respectively. Since the design was constructed involving 4 numerical factors with 2 replicates, thus 16-run of two-level fractional factorial design was performed.

These data were used as input into the DOE for analysis to determine the model equation. The Minitab 16 (Minitab Inc, USA) statistical software was used to perform statistical analysis and to develop empirical model. The adequacy of the models was further justified through analysis of variance (ANOVA), regression analysis and R-sq test. According to the design, generator of D is equal to ABC. The alias structures for this 2^{4-1} fractional factorial design are shown in Table 4.

3. Results and discussion

3.1. Phase and microstructure analysis

Fig. 2 illustrates XRD patterns for a set of replication which was chosen randomly. XRD pattern of all mechanically alloyed samples produced according to the created design showed the presence of phase α -Mg. Since samples 1, 4, 6 and 7 were alloyed with only 3 wt% of Zn, all the added alloying element (Zn) were solid-solved into the host Mg forming an α -Mg solid solution.

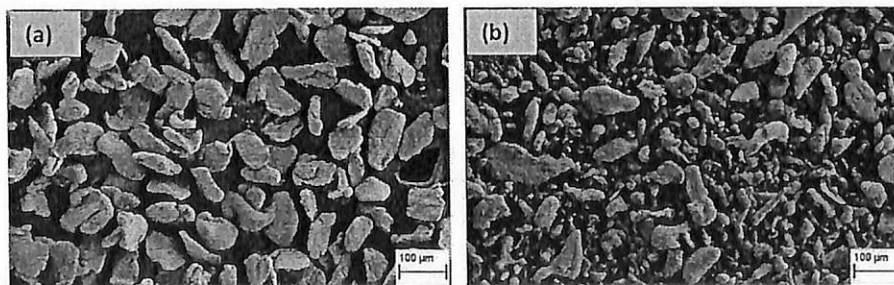


Fig. 1. SEM micrographs of elemental (a) magnesium and (b) zinc powders.

Table 2
Factors and levels evaluated in the experiments.

Factor	Code	Unit	Level	
			-1	+1
Milling time	A	H	2	10
Milling speed	B	Rpm	100	300
Ball-to-powder weight ratio	C	-	5	15
Percentage of Zn	D	wt%	3	10

According to binary diagram of Mg–Zn, the single phase in this binary alloy was solid-solution α -Mg. In this alloy system, solubility limit of Zn in Mg phase is 6.2 wt% at 340 °C but the solubility is very small at room temperature. Since only single α -Mg phase existed in the Mg–Zn alloy matrix, the result clearly suggested that Mg and Zn form a homogeneous solid solution without any diffusive or combustion reaction occurring between pure metals forming intermetallic compound or intermediate phase alloy (secondary solid solution). However, the α -Mg and MgZn phase peaks can be clearly identified in the sample 2, 3, 5 and 8. These four samples were alloyed with 10 wt% of Zn. Since the added Zn into Mg matrix was high, thus provided the high chances for the formation of secondary phase of MgZn.

From the diffractogram in Fig. 2, it can be seen that most of the peaks of sintered alloys were shifted to the left-hand side (lower angle) associated with the α -Mg solid solution formation. During the formation of solid solution, smaller radius of Zn (134 pm) atoms took place as impurities in the larger Mg (160 pm) atom lattice. The replacement of Zn in the host sites caused a reduction of the Mg lattice. In addition, the shifted angles were also caused by a reduction of crystallite size and/or the accumulation of lattice strain during mechanical alloying as shown in Table 5. This indicated that the formation of fine crystallite was typically affected by increasing the number of collisions per unit time during milling process [15,16].

Fig. 3 shows the optical microstructure of mechanically milled Mg–Zn alloy which were subsequently compacted under 400 MPa and sintered at 350 °C in argon atmosphere. From the illustrations, it can be seen that the distribution of fine pores that presented as black spots in the sintered alloy was uniformly distributed. The refinement of pore size and its homogeneous distribution are good as it could increase the contact area between grains leading to enhance densification effect, sinterability and its properties afterward [17]. According to Table 3, experimental result shows a relatively high density of all samples. Final density

Table 3
The 2^{4-1} experimental design and actual responses of binary Mg–Zn alloy.

Run (#)	Basic design				Density (g/cm^3) Y1	Microhardness (HV) Y2
	A	B	C	D = ABC		
1	-	-	-	-	1.8024	53.76
2	+	-	-	+	1.8870	77.85
3	-	+	-	+	1.9938	94.37
4	+	+	-	-	1.8526	89.10
5	-	-	+	+	1.9174	74.13
6	+	-	+	-	1.8074	63.28
7	-	+	+	-	1.8106	67.02
8	+	+	+	+	1.8617	65.82
9	-	-	-	-	1.8016	54.95
10	+	-	-	+	1.8900	77.74
11	-	+	-	+	1.9904	93.55
12	+	+	-	-	1.8503	90.74
13	-	-	+	+	1.919	73.67
14	+	-	+	-	1.8067	62.08
15	-	+	+	-	1.8118	67.74
16	+	+	+	+	1.8603	64.45

was predicted by simple rule of mixture (ROM) model which to be in range of 1.70–7.10 g/cm^3 since original density of Mg and Zn are 1.738 g/cm^3 and 7.140 g/cm^3 respectively. The measured data showed density values were in the range of 1.800–1.990 g/cm^3 . Results indicated that the density was not only dependent on composition and starting raw materials but it was also affected by the processing parameters studied in the present work. Density values of Mg–Zn alloy obtained in this was considerably accepted to be used as implant materials since the density of natural bone is between 1.70 and 2.10 g/cm^3 [18].

Measurement of internal strain as a function of milling time and percentage of Zn is shown in Table 5. Higher milling time reduced the crystallite size since repeated deformation occurred at a higher rate. As more energy was supplied to the powders, each crystallite remains constrained by its surrounding crystallites and produced stress/strain in the alloy. Continuous deformation of the powder throughout milling refined crystallite size, leading to continuous accumulation of internal defects. The accumulation of the internal defects resulted in increasing in hardness with a slight reduction of density.

Interestingly, alloying Mg with Zn significantly increased the hardness of pure Mg (pure Mg powder produced according to high level parameters and subsequently was consolidated with the same parameter of producing Mg–Zn alloy) from 27 HV up to 94 HV. The improvement of Mg hardness is indirectly beneficial in altering other mechanical properties including elastic modulus, compressive strength, wear resistance and fatigue resistance [19]. According to the method developed by Oliver and Pharr [20], elastic modulus might be directly determined by hardness in accordance to nanoindentation load-displacement data. From the developed equation, elastic modulus is proportionally related to the obtained nanohardness [21]. Accordingly, the concept of the derivative theory can be applied in this study to assume the estimated elastic modulus of the alloy by saying that increasing in hardness might increase its elastic modulus. The enhancement of those properties must be necessarily sufficiently acceptable for producing bio-implant in order to avoid stress shielding problem due to mismatching of certain mechanical behaviors during implantation duration.

3.2. Experimental design and data analysis

After data collection of the responses was completed, the results were analyzed for its adequacy using the analysis of variance (ANOVA) technique. The ANOVA for density (Y1) and hardness (Y2) are summarized in Tables 6 and 7. Statistical effect of variables was calculated within 95% confidence interval. The "Model F-value" of 554.59 for Y1 and 660.74 for Y2 implies that the models were significant relative to noise. For both properties, only 0.001% chance that the "Model F-value" this large could occur due to noise for each case. In general, the smaller *p*-value, the more significant the terms observed. In both cases of density and hardness, all of study factors of A, B, C, D and interactions of AB, AC and AD were significant as the *p*-values were less than 0.05.

Table 4
Aliases for 2^{4-1} fractional factorial design.

Alias structure		
[A]	→	A + BCD
[B]	→	B + ACD
[C]	→	C + ABD
[D]	→	D + ABC
[AB]	→	AB + CD
[AC]	→	AC + BD
[AD]	→	AD + BC

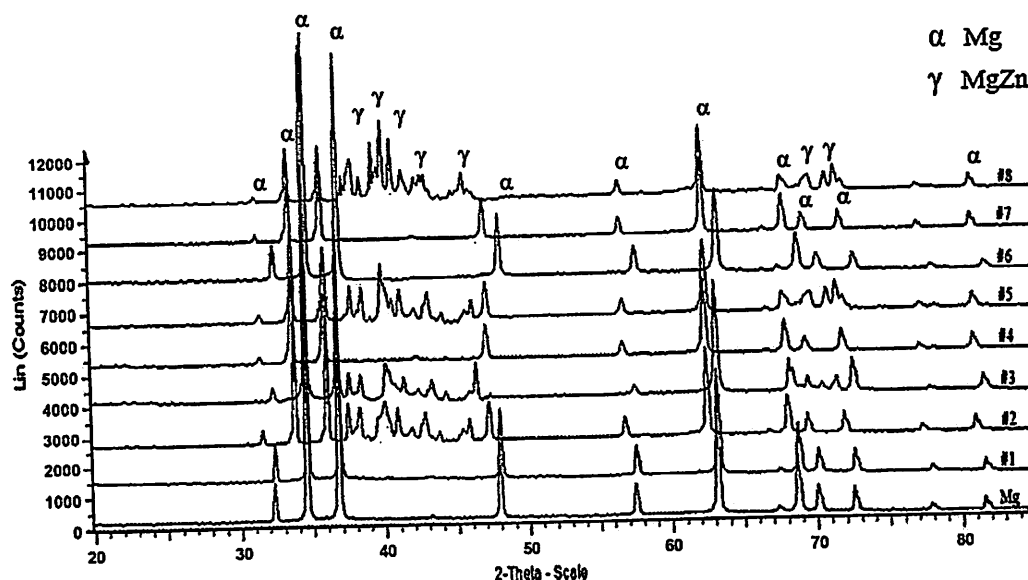


Fig. 2. XRD patterns of pure Mg and Mg–Zn alloys of single replication.

Table 5
Internal strain of Mg–Zn alloy at different milling time and percentage of Zn.

Run	Milling time (h)	Percentage of Zn (wt%)	Internal strain (%)
1	2	3	0.03
3	2	10	0.21
5	2	10	0.13
7	2	3	0.06
2	10	10	0.15
4	10	3	0.17
6	10	3	0.07
8	10	10	0.09

A regression analysis was carried out to obtain the best-fit model to the experimental data. The regression analysis for each response was done using coded units and summarized into Tables 8 and 9. In addition, coefficient of correlation (R -sq) test is one of the most conveniently accepted methods which allow a researcher to examine the fitted model to ensure that it provides an adequate approximation to the true system and verify that none of the least squares regression assumptions are violated [22]. R -sq value gives a correlation between the experimental response and the predicted response and should be high for a particular model to be significant. R -sq for both density and hardness were 99.96% and 99.83%, respectively and the standard deviation for Y1 was 4.69×10^{-3} and Y2 was 0.743 which were very small in quantities. This implies that all responses were fairly closer to the predicted values and thus the regression equation generated in this experimental study could be used in the prediction of properties of binary Mg–Zn alloy with a fair degree of accuracy. Furthermore, the obtained data showed the predicted R -sq values were in good agreement with the adjusted R -sq values for each case. The regression analysis suggested that the relationship between both responses of binary Mg–Zn alloy and the four factors was best fitted with a quadratic model. For each case, the coded models are listed as follow:

$$Y1 = 1.877 - 0.012A + 0.024B + 0.017C + 0.045D - 0.005AB - 0.005AC + 0.009AD$$

$$Y2 = 73.141 + 0.742A + 5.958B - 5.867C + 4.557D - 2.313AB - 4.108AC - 6.974AD$$

3.3. Effect of milling time, milling speed, BPR and percentage of Zn on responses

There are many factors that affect the milling process and also the product developed using mechanical alloying, which are important to be considered in fabrication of homogenous materials including alloys [13]. The parameters must be seriously controlled to ensure the mechanically alloyed product with better desired properties could be obtained. The main effect plots of the studied variables are presented in Figs. 4 and 5 corresponds to density and hardness, respectively.

Milling time is one of important parameters in milling process. Milling time depends on types of mill used, intensity of milling, ball-to-powder weight ratio, and temperature of milling. The time should be chosen to achieve a steady state between fracturing and cold welding of powder particles to facilitate alloying. Theoretically, higher milling time is preferred since it could increase homogeneity of powders and refine structure up to nanostructured scale. However, higher milling time causes the presence of contamination in milled powders especially for reactive metal like titanium [23]. This consideration is also applicable for Mg–Zn alloy as Mg is one of reactive metal element.

As reported by Datta et al. [24], a homogenous alloy mixture of Mg, Zn and Ca was formed up to 1 h of milling without any diffusive or combustion reaction occurring between pure metals which may cause increasing in density. In addition, prolonged milling time up to 8 h resulted in formation of amorphous phase. However, in this study although the milling time was considerably a bit longer (maximum 10 h), there was no formation of amorphous phase in Mg–Zn alloy which indicated no diffusive mixing mechanism was initiated in this binary alloy system within the milling time. Therefore, the results suggest that the milling time used in this work is suitable in order to obtain required density and hardness without formation of any amorphous phase or existence of contaminant.

Main effect plots shows that increasing milling time reduced density (Fig. 4) and increased hardness (Fig. 5). It was found that milling time gave a contradict effect on both density and hardness. Increasing in milling time reduced the density of sintered alloys. This result is probably related to mechanism of work hardening or strain hardening occurred in the powder particles during mechanical alloying of Mg–Zn powder. Hardened Mg–Zn mixture

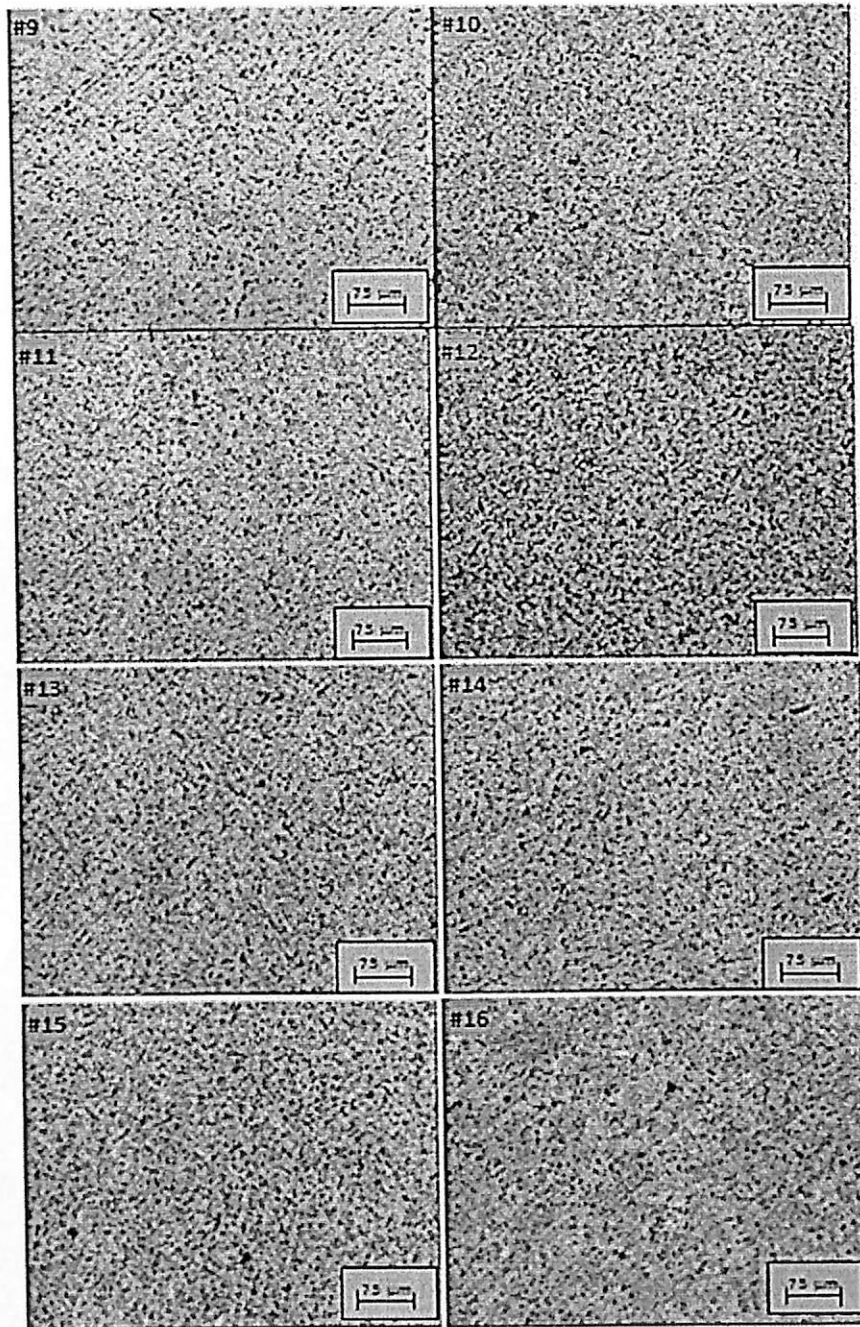


Fig. 3. Microstructure of Mg-Zn alloys of single replication.

Table 6
ANOVA for quadratic model of density (Y1).

Source	Sum of squares	DF	Mean square	F-value	p-value
Model	0.0488138	4	0.0122034	554.59	0.000
A	0.0023064	1	0.0023064	104.82	0.000
B	0.0089161	1	0.0089161	405.20	0.000
C	0.0048755	1	0.0048755	221.57	0.000
D	0.0327158	1	0.0327158	1486.78	0.000
AB	0.0004421	1	0.0004421	20.09	0.002
AC	0.0003658	1	0.0003658	16.62	0.004
AD	0.0012763	1	0.0012763	58.00	0.000
Residual error	0.0001760	8	0.0000220		
Pure error	0.0001760	8	0.0000220		
Total	0.0510739	15			

Table 7
ANOVA for quadratic model of microhardness (Y2).

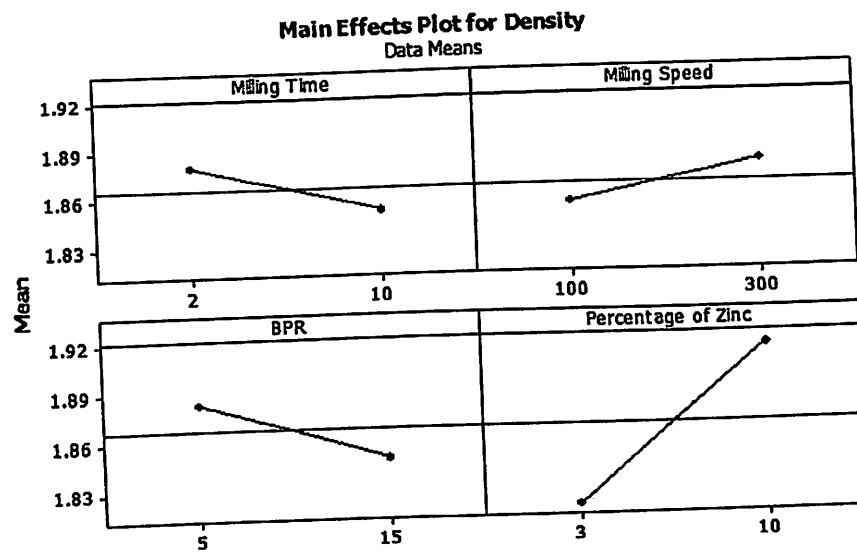
Source	Sum of squares	DF	Mean square	F-value	p-value
Model	1459.76	4	364.940	660.74	0.000
A	8.81	1	8.806	15.94	0.004
B	567.99	1	567.988	1028.37	0.000
C	550.72	1	550.724	997.11	0.000
D	332.24	1	332.242	601.54	0.000
AB	85.61	1	85.609	155.00	0.000
AC	270.03	1	270.027	488.90	0.000
AD	778.27	1	778.271	1409.10	0.000
Residual error	4.42	8	0.552		
Pure error	4.42	8	0.552		
Total	2598.08	15			

Table 8
Effects and regression coefficient for density (Y1).

Term	Effect	Coef	SE Coef	T	P
Constant		1.87738	0.001173	1600.88	0.000
A	-0.02401	-0.01201	0.001173	-10.24	0.000
B	0.04721	0.02361	0.001173	20.13	0.000
C	0.03491	0.01746	0.001173	14.89	0.000
D	0.09044	0.04522	0.001173	38.56	0.000
AB	-0.01051	-0.00526	0.001173	-4.48	0.002
AC	-0.0056	-0.00478	0.001173	-4.08	0.004
AD	0.01786	0.00893	0.001173	7.62	0.000
S = 0.00469088	Press = 0.00070414	R-Sq(pred) = 98.62%			
R-Sq = 99.66%	R-Sq(adj) = 99.35%				

Table 9
Effects and regression coefficient for microhardness (Y2).

Term	Effect	Coef	SE Coef	T	P
Constant		73.141	0.1858	393.66	0.000
A	1.484	0.742	0.1858	3.99	0.004
B	11.916	5.958	0.1858	32.07	0.000
C	-11.734	-5.867	0.1858	-31.58	0.000
D	9.114	4.557	0.1858	24.53	0.000
AB	-4.626	-2.313	0.1858	-12.45	0.000
AC	-8.216	-4.108	0.1858	-22.11	0.000
AD	-13.949	-6.974	0.1858	-37.54	0.000
S = 0.743182	Press = 17.6742	R-Sq(pred) = 99.32%			
R-Sq = 99.83%	R-Sq(adj) = 99.68%				

**Fig. 4.** Main effect of studied factor on density (Y1).

powder has poor compressibility, which make it more difficult to be deformed during compaction [25]. In common, hardness is proportionally related to density. However, in this finding with a prolonged milling time, hardness increased although density was decreased. The increasing in hardness was slightly resulted from the strain-hardened alloy particles as a function of milling time [15].

Based on a study by Shehata et al. [26], faster milling speed transfers higher kinetic energy into powders and higher kinetic energy leads to the presence of refined microstructure and also decreases the diffusion distance. At higher milling speed, milling process promotes homogenization and alloying occurred. As shown in Figs. 4 and 5, increasing in milling speed increased both density and hardness. The result is caused by refinement of alloy particles which then increased the compressibility of powder particles. As the compressibility was improved, load bearing area

between the particles increased thus reduced the porosity. Reduction of porosity is good for density and hardness improvement [17]. In addition, cold-worked particles provided high hardness of Mg–Zn alloy and the combination effect of high density improved hardness further. In this study, complete alloying occurred though at milling speed as low as 100 rpm. It can be said that, 100 rpm was sufficient to provide energy in refining the milled grains and initiating the formation of α -Mg solid solution during mechanical alloying and subsequent consolidation.

The ratio of the weight of the ball to the powder (BPR) is an important variable in the milling process. The ratio is depending on material used and certain properties and application needed to investigate. Lower ratio as 1:1 and up to higher ratio 1000:1 have been used by researchers [23] to investigate a variety of materials. Increasing in the BPR values can be obtained either by increasing the weight of ball or decreasing the powders weight.

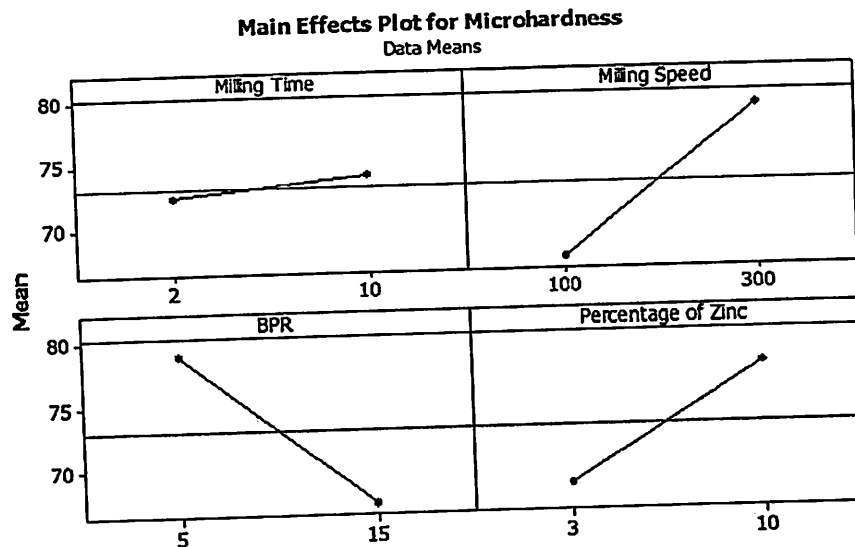


Fig. 5. Main effect of studied factor on microhardness (Y2).

In the present work, density and hardness were reduced with the increasing in BPR. This is because for soft and ductile Mg, excessive heat generated during mechanical alloying process with high BPR caused the occurrence of cold welding which then led to the formation of flaky powder mixture [23]. Once the flaky powder formed, the densification of powder and bonding between particles were deteriorated which then resulted in high formation of porosity. High porosity due to the flaky powder consequently caused a reduction in both density and hardness.

Both Figs. 4 and 5 display that increasing the amount of Zn increased both density and hardness. Zn was added into pure Mg in order to improve its hardness by forming Mg–Zn alloy. Higher Zn content means there are more solute Zn atoms that could restrict dislocation motion in the Mg lattice structure leading to an improvement in hardness. From XRD analysis there were alloys with single α -Mg solid solution while alloys with 10 wt% Zn consisted of a mixture of α -Mg and MgZn. Adding 10 wt% Zn was exceeded its solubility limit in Mg matrix (6.2 wt%), thus secondary phase (MgZn) started to form. In most cases, the presence of secondary phase needs to be avoided due to its hard and brittle properties. By referring to Table 10 that shows the effect of amount of Zn to the relative density (TD%) of the alloys, we discover that the existence of this phase deteriorates the theoretical density of the alloys, which is not beneficial for mechanical properties. Maximum relative density of Mg–10 wt% Zn (87.45 TD%) was lower than the minimum relative density of Mg–3 wt% Zn (94.76 TD%). The low relative density suggests the high porosity in the 10%Zn alloy was due to the association of MgZn phase in the Mg metallic which was supported by XRD analysis. The compressibility of soft Mg matrix during consolidation was inhibited by secondary

metallic phase MgZn which explains the low relative density with high content of Zn.

3.4. Analysis of responses: density and microhardness

The effects of studied principal factors and interaction between parameters on the density and hardness of binary Mg–Zn alloy are presented comparatively in Figs. 6 and 7, respectively. According to the sparsity-of effects principle in factorial design, it was most likely that main (single factor) effects and two-factor interactions were the most significant effects, and the higher order interactions were negligible. In other words, higher order interactions such as four-factor interactions were very rare and the contribution to the overall results insignificant the residual which were dispersed randomly. As shown in Figs. 6 and 7, they were positive and negative gradients in the interactions among the factors and that could balance out each other. This caused the residuals were dispersed randomly which lead the overall higher order interactions into insignificant or very lower contribution. For density, interaction effects between milling speed–percentage of Zn and BPR–percentage of Zn were very low and neglected as the lines lied in nearly parallel direction toward each other. Analysis of the effect of principal factors showed that in the considered range parameters, percentage of Zn was the most significant variable in achieving maximum density. According to the positive effect of this parameter, increasing in Zn amount enhanced Mg–Zn alloy density since Zn element has higher density compared to Mg.

In the case of microhardness, interaction effects between milling speed–percentage of Zn and BPR–percentage of Zn were very low and neglected. In the considered range parameter, principal factor of milling speed was the most significant variable in attaining maximum hardness. High speed rotation of the vial and revolution of the disk caused the milling balls move strongly and violently, leading to fine grinding of alloy powder due to generation of high ball impact energy onto the powder. The impact energy of balls during milling is dependent on operating parameters, especially, rotational speed and its direction of the vial to that of the revolution of the disc. High impact refines powder particles that caused increasing in densification and cold working of the alloy powder which then increased the hardness.

Higher densification of Mg–Zn powder provided a stronger bonding between powder particles which consequently resulted in improvement of alloy hardness. In addition to the effect of

Table 10
Relative density of a single replicate.

Run	Percentage of Zn (wt%)	Relative density (%TD)
1	5	94.76
4	3	97.40
6	3	95.03
7	3	95.19
2	10	82.76
3	10	87.45
5	10	84.10
8	10	81.65

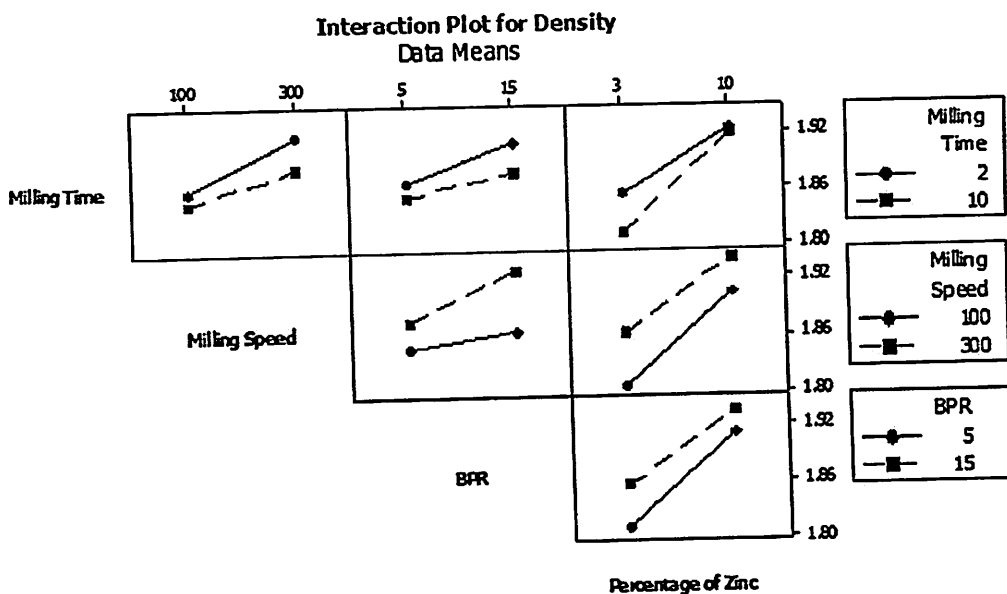


Fig. 6. Interaction effects for density (Y1).

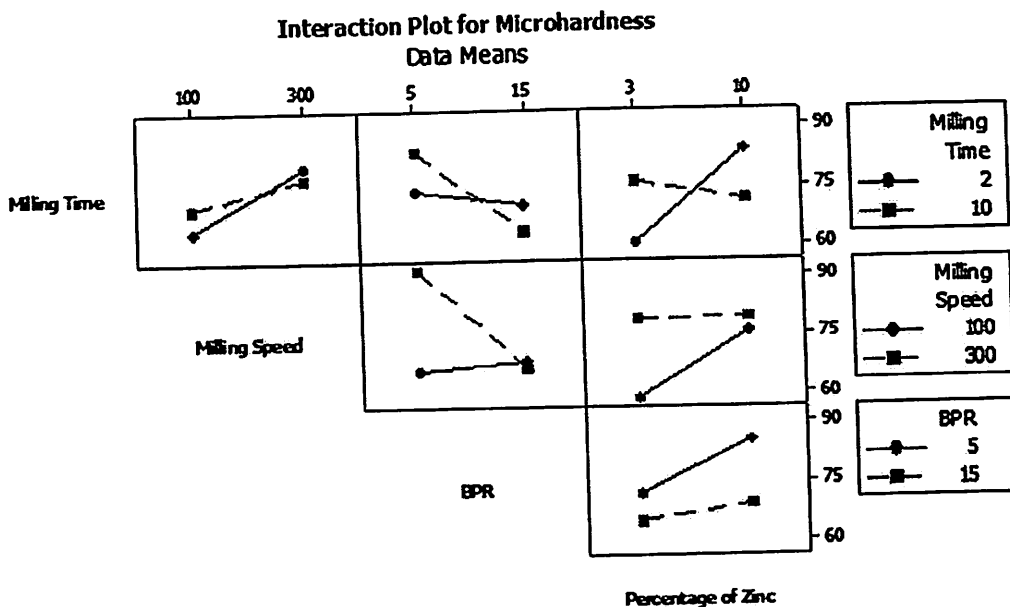


Fig. 7. Interaction effects for microhardness (Y2).

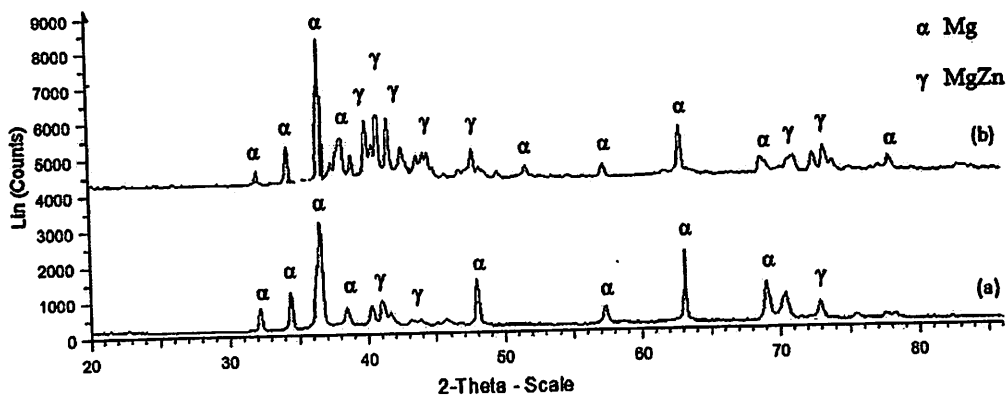


Fig. 8. XRD patterns of (a) as-milled Mg-Zn powder and (b) sintered Mg-Zn alloy for sample #8.

densification, the existence MgZn phase (Fig. 1) has a significant effect to the increment of microhardness as well. As shown in Fig. 8, the peaks of MgZn compounds started to form during milling, consequently affected the compressibility of alloy powder. The intensity of peaks of the sintered alloy increased which then influenced its final properties. In most cases, secondary phase that existed in the metallic matrix provided strengthening effect due to its inherent hard and brittle properties of intermetallic compound [27]. However, as reported by Zhang et al. [28], formation of secondary phase in the Mg matrix commonly deteriorated machinability of Mg alloys due to reduction of its elongation. In this study, compressibility of alloy powders was reduced with the presence of MgZn compound. Thus, the addition of Zn in the present work must be strictly controlled in order to improve its hardness without sacrificing its ductility too much.

4. Conclusion

A reliable statistical model based on fractional factorial experiment design has been developed which can be used for the optimization of binary Mg–Zn alloy synthesized by mechanical alloying. In the present work, Mg–Zn binary alloy was obtained between 1.80 g/cm³ and 1.99 g/cm³ which close to density of natural bone (i.e., 1.70–2.10 g/cm³). Microhardness of pure Mg (27 HV) was increased with addition of 3–10 wt% Zn which was between 54 HV and 94 HV. Experimental design using 2^{4–1} fractional factorial design enabled to establish the polynomial functions that described the effects of processing condition on the density and hardness of Mg–Zn alloy that was prepared by mechanical alloying and followed by sintering. The statistical analysis demonstrated main factor of milling time (A), milling speed (B), ball to powder weight ratio (C) and percentage of Zn (D) and interactions of AB, AC and AD are significant for both responses density (Y1) and hardness (Y2) as the p-value is less than 0.05. The higher order interactions such four-factor interactions were very rare and considerably negligible. The role of each milling parameters and their interactions on varying density and hardness of the alloy was described comprehensively.

Acknowledgements

The authors would like to thank to Universiti Sains Malaysia RU-PRGS Grant No. 8046026, Universiti Sains Malaysia RU Grant No. 811224 and scholarship scheme of Ministry of High Education (Malaysia).

References

- [1] F. Witte, V. Kaese, H. Haferkamp, E. Switzer, A.M. Lindenberg, C.J. Wirth, H. Windhagen, In vivo corrosion of four magnesium alloys and the associated bone response, *Biomaterials* 26 (2005) 3557–3563.
- [2] W. Li, S. Guan, J. Chen, J. Hu, S. Chen, L. Wang, S. Zhu, Preparation and in vitro degradation of the composite coating with high adhesion strength on biodegradable Mg–Zn–Ca alloy, *Mater. Charact.* 62 (12) (2011) 1158–1165.
- [3] H. Bahman, A. Abdollah, Microstructure, mechanical properties, corrosion behavior and cytotoxicity of Mg–Zn–Al–Ca alloys as biodegradable materials, *J. Alloys Comp.* 607 (2014) 1–10.
- [4] H.R. Bakhsheshi-Rad, M.H. Idris, M.R. Abdul-Kadir, A. Ourdjini, M. Medraj, M. Daroonparvar, E. Hamzah, Mechanical and bio-corrosion properties of quaternary Mg–Ca–Mn–Zn alloys compared with binary Mg–Ca alloys, *Mater. Des.* 53 (2014) 283–292.
- [5] G.L. Song, Control of biodegradation of biocompatible magnesium alloys, *Corros. Sci.* 49 (4) (2007) 1696–1701.
- [6] M.P. Laura, L. Rink, H. Haase, The essential toxin: impact of zinc on human health, *Int. J. Environ. Res. Public Health* 7 (4) (2010) 1342–1365.
- [7] X. Gu, Y. Zheng, Y. Cheng, S. Zhong, T. Xi, In vitro corrosion and biocompatibility of binary magnesium alloys, *Biomaterials* 30 (4) (2009) 484–498.
- [8] J.S. Benjamin, T.E. Volin, The mechanism of mechanical alloying, *J. Metall. Trans.* 5 (1974) 1929–1934.
- [9] F. Karimzadeh, M.H. Enayati, M. Tavoosi, Synthesis and characterization of Zn/Al₂O₃ nanocomposite by mechanical alloying, *Mater. Sci. Eng., A* 486 (1–2) (2008) 45–48.
- [10] N. Plesu, I. Grozav, S. Ilescu, G. Iliu, Acrylic blends based on polyaniline: factorial design, *Synth. Met.* 159 (5–6) (2009) 501–507.
- [11] D.C. Montgomery, *Design and Analysis of Experiments*, eight ed., John Wiley and Sons, USA, 2013.
- [12] V. Satheshkumar, P.R. Lakshminarayanan, Developing mathematical models on tensile strength and acoustic emission count of ZE41A cast magnesium alloy, *J. Alloys Comp.* 537 (2012) 35–42.
- [13] M.S.E. Eskandarany, *Mechanical Alloying for Fabrication of Advanced Engineering Materials*, William Andrew Publishing, USA, 2001, 14–17, 62–67.
- [14] F. Neves, F.M. Braz Fernandes, I. Martins, J.B. Correia, Parametric optimization of Ti–Ni powder mixtures produced by mechanical alloying, *J. Alloys Comp.* 509 (2011) 271–274.
- [15] H. Zuhailawati, Y. Mahani, Effects of milling time on hardness and electrical conductivity of in situ Cu–NbC composite produced by mechanical alloying, *J. Alloys Comp.* 476 (1–2) (2009) 142–146.
- [16] B. Madavali, J.H. Lee, J.K. Lee, K.Y. Cho, C. Suryanarayana, S.J. Hong, Effects of atmosphere and milling time on the coarsening of copper powders during mechanical milling, *Powder Technol.* 256 (2014) 251–256.
- [17] H. Zuhailawati, H.M. Salihin, Y. Mahani, Microstructure and properties of copper composite containing in situ NbC reinforcement: effects of milling speed, *J. Alloys Comp.* 489 (2) (2010) 369–374.
- [18] M. Gupta, N.M.L. Sharon, *Magnesium, Magnesium Alloys, and Magnesium Composites*, John Wiley and Sons, USA, 2011.
- [19] S. Nag, R. Banerjee, H.L. Fraser, A novel combinatorial approach for understanding microstructural evolution and its relationship to mechanical properties in metallic biomaterials, *Acta Biomater.* 3 (3) (2007) 369–376.
- [20] W.C. Oliver, G.M. Pharr, An improved technique for determining hardness and elastic modulus using load and displacement sensing indentation experiments, *J. Mater. Res.* 7 (6) (1992) 1564–1583.
- [21] R. Rodriguez, I. Gutierrez, Correlation between nanoindentation and tensile properties Influence of the indentation size effect, *Mater. Sci. Eng. A* 361 (2003) 377–384.
- [22] M. Muthukumar, D. Mohan, Optimization of mechanical properties of polymer concrete and mix design recommendation based on design of experiments, *J. Appl. Polym. Sci.* 94 (3) (2004) 1107–1116.
- [23] C. Suryanarayana, Mechanical alloying and milling, *Prog. Mater. Sci.* 46 (2001) 1–184.
- [24] M.K. Datta, D.T. Chou, D. Hong, P. Saha, S.J. Chung, B. Lee, A. Sirinterlikci, M. Ramanathan, A. Roy, P.N. Kumta, Structure and thermal stability of biodegradable Mg–Zn–Ca based amorphous alloys synthesized by mechanical alloying, *Mater. Sci. Eng., B* 176 (2011) 1637–1643.
- [25] H. Zuhailawati, T.L. Yong, Consolidation of dispersion strengthened copper–niobium carbide composite prepared by in situ and ex situ methods, *Mater. Sci. Eng., A* 505 (1–2) (2009) 27–30.
- [26] F. Shehata, A. Fathy, M. Abdelhameed, S.F. Moustafa, Preparation and properties of Al₂O₃ nanoparticle reinforced copper matrix composites by in situ processing, *Mater. Des.* 30 (7) (2009) 2756–2762.
- [27] J. Chen, Z. Chen, H. Yan, F. Zhang, Microstructural characterization and mechanical properties of a Mg–6Zn–3Sn–2Al alloy, *J. Alloys Comp.* 467 (2009) 1–7.
- [28] S. Zhang, X. Zhang, C. Zhao, J. Li, Y. Song, C. Xie, H. Tao, Y. Zhang, Y. He, Y. Jiang, Y. Bian, Research on an Mg–Zn alloy as a degradable biomaterial, *Acta Biomater.* 6 (2010) 626–640.

Cold spray deposition of hydroxyapatite powder onto magnesium substrates for biomaterial applications

M. Hasniyati¹, H. Zuhailawati*¹, S. Ramakrishnan¹, B. K. Dhindaw² and S. N. F. M. Noor³

A simple, modified, cold spray process was developed in which hydroxyapatite powder was coated onto pure magnesium substrates preheated to 350 or 550°C and ground to either 240 or 2000 grit surface roughness, with stand-off distances of 20 or 40 mm. The procedure was repeated five and 10 times. The hydroxyapatite coatings did not show any phase changes. Atomic force microscopy revealed a uniform coating topography, and scanning electron microscopy revealed good bonding between the coated layers and the substrates. As the *p* values were <0.05, all factors except the number of sprays were considered to be significant. The response optimiser indicated that a 22.7 mm stand-off distance, a 649.2 grit surface roughness and a 496°C substrate heating temperature produced good hydroxyapatite coatings of 46.3 µm thickness, 436.5 MPa nanohardness and 43.9 GPa elastic modulus. The modified cold spray technique with substrate heating showed promising results in terms of product coating thickness and mechanical properties.

Keywords: Cold spray, Magnesium, Hydroxyapatite, Surface response methodology, Fractional factorial design, Characterisation

Introduction

Magnesium stands out as a potential candidate for temporary implants in biomedical applications due to its light weight, as well as its elastic modulus and compressive yield strength that are compatible with those of natural bone.¹ The density of Mg is 1.738 g cm⁻³, which is only slightly less than that of natural bone (1.8–2.1 g cm⁻³), while the elastic modulus of pure Mg is 45 GPa, compared to human bone (40–57 GPa). The use of pure Mg in bioimplants has been seriously considered.² Magnesium participates in human metabolic reactions and is therefore non-toxic. It is biocompatible and biodegradable in human body fluid, thus eliminating the need for a second operation to remove a temporary implant. The use of Mg alloys is generally not advisable because most alloying elements can be toxic to the human body (except for Ca alloys, for example). Furthermore, preparation of these alloys adds to the cost of the implant without giving any distinct advantages. As the main limitation of the use of Mg in medical applications is its extremely rapid degradation

rate due to corrosion, its surface must be coated with materials of high corrosion resistance. One coating material with a potential to retard the biodegradation rate of Mg in human body fluid is hydroxyapatite {HAP; [Ca₁₀(PO₄)₆OH₂]}, whose primary component consists of the same ions that are responsible for the construction of the mineral part of bone and teeth. It is bioactive with bone bonding ability, thus making it suitable for clinical use as bone spacers and fillers. The absence of cytotoxic effects makes HAP biocompatible with both hard and soft tissues.³

To coat HAP powder onto highly degradable Mg substrates, any processing technique that melts the Mg substrate or accelerates the dissolution of Mg in fluid must be avoided. Thus, this work proposes a cold spray technique as a method that is suitable for coating HAP onto Mg substrates. This technique is also known as cold gas dynamic spraying, kinetic spraying, high velocity powder deposition or supersonic powder deposition.⁴ In principle, deformable metallic particles (or other feedstock powders) are introduced into a high velocity, gas dynamic stream and directed onto a substrate surface where they impact and form a coating.⁵ Coldspray technology overcomes the shortcomings of thermal spraying, which involves melting and solidification of the coating,⁶ as well as those of the dipping technique, notably the dissolution of Mg. Cold spraying has been reported to produce coatings of proper density and adhesion with substrates such as Cu, Al, Fe, Ti, Zn, Ni and Mg alloys.^{7–11} However, to date, there have been

¹Structural Materials Niche Area Group, School of Materials and Mineral Resources Engineering, Engineering Campus, Universiti Sains Malaysia, Nibong Tebal, Penang 14300, Malaysia

²Faculty of Engineering, Christ University, Bangalore 560060, India

³Paediatric Dentistry Unit, Advanced Medical and Dental Institute, Universiti Sains Malaysia, Bertam, Kepala Batas, Penang 13200, Malaysia

*Corresponding author, email zuhalla@usm.my

few reports dealing with the cold spraying of HAP powder to form a coating layer on a pure Mg substrate.

To determine the conditions that produce high quality HAP coating on a Mg substrate, a trial and error method is not a good option. Several factors influence the properties of the coating prepared by the cold spray technique, so evaluation of the effects of individual factors is time consuming, and the process of determining the factors that would give optimum results is difficult and erratic. Instead, the design of experiment (DOE) statistical approach, in which a mathematical model is developed using experimental runs, can be used, as it is a powerful and efficient approach for solving challenging quality problems.¹² In practice, DOE has been used successfully in several industrial applications for optimising manufacturing processes. For example, DOE has been applied to optimise the plasma spray process of yttria stabilised zirconia coatings.¹³ Of the available DOE methods, response surface methodology is the method commonly used for mathematical modelling and analysis of problems in which a response is influenced by multiple variables.¹⁴ Response surface methodology also helps to reduce the number of experimental runs required to generate statistically validated results, as well as the repetition of experiments for multiple factor experiments. Response surface methodology coupled with a desirability function is a useful method for optimising multiple responses, enabling clarification of the functional relationships between the independent factors across the responses.

This work proposes a novel approach of adapting the cold spray technique to coat HAP onto a Mg substrate at low temperature. The work evaluates the effects of several cold spraying process variables (stand-off distance between nozzle spray and substrate, surface roughness of the substrate, substrate temperature and number of sprays) on the properties of the HAP coating on the heated Mg substrate. The results chosen for optimisation comprised only physical properties: coating thickness, hardness and modulus of the coating. Fractional factorial design, which reduces the number of experimental runs to half of that required by conventional full factorial design, is utilised to reduce the time and cost of the experimental work. The optimised coating is then characterised using atomic force microscopy (AFM) and scanning electron microscopy (SEM) studies.

Materials and methods

Materials

The substrate material was pure Mg plate (Xi'an Yuechen Metal Products, China). The specimens were cut into small pieces measuring $15 \times 15 \times 5$ mm. The specimen surfaces were serially ground with either 240 or 2000 grit SiC papers. Then, the specimens were ultrasonically cleaned in acetone for 5 min. For HAP, $\text{Ca}_{10}(\text{PO}_4)_6\text{OH}_2$ powder (Sigma-Aldrich, Malaysia) was used as the feed-stock of the cold spray process.

Design of experiment

Design of experiment was carried out using Minitab 16 (Minitab Inc, USA). Response surface methodology was used with fractional factorial design to obtain a mathematical correlation between stand-off distance,

surface roughness, substrate heating temperature and number of sprays of HAP coated onto pure Mg substrates, to yield the highly desirable mechanical properties (thickness, nanohardness and elastic modulus) of the samples.

This present work used a 2^{4-1} fractional factorial design to identify factors that significantly influence the mechanical properties of the coated samples, so that insignificant factors could be eliminated. In this way, the thickness, nanohardness and elastic modulus of the coatings were selected as the response variables to represent the mechanical properties and soundness of the HAP coatings. To avoid too wide a range in the screening tests, the range of factors used was designated as +1 (high) or -1 (low), as given in Table 1. The levels of the factors were chosen based on preliminary experiments. A minimum stand-off distance of 20 mm was required for convenient location of the nozzle with respect to the sample in the furnace. Beyond a 60 mm stand-off distance, the stream of particles tended to flare. An upper boundary of substrate temperature was chosen that was well below the melting point of Mg. A lower boundary of substrate temperature was chosen so that a reasonable thickness of coating could be obtained. Surface roughness levels were varied from near smooth (2000 grit) to rough (240 grit). In the present work, a 2^{4-1} fractional factorial design was formulated for four factors with two replications, leading to a total of 16 sets of samples.

Analysis of variance (ANOVA) was used to determine the adequacy of the factorial model. Then, optimisation experiments were performed to determine the best settings and define the nature of curvature of the response curves.

Preparation of HAP coatings

For the present study, the cold spray technique was modified so that the spraying ambience was at room temperature ($\sim 24^\circ\text{C}$) in order to aid retention of the HAP properties that usually show phase changes with high temperature deposition. The spraying ambience in this case was defined as the zone between the nozzle and an ~ 10 mm distance from the sample towards the nozzle. The pure Mg substrate was placed inside a furnace, where it was preheated to a temperature of either 350 or 550°C for 1 h, and then the HAP powder was cold sprayed onto the substrate. The nozzle was positioned at either 20 or 40 mm from the preheated substrate with the spray angle between the nozzle and substrate maintained at 90° . The air pressure was 1 MPa, and the air temperature was maintained at room temperature. The procedure was repeated either five or 10 times.

Table 1 Levels of factors for screening

Variable	Notation	Units	Level	
			-	+
Stand-off distance	A	mm	20	60
Surface roughness	B	grid	240	2000
Substrate heating temperature	C	°C	350	550
Number of sprays	D	...	5	10

Characterisation of HAP coatings

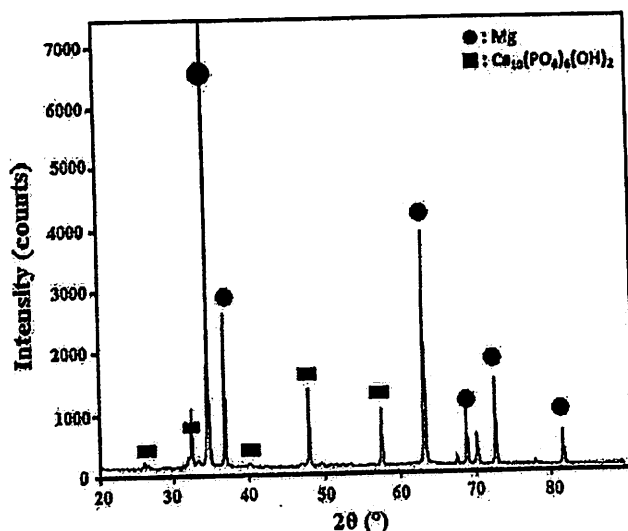
X-ray diffraction (XRD; Bruker AXS D8, USA) analysis, performed to identify phases in the HAP coating deposited by the cold spray technique, was conducted through a range of Bragg angles (2θ) of 20–80° using Cu K_α radiation ($\lambda = 0.15406$ nm). The voltage was set to 40 kV, with a current of 40 mA. An atomic force microscope (NanoNavi SII, Japan) was used to image the structure of the HAP coating at the atomic level. The atomic force microscope provided two-dimensional images of the samples and surface profiles of the coatings. The surface morphology and the composition of the as deposited coating were studied using a field emission scanning electron microscope (Zeiss SUPRA 35VP, Germany) equipped with energy dispersion X-ray spectrometry. Energy dispersion X-ray spectrometry was carried out at a voltage of 15 kV and a working distance of 10 mm, while morphology was studied at a 5 kV voltage and a 5 mm working distance. Coating thickness was measured using a metallurgical microscope (MT8000 Series, Meiji Techno, Japan).

Hardness and elastic modulus of the coating were evaluated by nanoindentation with a nanotest instrument (Micro Materials Ltd, Wrexham, UK) at minimum and maximum loads of 10 and 300 mN. The indentations were made under load control mode, where the loads were applied and then released after the set peak, with dwell times of 5 s at the maximum loads.

Results and discussion

Phase studies

Figure 1 shows XRD patterns of the HAP and pure Mg with the HAP coating. The XRD pattern of the coating demonstrates the presence of HAP. The XRD patterns in Fig. 1 indicate that the cold spray process does not affect the pure HAP phase, even at a substrate preheated temperature of 550°C. As the coating is thin (10–50 μm), peaks of pure Mg are seen in the XRD pattern due to the high penetration of the X-ray radiation beneath the coating, which reveals the presence of the substrate metal.



1 X-ray diffraction spectrums for *a* hydroxyapatite and *b* magnesium and hydroxyapatite coatings at 550°C

Screening factors

The properties of the cold spray coatings depend on the parameters used in the spraying process. Establishing relationships between the properties and the processing parameters is important for producing coatings with the desired characteristics. The results of the screening stages of the two-level fractional factorial experimental design are presented in Table 2. Analysis of the regression coefficients of the linear polynomial models describing the relationships between the responses of coating thickness, hardness and elastic modulus against the four factors (*A*, *B*, *C* and *D*) is presented in the section on 'Analysis of variance'.

Analysis of variance

Little work has been reported in the literature that discusses the effects on the spraying process of the individual, as well as combined, process parameters. To gain a better understanding of the role of individual and combined process parameters, data are analysed statistically to relate the response variables to the independent process parameters. After the effects are estimated, the factors affecting the mechanical properties of the coating are determined by performing ANOVA.

A half normal plot and ANOVA were generated using the 2^{4-1} fractional factorial design in the screening experiment, as shown in Fig. 2 and in Table 3. Figure 2*a* shows that the factors *A*, *B*, *C* and the interaction *AB* are positioned away from the straight line, indicating that variables *A*, *B*, *C* and interaction *AB* are significant model terms. This finding is also supported by ANOVA, as shown in Table 3 for thickness, which gives a *p* value of the individual factors *A*, *B*, *C* and of the combined factor *AB* as <0.005 . Figure 2*b* and *c* demonstrates that the factors *A*, *B*, *C* and the interactions *AB* and *AC* are significant model terms. The ANOVA for both responses shows that these factors are significant with $p < 0.05$. From the response results, an approximate polynomial relationship between variables and responses can be determined and expressed as the following mathematical equations:

$$Y_1 = 26.38 - 5.87A - 5.20B + 3.47C + 0.036D + 3.27AB - 1.04AC + 0.85AD \quad (1)$$

$$Y_2 = 155.83 - 84.29A - 73.49B + 46.96C + 0.22D + 54.21AB - 26.58AC - 4.25AD \quad (2)$$

$$Y_3 = 23.23 - 8.02A - 5.67B + 4.24C - 0.78D + 2.66AB - 1.60AC + 0.26AD \quad (3)$$

Factors with positive coefficients show that the factors have to be increased, and those with negative coefficients have to be lowered to maximise the responses.

Optimisation of factors

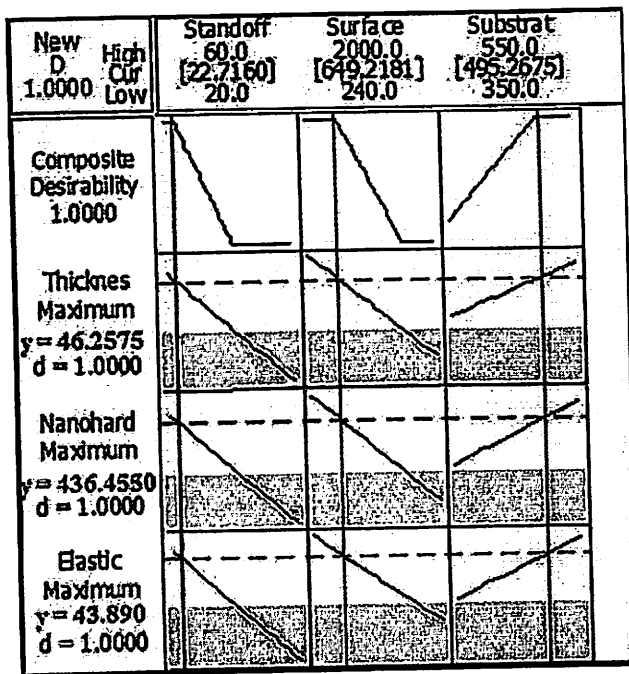
The interaction effects in equations (1)–(3) show that the combined effects of *A* and *B*, manifesting as interaction coefficient *AB*, and those of *A* and *C*, manifesting as *AC*, are significant and strong. Therefore, the effects of individual variables are not linear. A special response optimiser needs to be invoked to obtain the optimal values for the variables. The response optimiser in Minitab identifies the combination of input variable settings that jointly optimises a single response or a set of responses. It provides an optimal solution for

Table 3 Analysis of variance for thickness, nanohardness and elastic modulus

Source	p value (Prob>F)		
	Thickness	Nanohardness	Elastic modulus
A	0.0002	<0.0001	<0.0001
B	0.0004	<0.0001	<0.0001
C	0.0044	0.0002	<0.0001
D	0.9682	0.9771	0.1169
AB	0.0061	<0.0001	0.0003
AC	0.2757	0.0068	0.0071
AD	0.3660	0.5785	0.5711

values of stand-off distance as 22.7 mm, surface roughness as 649.2 grit and substrate heating temperature as 495.27°C. These parameters accommodate the optimum requirements of the cold spray process. In Fig. 3, all the responses are treated as equally important, and therefore, the default value 1.0 is given for $d = 1$.

To test the validity and reliability of the response optimiser suggestions, simple experimental work was conducted in the laboratory using the optimum trade-off values of stand-off as 23 mm, surface roughness as 650 grit and substrate heating temperature as 495°C. The experimentally measured values and the values from the optimisation procedure are listed in Table 4.



3 Optimal solution for input variable combinations along with optimisation plot

Table 4 Experimental and calculated values for response optimiser

Response variables	Experimental values	Values from optimisation procedure
Thickness $Y_1/\mu\text{m}$	48.97	46.26
Nanohardness Y_2/MPa	423.71	436.46
Elastic modulus Y_3/GPa	43.26	43.89

The comparison between the experimental values and values from optimisation procedure shows the significance of these values in the comparison t test for the theoretical model and experimental work.

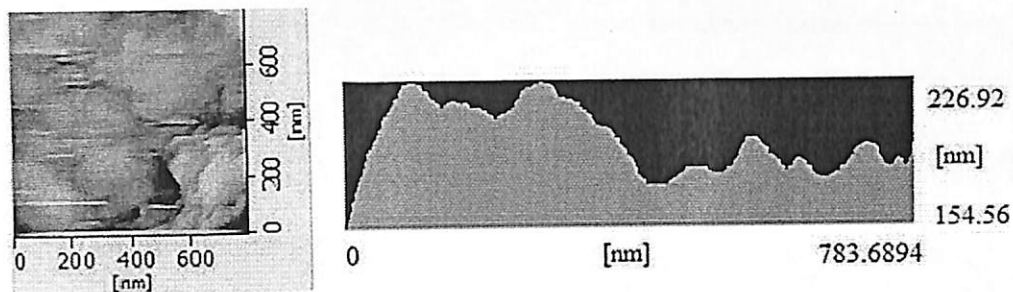
Characterisation

A comparison characterisation of the coatings obtained in runs 11 and 4 (Table 2) was conducted. The surface topography in two-dimensional images of the HAP coating surfaces was visualised by AFM, as shown in Fig. 4, which shows the coating roughness to be uniform, varying for sample run 11 from ~226.92 to 154.55 nm and for sample run 4 from 75.66 to 156.74 nm. The variation in colour in different regions reflects the signal variation with depth, which corresponds to the height difference or roughness of the sample. The size of the nodules is distinctly larger for sample run 11 than for sample run 4, and varies from 50 to 200 nm for sample run 11 and from 25 to 100 nm for sample run 4. It is expected that the higher nodule sizes for sample run 11 arise from better bonding between the particles of HAP.

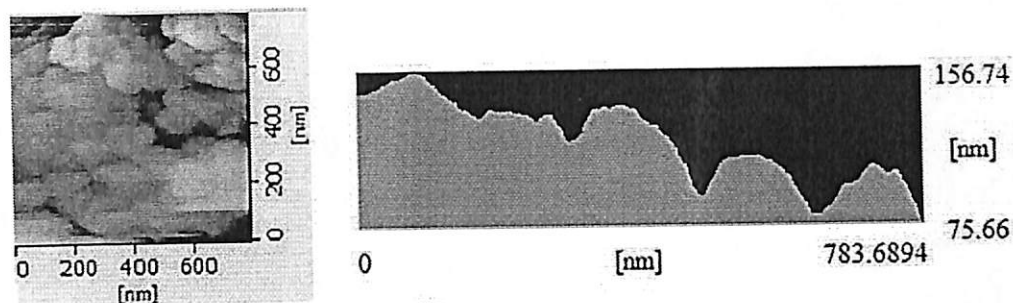
Figure 5a and b shows SEM images of the surface morphology and chemical analysis of the HAP coating on the samples of runs 11 and 4 respectively. As shown in Fig. 5a, the HAP particles are well bonded, forming a thin coating on the Mg substrate. Energy dispersion X-ray spectrometry chemical analysis on the coated and substrate areas shows that the main elements in the coating are Ca, P and O, with Mg as the substrate. Interestingly, in the sample for run 11, a few HAP particles bonded well with each other due to sintering, which was possibly caused by high impact velocities onto the substrate with the elevated substrate temperature (550°C). However, the sample for run 4, whose substrate was heated to 350°C, showed poor bonding between the HAP particles and the Mg substrate, suggesting that higher preheating of the substrate improved the bonding between the HAP particles and the substrate, as well as between the HAP particles. These observations for samples from runs 11 and 4 are also corroborated by AFM studies which shown that sample run 11 has better bonding between the particles of HAP compared to sample run 4.

Figures 6a and b shows cross-sectional views of the coatings on the samples for runs 4 and 11 respectively. As the spraying distance decreases, adherence of the HAP coating increases, with the particles forming good mechanical bonds with the substrate. The spray stand-off distance is directly correlated with the velocity of impingement of the powder on the substrate and, hence, on the quality of adhesion of the coating to the substrate. Higher spray velocity is expected to lead to breakage of the agglomerates into fine particles. In earlier work,^{15,16} it was demonstrated that deposition efficiency depends upon the substrate ductility. Higher ductility leads to shear deformation, resulting in viscose flow zones causing shear instabilities. This effect also manifests in subsurface layers, which occur due to thermal softening. The above conditions are conducive to better bonding and adhesion of sprayed particles to the substrate. Table 5 gives the hardness values for pure Mg¹⁷ at the temperatures of 350 and 550°C, and also at room temperature.

It can be seen from Table 5 that the hardness of Mg decreases drastically upon heating to higher temperatures, especially to 550°C. Thus, the possibilities of softening of the substrate and shear instabilities also

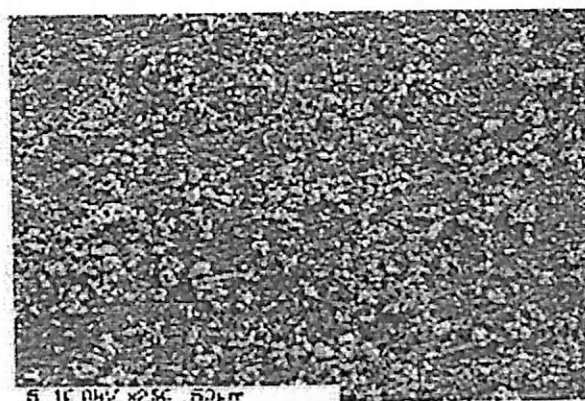
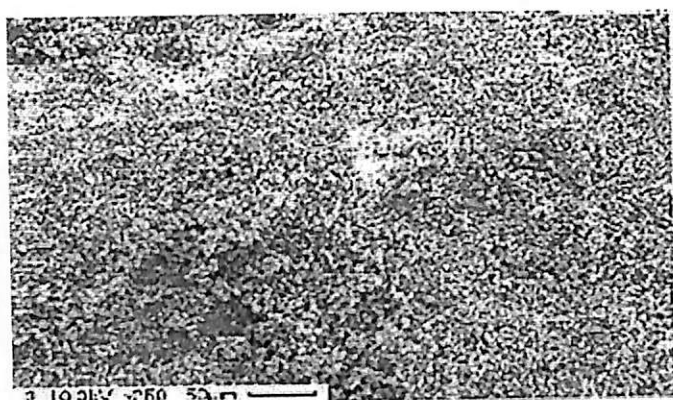


(a)



(b)

4 Two-dimensional AFM image of HAP coating sprayed and its surface roughness sprayed at a 550°C (run 11) and b 350°C (run 4)



Element	Wt%	At%
OK	30.15	48.01
MgK	08.00	08.39
PK	22.95	18.88
CaK	38.89	24.72

(a)

Element	Wt%	At%
OK	15.63	23.42
MgK	63.33	62.45
PK	08.82	06.83
CaK	12.21	07.31

(b)

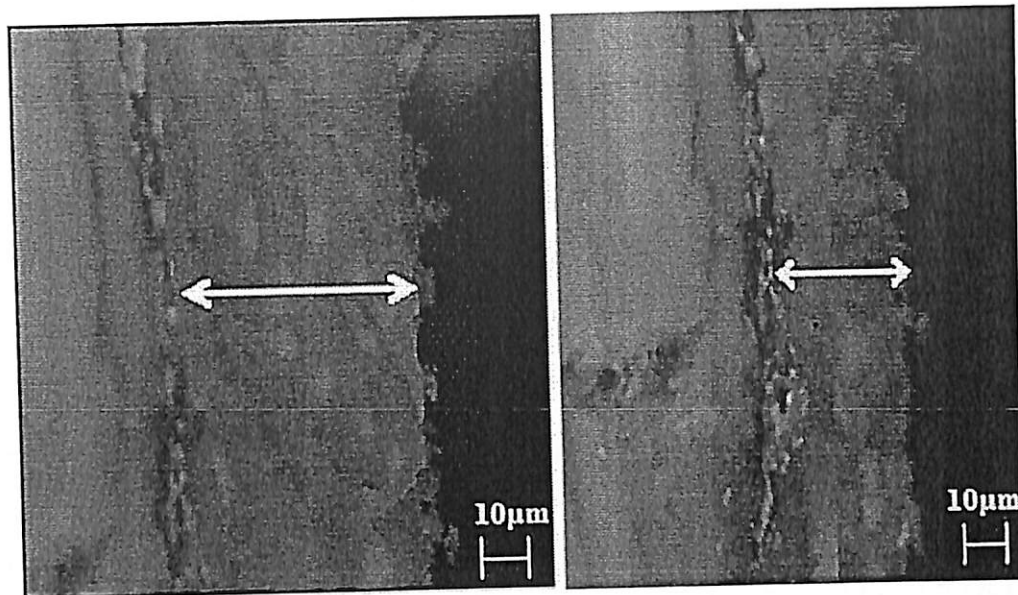
5 Scanning electron microscopy and EDX spectrum of pure magnesium substrate coated with HAP particle sprayed at a 550°C (run 11) and b 350°C (run 4)

increase significantly. The better adherence and build-up of sprayed HAP on the Mg substrate, resulting in better mechanical properties of the coating, corroborate the above mechanism.

It has been shown¹⁸ that surface roughness leads to better interlocking among the particles in the coating. High resolution imaging studies show¹⁸ that the adhesion is much improved between the coating and the substrate and that the particles have better interlocking. In the present work, AFM studies, as reported in Fig. 4, show larger nodules at higher strength levels. On the

contrary, on surfaces with low roughness, the first stream of particles to hit the surface would have less area to bind to, resulting in weaker bond strengths. Thus, particles would have greater difficulty in adhering to the substrate, resulting in an initial reduction in the deposited mass.

This breakage of the agglomerates into fine particles, combined with the high substrate temperature that enhances deformation of the substrate, leads to better adhesion and mechanical properties. However, there is an optimum velocity beyond which the particles could



6 Cross-sectional view of HAP coating on magnesium substrate sprayed at a 60 mm (run 4) and b 20 mm (run 11)

Table 5 Hardness of pure Mg at various temperatures

Temperature/°C	Hardness/kg mm ⁻²
Room temperature	27
350	8
550	2

possibly start rebounding, thus cancelling the beneficial effect of the higher velocity. The optimum velocity becomes enhanced when the surface is heated. Thus, even at higher velocities, the particles can attach to the surface. In the present work, when the substrate is heated, shorter stand-off distances give better coatings. At shorter stand-off distances, less flaring of the particle streams occurs, and so the velocity and kinetic energy of the particles are higher.

High surface roughness and shorter spray stand-off distance both appear to enhance the mechanical properties of the coatings. The effect of interaction between processing variables on the coating properties brings out some interesting observations. The interaction between stand-off distance and surface roughness *AB* shows a positive influence on the enhancement of strength and coating thickness. Individually, the effect of an increase in the stand-off distance is negative. However, when it is increased simultaneously along with the surface roughness of the substrate, the effect is positive. This may be related to the critical velocity to obtain quality coating. In the previous work, critical velocity has been related to the pressure of the stream of gas.¹⁹ However if the surface roughness is enhanced simultaneously with an increase in the stand-off distance, the interaction may result in effectively lowering of the critical velocity. Thus, even with the decrease in the stream velocity due to an increase in the stand-off distance, the quality of the coating would be enhanced as the critical velocity is also lowered. This shows the predominant effect of the increase in surface roughness leading to a better interlocking of the particles with the substrate.²⁰

On the other hand, the negative coefficient for the combined effect of the stand-off distance and the

substrate heating temperature *AC* shows that reduction of velocity along with an increase in the substrate heating temperature is not able to effectively decrease the critical velocity. Thus, the quality of the coating is lowered.

Conclusions

1. A simple and effective modified cold spray processing method has been used to coat HAP powder onto pure Mg substrates. An XRD phase study showed that the HAP coatings on the substrates did not undergo any phase changes during processing. Results from AFM and SEM confirmed the presence of compact HAP coatings on the samples.
2. Stand-off distance, surface substrate roughness and substrate heating temperature were determined to be significant parameters. A stand-off distance of 22.7 mm, a surface roughness of 649.2 grit and a substrate heating temperature of 496°C were found to be the optimum conditions for achieving the best mechanical properties of the cold sprayed HAP coatings on the Mg substrates.
3. It is noteworthy that optimising the mechanical properties using the DOE approach identified the variables, resulting in the modulus value of the coating being close to that of human bone and the hardness value close to that of the metallic state. Characterisations of the coatings with AFM and SEM studies showed that the coatings had large nodules of HAP, indicating better bonding, resulting in high hardness and reasonable modulus values.
4. Shear deformation of the substrate surface and interlocking seem to be the main mechanisms in this variant of the cold spray process.

Acknowledgements

The authors would like to thank Universiti Sains Malaysia (RU grant no. 811224) for the financial support and scholarship scheme (MyBrain15) of the Ministry of Higher Education, Malaysia. The use of the

nanindentation technology granted by the School of Mechanical Engineering, Universiti Sains Malaysia, is gratefully acknowledged.

References

1. V. K. Champagne: 'The cold spray materials deposition process: fundamentals and applications', 25-27; 2007, New York, Woodhead Publishing.
2. G. E. J. Poinern, S. Brundavanam and D. Fawcett: 'Biomedical magnesium alloys: a review of material properties, surface modifications and potential as a biodegradable orthopaedic implant', *J. Biomed. Eng.*, 2012, 6, 218-240.
3. A. Choudhuri, P. S. Mohanty and J. Karthikeyan: 'Bio-ceramic composite coatings by cold spray technology', Proc. Int. Conf. on 'Thermal spray', Las Vegas, NV, USA, May 2009, ASM International, 391-396
4. R. S. Lima, A. Kucuk, C. C. Berndt, J. Karthikeyan, C. M. Kay and J. Lindemann: 'Deposition efficiency, mechanical properties and coating roughness in cold-sprayed titanium', *J. Mater. Sci.*, 2002, 21, 1687-1689.
5. C. Li and W. Li: 'Deposition characteristics of titanium coating in cold spraying', *Surf. Coat. Technol.*, 2003, 167, 278-283.
6. H. K. Kang and S. B. Kang: 'Tungsten/copper composite deposits produced by a cold spray', *Scr. Mater.*, 2013, 49, 1169-1174.
7. H. Lee, S. Jung, S. Lee, Y. You and Y. Ko: 'Correlation between Al_2O_3 particles and interface of Al- Al_2O_3 coatings by cold spray', *Appl. Surf. Sci.*, 2005, 252, 1891-1898.
8. T. Van Steenkiste: 'Kinetic sprayed rare earth iron alloy composite coatings', *J. Therm. Spray Technol.*, 2006, 15, 501-506.
9. X. Zheng, M. Huang and C. Ding: 'Bond strength of plasma sprayed hydroxyapatite/Ti composite coatings', *Biomaterials*, 2000, 21, 841-849.
10. P. King, S. Zahiri and M. Jahedi: 'Rare earth/metal composite formation by cold spray', *J. Therm. Spray Technol.*, 2007, 17, 221-227.
11. C. W. Abdullah, H. Zuhailawati, V. Aishvarya and B. K. Dhindaw: 'Hydroxyapatite-coated magnesium-based biodegradable alloy: cold spray deposition and simulated body fluid studies', *J. Mater. Eng. Perform.*, 2013, 10, 2997-3004.
12. C. D. Montgomery: 'Design and analysis of experiments', 7th edn; 2009, New York, John Wiley & Son.
13. J. F. Li, H. L. Lioa, C. X. Ding and C. Coddet: 'Optimizing the plasma spray process parameters of yttria stabilized zirconia coatings using a uniform design of experiments', *J. Mater. Process. Technol.*, 2005, 160, 34-42.
14. A. I. Khuri and J. A. Cornell: 'Response surface: design and analyses', 2nd edn, 105-110; 1996, New York, Marcel Dekker.
15. J. O. Klieman, H. Gutzman, F. Gartner, T. Klassen and I. Jursic: 'Formation of cold sprayed ceramic titanium dioxide layers on metal surfaces', *J. Therm. Spray Technol.*, 2010, 20, 292-298.
16. S. Tarasov, V. Rubtsov and A. Kolubaev: 'Subsurface shear instabilities and nanostructuring of metals in sliding', *Wear*, 2010, 268, 1-2, 59-66.
17. E. M. Savitsky: 'The influence of temperature on the mechanical properties of metals and alloys'; 1957, Moscow, Publishing House of the Academy of Sciences.
18. H. Y. Lee, Y. H. Yu, Y. P. Hong and K. H. Ko: 'Thin film coatings of WO by cold gas dynamic spray', *J. Therm. Spray Technol.*, 2005, 14, 183-186.
19. H. Assadi, T. Schmidt, H. Richter, J. O. Kliemann, K. Binder, F. Gartner, T. Klassen and H. Kreye: 'On parameter selection in cold spraying', *J. Therm. Spray Technol.*, 2011, 6, 1161-1176.
20. A. Moridi, S. M. H. Gangaraj, M. Guagliano and M. Dao: 'Cold spray coating: review of material systems and future perspectives', *Surf. Eng.*, 2014, 36, 369-395.



Optimization of multiple responses using overlaid contour plot and steepest methods analysis on hydroxyapatite coated magnesium via cold spray deposition



M.R. Hasniyati^a, H. Zuhailawati^{a,*}, R. Sivakumar^a, B.K. Dhindaw^b

^a Biomaterials Niche Area Group, School of Materials and Mineral Resources Engineering, Engineering Campus, Universiti Sains Malaysia, 14300 Nibong Tebal, Penang

^b Faculty of Engineering, Christ University, Bangalore 560060, India

ARTICLE INFO

Article history:

Received 16 June 2015

Revised 3 September 2015

Accepted in revised form 4 September 2015

Available online 10 September 2015

Keywords:

Multiple responses

Overlaid method

Steepest method

Hydroxyapatite

Cold spray

Coating

ABSTRACT

In this work, sequential optimization strategy based statistical design was employed to enhance the mechanical properties of hydroxyapatite coatings onto a pure magnesium substrate using a cold spray technique. A fractional factorial design (2^{4-1}) was applied to elucidate the process parameters that significantly affected the mechanical properties of the coating samples. Standoff distance, surface roughness, and substrate heating temperature were identified as important process parameters affecting thickness, nanohardness, and the elastic modulus of the coating sample. The overlaid method analysis was employed to determine tradeoff optimal values from multiple regressive equations. Then, finally, steepest method analysis was used to reconfirm and relocate the optimal domain from which the factor levels for maximum mechanical properties of the coating were determined at 49.77 mm standoff distance, 926.4 grit surface roughness, and 456 °C substrate heating temperature, which can accommodate the optimum requirements for the cold spray process with a coating of 49.77 μm thickness, 462.61 MPa nanohardness, and 45.69 GPa elastic modulus. Scanning electron microscopy revealed that a short standoff distance, high surface roughness, and high substrate temperatures improved the bond between the coated layers and substrates.

© 2015 Elsevier B.V. All rights reserved.

1. Introduction

Hydroxyapatite [$\text{Ca}_{10}(\text{PO}_4)_6(\text{OH})_2$], (HAP), has been widely used in dental and orthopedic implants, due to its chemical and crystallographic similarity with bone minerals [1–3]. The use of HAP coatings has a number of advantages besides improving the corrosion resistance of Mg and Mg Alloys in the physiological environment. HAP is a major inorganic component found in natural bone tissues, therefore using HAP as a biological coating on Mg offers a number of attractive properties [4]. A lack of cytotoxic effects makes HAP biocompatible with hard tissues, skin, and muscle tissues. Thus, it can be bonded directly to bone. Despite its ideal bioactive properties, poor mechanical strength hinders the use of HAP as a load bearing implant. As a result, the combination of bioactive HAP coating and mechanically strong metals has become a promising approach to fabricate surgical implants for load-bearing applications [5].

A recent study indicated that HAP was deposited onto a magnesium (Mg) alloy to improve its biodegradable performance. Magnesium ions present in the human body, whereby approximately 1 mol of Mg is sorted in a 70 kg adult human body and an estimated amount of half of total physical Mg in the bone tissue. Magnesium is also present in human metabolic reactions and nontoxic to the human

body. Magnesium has good biocompatibility and is biodegradable in human body fluids by corrosion, which eliminates the need for another operation to remove the implants. Furthermore, it has been shown that the elastic modulus of pure Mg is 45 GPa, which is comparable to that of natural bone (40–57 GPa) than other commonly used metallic implants.

Among HAP coating techniques, plasma spraying is by far the most widely adopted process [6,7]. However, Moridi et al. [8] indicated that the plasma spray technique is difficult to use with Mg because it may convert HAP into other calcium phosphate phases i.e. α - or β -tricalcium phosphate, tetra calcium phosphate, or calcium oxide due to the high temperature used. These disadvantages are overcome with the aid of a new thermal spray process known as cold spraying. Cold spraying uses high velocity rather than high temperature to produce coatings, which avoids or minimizes the primary deleterious high temperature reactions. Cold spraying has been reported to produce coatings of proper density and adhesion with substrates such as Cu, Al, Fe, Ti, Zn, Ni and Mg alloys [9–13]. In the present study, the cold spray technique was modified by using ambient air at room temperature (~ 24 °C) as the spraying medium. This modification helped to retain the HAP properties, which usually show phase changes at high temperature deposition.

Prior knowledge and understanding under investigation are necessary to achieve a more realistic model to produce a good HAP coating from this technique. Recently, various industries have employed the designs of experiments (DOE) method to improve products or

* Corresponding author.

E-mail address: zuhaila@usm.my (H. Zuhailawati).

manufacturing processes [14]. It is a powerful and effective method to solve challenging quality problems. In practice, the DOE method has been used successfully in several industrial applications for optimizing manufacturing processes. For example, DOE has been applied to optimize the plasma spray process of yttria-stabilized zirconia coatings [15]. Moreover, Azarmi et al. [16] applied DOE method to optimize the atmospheric plasma spray process parameters for alloy 625 coatings. Dyshlovenko et al. [17] used DOE to examine the effect of power densities on phase composition and microstructure of pulsed laser treatment of hydroxyapatite coatings using plasma spraying technique. Of the available DOE methods, a fractional factorial design is a variation of the basic factorial design in which only a subset of the run is used. These fractional factorial designs are among the most widely used types of designs for product and process designs and for process improvements. In developing the regression equation, the test variables were coded according to the following equation:

$$X_j = (Z_j - Z_{0j})/\Delta_j \quad (1)$$

where X_j is the coded value of the independent variable, Z_j is the real value of the independent variable; Z_{0j} is the value of the independent variable on the center point, and Δ_j is the step change value. The linear model observed is expressed as follows:

$$Y = \beta_0 + \sum_{j=1}^n \beta_j X_j \quad (2)$$

where Y is the predicted response, X_j are input variables that influence the response variable Y ; β_0 is the intercept; and β_j is the j th linear coefficient.

On the other hand, multiple response optimization methodology is a collection of mathematical and statistical techniques for designing experiments, building models, evaluating the effects caused by factors, and searching for optimum conditions for the modeling and analysis of multiple response optimization problems. The multiple responses of interest are influenced by several variables. The aim is to optimize these responses [18]. Frequently, the overlaid method analysis is employed to determine the tradeoff optimal values from multiple regressive equations. If the mean of the center points exceeds the mean of factorial points, the optimum would be near or with the experimental design space. If the mean of the center points was less than the mean of the factorial points, then the optimum would be outside the experimental design space and the method of the steepest analysis should be applied. The steepest ascent method analysis is a procedure for moving sequentially in the direction of the maximum increase in the response. If the minimization is desired, then the technique is called the method of steepest descent [19].

In this work, a novel approach by adopting the cold spray technique to coat HAP on a magnesium substrate at low temperature is proposed. As far as the authors are concerned, most of published reports are limited to the effects of the process parameters on a single response. Thus, the aim of this work is to highlight the use of overlaid contour plots and the steepest methods to analyze multiple responses of thickness, nanohardness, and the elastic modulus of the coating. Then, the tradeoff optimal values of the responses were derived.

2. Materials and methods

2.1. Sample preparation

Pure Mg plate provided by Xi'an Yuechen Metal Products, China was cut into 15 mm × 15 mm × 5 mm. Before the cold spray process, the samples were pre-treated as follows: (1) the specimen surfaces were serially ground with either 240 grit or 2000 grit SiC papers and (2) the specimens were cleaned ultrasonically in acetone for 5 min. For HAP, $\text{Ca}_{10}(\text{PO}_4)_6\text{OH}_2$ powder (Sigma-Aldrich, Malaysia) was used as the feedstock for the cold spray process. The average HAP powder size used in

this experiment was 5 μm. The pure Mg substrate was placed inside a furnace, where it was preheated to a temperature of either 350 °C or 550 °C for 1 h, and then the HAP powder was cold-sprayed onto the substrate. The particles were accelerated through a standard de Laval type of nozzle with rectangular exit cross-section (aperture of 4 mm × 6 mm and throat diameter of 1 mm). The nozzle was positioned at either 20 mm or 40 mm from the preheated substrate with the spray angle between the nozzle and substrate maintained at 90°. The air pressure was 1 MPa and the air temperature was maintained at room temperature. The procedure was repeated either five or ten times. Each spray procedure takes around 10 to 15 min to be completed. The particle velocity obtained from this procedure was 14.5 m/s.

2.2. Multi regression equation modeling using fractional factorial design

A $2^4 - 1$ fractional factorial design with two replications was used to pick factors that influenced the mechanical properties of the coating sample significantly and any insignificant ones were eliminated to obtain a smaller and more manageable set of factors. This DOE design was carried out using Minitab 16 (Minitab Inc. USA). To avoid too wide a range in the screening tests, the range of factors used was designated as +1 (high) or -1 (low), as given in Table 1. The levels of the factors were chosen based on preliminary experiments. Analysis of variance (ANOVA) was used to determine the adequacy of the factorial model. Then, optimization experiments were performed to determine the best settings and define the nature of curvature of the response curves. Lastly, the experiments were performed along the steepest ascent and descent paths until the response did not increase or decrease any more to find the optimal value for the responses.

2.3. Characterizations of HAP coatings

The coating thickness of the as-deposited coating was studied using a field emission scanning electron microscope (Zeiss SUPRA 35VP, Germany). Hardness and the elastic modulus of the coating were evaluated by nanoindentation with a nano test instrument (Micro Materials Ltd., Wrexham, UK) at minimum and maximum loads of 10 mN and 300 mN. The indentations were made under load control mode, where the loads were applied and then released after the set peak with dwell times of 5 s at the maximum loads.

3. Results and discussion

3.1. Fractional factorial design

Optimization of parameters like standoff distance (X_1), surface roughness (X_2), substrate heating temperature (X_3), and number of sprays (X_4) were investigated. In this study, the influence of various process parameters on HAP coated onto pure Mg substrate were investigated via a screening process using fractional factorial design. Table 2 shows the results of the experiment.

The factorial analysis of variance in Table 3 indicates that the standoff distance, surface roughness, and substrate heating temperature were significant factors (p value of <0.05 was used as a cutoff point for significance differences), which affects the mechanical properties of the

Table 1
Level of factors of fractional factorial design.

Variable	Notation	Unit	Level	
			-	+
Standoff distance	X_1	mm	20	60
Surface roughness	X_2	grid	240 ($R_a = 0.6$)	2000 ($R_a = 0.11$)
Substrate heating temperature	X_3	°C	350	550
Number of sprays	X_4	-	5	10

Table 2
The experimental design and measured responses.

Run no	Variables in coded levels				Actual responses		
	Standoff distance (X ₁)	Surface roughness (X ₂)	Substrate heating temperature (X ₃)	Number of sprays (X ₄)	Thickness of coating, μm (Y ₁)	Nanohardness, MPa (Y ₂)	Elastic modulus, GPa (Y ₃)
1	+	+	+	+	21.96	69.49	13.96
2	–	+	–	+	18.73	47.58	16.81
3	–	+	–	–	18.19	39.12	15.26
4	+	+	–	–	13.03	36.82	9.09
5	+	–	+	–	23.56	156.87	23.46
6	+	–	+	–	24.43	73.60	19.30
7	+	+	–	+	21.84	67.72	14.70
8	+	–	–	+	20.31	67.23	13.80
9	–	+	+	–	32.63	197.65	30.73
10	+	+	–	–	17.48	35.01	11.08
11	–	–	–	+	49.77	462.61	45.69
12	+	–	–	+	21.48	65.61	16.32
13	–	–	+	–	39.08	429.02	43.06
14	–	–	–	–	35.09	255.92	33.26
15	–	–	–	–	38.97	323.71	36.33
16	–	+	+	–	25.58	156.87	23.46

coating sample and number of spray factor were found to be insignificant parameters and were maintained as a constant. A linear regression equation could be obtained from the regression results of the fractional factorial experiment:

$$Y_1 = 29.1 - 0.294X_1 - 0.591X_2 + 0.347X_3 \quad (3)$$

$$Y_2 = 207 - 4.21X_1 - 1.8835X_2 + 0.47X_3 \quad (4)$$

$$Y_3 = 27.4 - 0.401X_1 - 0.644X_2 + 0.424X_3 \quad (5)$$

Based on Eqs. (3), (4), and (5), the standoff distance (Y₁), surface roughness (Y₂), and substrate heating temperatures (Y₃) have different effects on the responses. Standoff distances and surface roughness are negative while the substrate heating temperature is positive. This shows that the factors with positive coefficients have to be increased and those with negative coefficients have to be lowered for maximizing the responses.

3.2. Overlaid analysis for multiple regression

Response contour plots were generated from the model equations (Eqs. (3), (4), and (5)) obtained in the regression analysis. Fig. 1 shows the analysis of the contour plots for thickness, which revealed that high thickness (>40 μm) was obtained at any one of the following combinations: (a) standoff distance 20–25 mm, surface roughness <500 grit, substrate heating temperature 350 °C; (b) standoff distance 20–30 mm, substrate heating temperature 440–550 °C, surface roughness 240 grit; and (c) surface roughness 350–700 grit, substrate heating temperature 440–550 °C, standoff distance 20 mm.

The analysis of the contour plots for nanohardness revealed that high nanohardness (>400 MPa) was obtained at any one of the

following combinations: (a) standoff distance 20–35 mm, surface roughness 20–900 grit, substrate heating temperature 350 °C; (b) standoff distance 20–30 mm, substrate heating temperature 490–550 °C, surface roughness 240 grit; and (c) surface roughness 350–600 grit, substrate heating temperature 490–550 °C, standoff distance 20 mm. Meanwhile, for elastic modulus revealed that high elastic modulus (>40 MPa) was obtained at any one of the following combinations: (a) standoff distance 20–30 mm, surface roughness 20–600 grit, substrate heating temperature 350 °C; (b) standoff distance 20–30 mm, substrate heating temperature 450–550 °C, surface roughness 240 grit; and (c) surface roughness 350–800 grit, substrate heating temperature 460–550 °C, standoff distance. Apart from these combinations, which were based on low values of the hold variables when the other two factors were varied, other combinations based on high and low values of the variables, can be arrived at.

The coating thickness, nanohardness, and elastic modulus were overlaid using Eqs. (3), (4), and (5) and the contour plot to find the feasible region (shown as the white region) having the desired properties (Fig. 2). For overlaying, substrate heating temperature and surface roughness were chosen as variables keeping the values of standoff distance constant at low point (Fig. 2(a)). The desired values of all these properties could be obtained at any given combination within the optimized region. Two more feasible regions were obtained (Fig. 2(b), (c)). On random check the difference between the calculated and experimental values was found to be less than 3%.

3.3. Steepest method analysis

To further optimize the process based on the regression equations (Eqs. (3)–(5)); experiments were conducted as proposed by the steepest method. The regression coefficient of standoff Distance (X₁) in Eq. (4) was chosen as a standard because its coefficient is higher

Table 3
Effects and regression coefficients for thickness, nanohardness, and elastic modulus of coatings.

Variable	Thickness			Nanohardness			Elastic modulus		
	Regression coefficient	Estimated effect	p-Value	Regression coefficient	Estimated effect	p-Value	Regression coefficient	Estimated effect	p-Value
Constant	26.3843	29.774	0.000	155.830	21.237	0.000	23.2313	52.317	0.000
X ₁	–5.8720	–6.626	0.000	–84.286	–11.487	0.000	–8.0160	–18.052	0.000
X ₂	–5.2025	–5.871	0.000	–73.491	–10.016	0.000	–5.6711	–12.771	0.000
X ₃	3.4730	3.919	0.04	46.955	6.399	0.000	4.2376	9.543	0.000
X ₄	0.0365	0.041	0.968	0.218	0.030	0.977	–0.7803	–1.757	0.117
X ₁ X ₂	3.2702	3.690	0.006	54.208	7.388	0.000	2.6641	6.000	0.000
X ₁ X ₃	–1.0368	–1.170	0.276	–26.579	–3.622	0.007	–1.5954	–3.593	0.007
X ₁ X ₄	0.8493	0.958	0.366	–4.249	–0.579	0.579	0.2623	0.591	0.571

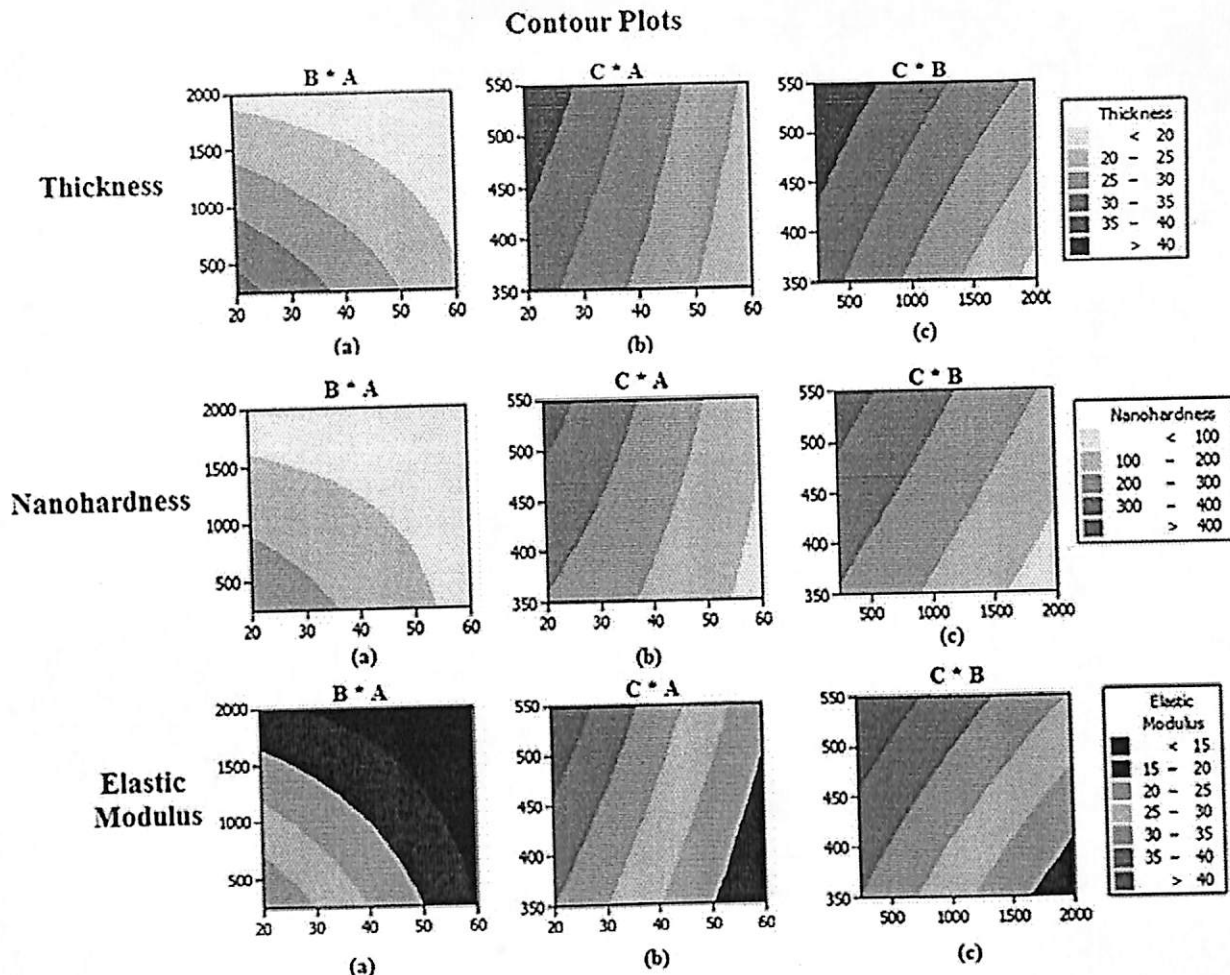


Fig. 1. Response contour plot of thickness, nanohardness and elastic modulus for (a) surface roughness vs standoff distance, (b) substrate heating temperature vs standoff distance and (c) substrate heating temperature vs surface roughness.

among the other coefficients in Eqs. (3), (4), and (5). Based on Table 1 and Eq. (4), X_i is noted by Δ_i , and the change in x_i be noted by δ_i . The coded variables are obtained by the following formula:

$$X_i = \frac{X_i - \bar{x}_i}{s_i} \tag{6}$$

where \bar{x}_i (respectively s_i) is the mean (respectively the standard deviation) of the two levels of x_i . Thus,

$$x_i + \delta_i = \frac{(X_i + \Delta_i) - \bar{x}_i}{s_i} \tag{7}$$

Then $\delta_i = \frac{\Delta_i}{s_i}$.

To the change in X_1 , $\Delta_1 = 10$ corresponds the change in x_1 , $\delta_2 = 10/20 = 0.5$ units.

In the relation $\frac{x_1}{b_1} = \frac{x_2}{b_2} = \frac{x_3}{b_3}$, we can substitute δ_i to x_i :

$\frac{\delta_1}{b_1} = \frac{\delta_2}{b_2}$, thus for X_1 , $\frac{0.5}{4.21} = \frac{\delta_2}{1.8835}$ and $\delta_1 = 0.22$, so $\Delta_2 = 0.22 * 880 = 193.6$ grit.

For X_3 , $\frac{0.5}{4.21} = \frac{\delta_3}{0.470}$ and $\delta_3 = 0.06$, so $\Delta_3 = 0.06 * 100 = 6^\circ\text{C}$.

Table 4 shows the results of steepest method experiment. According to Table 4, the increase in response is observed through the 4th step; however, all steps beyond this point result in a decrease in all responses. Therefore, the factors at run 4 were selected as the new optimal solution.

3.4. Effects of standoff distance, surface roughness, and substrate heating temperature on responses

Samples at run 1 and 4 were selected for characterization as both of the samples showed the lowest and highest value in the responses. Fig. 3(a) shows, for sample run 1, that the standoff distance of the substrate was 70 mm, surface roughness, 1700 grit, and substrate temperature 432 °C suggests that short standoff distance, high surface roughness, and high substrate temperature improved the bonding between the HAP powder and the substrate as well as between the HAP particles. Thus thicker coating layer was observed. In Fig. 3(b) HAP particles are forms a thin coating on the Mg substrate, which was possibly caused by high-impact velocities onto the substrate with the elevated substrate temperatures. These observations for samples from runs 1 and 4 are also corroborated by regression analysis in Eqs. (3)–(5), which shows factors like standoff distance and surface roughness have to be lowered while the substrate temperature has to be increased to find the maximum properties of the coating.

As spraying distance decreases, the adherence of the HAP coating increases with the particles forming a good mechanical bond with the substrate. The spray standoff distance is directly correlated with the velocity of the impingement of the powder on the substrate and on the quality of adhesion of the coating to the substrate. A higher velocity will lead to breakage of the agglomerates into fine particles. This combined with high substrate temperatures when the deformation of the substrate is also enhanced, then it leads to better adhesion and mechanical properties. However, there would

Overlaid Contour Plot of Thickness, Nanohardness and Elastic Modulus

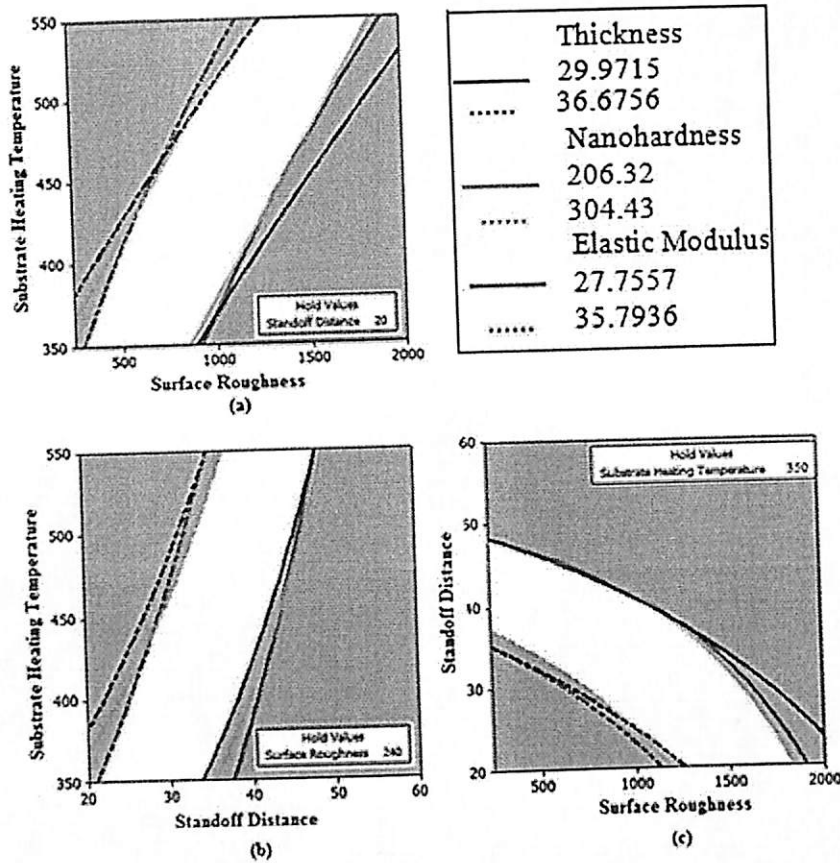


Fig. 2. Overlaid Contour plot of thickness, nanohardness and elastic modulus.

be an optimum velocity beyond which the particles may start rebounding and reverse this effect. Robert [20] assessed different processing parameters (oxygen and fuel flow, airflow, powder feed rate, standoff distance) on the structure and mechanical properties of Inconel 718 coatings. Results from this study showed that shorter spray distance increased the deposition efficiency and superficial hardness in the Inconel 718 coatings. Moreover, Morgan et al. [21] indicated that it is known that the particle velocity increased outside the nozzle and that the particles may lose velocity during the flight; however, this velocity can be further reduced due to the shock wave resulting from the previous particles impacting the substrate. The coating quality can be further improved by increasing the initial temperatures of substrate. The reason for this is that higher initial particle temperatures result in lower critical velocities as the materials are already softer at higher temperatures as well as less kinetic energy is needed to heat particle surface areas by plastic deformation.

Heat conduction will be less effective due to lower temperature gradients, which leave more time for diffusion and bonding. Increased material temperatures could enhance thermal softening, which is important for the bonding mechanism and potentiates the chemical reactions that may induce adhesion.

Defining the initial bonding mechanism at the substrate or coating interface becomes more important. One of the suggested theories for the bonding mechanism of cold sprayed coatings is associated to mechanical interlocking of the impinging powder particles to the substrate surface. It is reasonable to assume that increased the substrate roughness would further enhance bonding as it presents a greater array of nooks and recesses by which cold spray particles can be lodged. For surfaces with low roughness, the first particles to impact would have little surface area by which to bind and result in weaker bond strengths. These particles have greater difficulty adhering to the substrate, which results in an initial reduction in the deposited mass [22].

Table 4
Points along the path of steepest ascent and descent; and observed thickness of the nanohardness and elastic modulus of the sample at the points.

Run No		Standoff distance X_1	Surface roughness X_2	Substrate heating temperature X_3	Thickness	Nanohardness	Elastic modulus
1	Base	40	1120	450			
2	Base $- 3\Delta_1$	70	1700.8	432	5.92	31.86	9.28
3	Base $- 2\Delta_1$	60	1507.2	438	18.04	40.4	9.96
4	Base $- \Delta_1$	50	1313.6	444	35.38	51.31	11.21
5	Base	40	1120	450			
6	Base $+ \Delta_1$	30	926.4	456	49.77	462.61	45.69
7	Base $+ 2\Delta_1$	20	732.8	462	47.23	422.50	42.96
8	Base $+ 3\Delta_1$	10	539.2	468	45.08	419.85	42.57

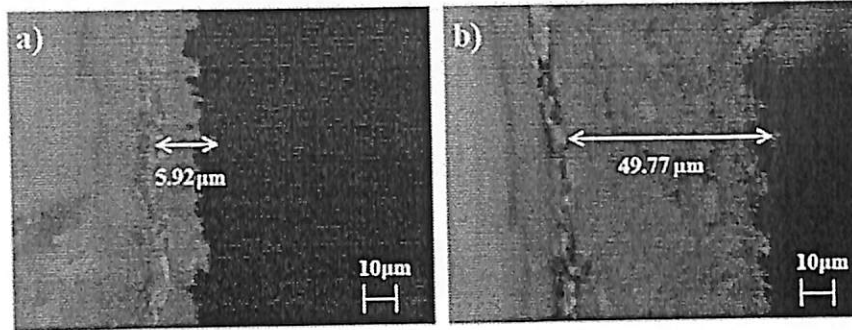


Fig. 3. Cross-sectional view of HAP coating on magnesium substrate at (a) run 1 and (b) run 4.

4. Conclusions

The effects of input factors such as standoff distance, surface roughness, substrate heating temperature, and the number of sprays on the mechanical properties (thickness, nanohardness, and elastic modulus) of the HAP coating on pure Mg have been investigated using fractional factorial design. The model terms attained for standoff distance, surface roughness, and substrate heating temperature were found to be significant for all responses. The overlaid contour plots from these responses are critical to determine the tradeoff optimal values. The optimal solution has been determined by maximizing the composite desirability. Steepest method analysis reconfirmed and relocated the optimal domains. The factor levels of maximum mechanical properties of coating were determined at 49.77 mm standoff distance, 926.4 grit surface roughness ($R_a = 0.14$), and 456 °C substrate heating temperature for the cold spray process. A coating of 49.77 μm thickness, 462.61 MPa nanohardness, and 45.69 GPa elastic modulus was achieved. SEM characterization of the coatings made with optimal combination of variables showed better bonding resulting in high hardness and reasonable modulus.

Acknowledgement

The authors would like to thank Universiti Sains Malaysia (RU Grant No. 811224) for the financial support and scholarship scheme (MyBrain15) of the Ministry of Higher Education, Malaysia. The use of the nanoindentation technology in the School of Mechanical Engineering, Universiti Sains Malaysia, is gratefully acknowledged.

References

- [1] Y.C. Tsui, C. Doyle, T.W. Clyne, Plasma sprayed hydroxyapatite coatings on titanium substrate part 1: mechanical properties and residual stress levels, *Biomaterials* 19 (1998) 2015–2029.
- [2] L. Sun, C.C. Berndt, K.A. Gross, A. Kucuk, Material fundamentals and clinical performance of plasma-sprayed hydroxyapatite coatings: a review, *J. Biomed. Mater. Res. B Appl. Biomater.* 58 (2001) 570–592.
- [3] P.K. Stephenson, M.A. Freeman, P.A. Revell, J. Germain, M. Tuke, C.J. Pirie, The effect of hydroxyapatite coating on ingrowth of bone into cavities in an implant, *J. Arthroplast.* 6 (1991) 51–58.
- [4] S. Brundavanam, G.E. Poinern, D. Faweett, Chemical immersion coatings to improve biological degradability of magnesium substrates for potential orthopaedic applications, *Int. J. Biomed. Mater. Res.* 2 (2014) 7–14.
- [5] A. Choudhuri, P.S. Mohanty, J. Karthikeyan, Bioceramic composite coating by cold spray technology, *Process. Int. Therm. Spray Conf.* (2009) 391–396.
- [6] V. Sergo, O. Sbaizero, D.R. Clarke, Mechanical and chemical consequences of the residual stresses in plasma sprayed hydroxyapatite coatings, *Biomaterials* 18 (1997) 477–482.
- [7] W. Tong, Z. Yang, X. Zhang, Patterns of plasma sprayed HAP coatings, *Biomed. Mater. Res.* 40 (1998) 407–413.
- [8] A. Moridi, S.M. Hassani-Gangaraj, M. Guagliano, M. Dao, Cold spray coating: review of material systems and future perspectives, *Surf. Eng.* 36 (2014) 369–395.
- [9] H. Lee, S. Jung, S. Lee, Y. You, Y. Ko, Correlation between Al_2O_3 particles and interface of Al- Al_2O_3 coatings by cold spray, *Appl. Surf. Sci.* 252 (2005) 1891–1899.
- [10] T. Van Steenkiste, Kinetic sprayed rare earth iron alloy composite coatings, *J. Therm. Spray Technol.* 15 (2006) 501–506.
- [11] X. Zheng, M. Huang, C. Ding, Bond strength of plasma sprayed hydroxyapatite/Ti composite coatings, *Biomaterials* 21 (2000) 841–849.
- [12] P. King, S. Zahiri, M. Jahedi, Rare earth/metal composite formation by cold spray, *J. Therm. Spray Technol.* 17 (2007) 221–227.
- [13] C.W. Abdullah, H. Zuhailawati, V. Aishvarya, B.K. Dhindaw, Hydroxyapatite-coated magnesium-based biodegradable alloy: cold spray deposition and simulated body fluid studies, *J. Mater. Eng. Perform.* 10 (2013) 2997–3004.
- [14] C. Douglas Montgomery, *Design and Analysis of Experiments*, seven ed. John Wiley & Son, Asia, 2009.
- [15] J.F. Li, H.L. Liao, C.X. Ding, C. Coddet, Optimizing the plasma spray process parameters of yttria stabilized zirconia coatings using a uniform design of experiments, *J. Mater. Process. Technol.* 160 (2005) 34–42.
- [16] F. Azarmi, T.W. Coyle, J. Mostaghimi, Optimization of atmospheric plasma spray process parameters using a design of experiment for alloy 625 coatings, *J. Therm. Spray Technol.* 17 (2008) 144–155.
- [17] S. Dyshlovenko, C. Pierlot, L. Pawlowski, R. Tomaszek, P. Changnon, Experimental design of plasma spraying and laser treatment of hydroxyapatite coatings, *Surf. Coat. Technol.* 201 (2006) 2054–2060.
- [18] L.F. Alvarez, Approximation model building for design optimization using the response surface methodology and genetic programming (PHD Dissertation) University of Bradford, 2000.
- [19] R. Muthuvelayudham, T. Viruthagiri, Application of Central Composite Design Based Response Surface Methodology in Parameter Optimization and on Cellulose Production Using Agricultural Waste, *World Academy of Science, Engineering and Technology*, 2010 890–897.
- [20] A.M. Robert, Thermal spray: international advances in coatings technology, *J. Therm. Spray Technol.* 1 (1992) 283–284.
- [21] J. Pattison, S. Celotto, A. Khan, W. O'Neill, Standoff distance and bow shock phenomena in the cold spray process, *Surf. Coat. Technol.* 202 (2008) 1443–1454.
- [22] T.H. Van Steenkiste, J.R. Smith, R.E. Teets, Aluminum coatings via kinetic spray with relatively large powder particles, *Surf. Coat. Technol.* 154 (2002) 237–252.

Characterization of Binary Mg-Mn Alloy Synthesized Through Mechanical Alloying: Effect of Milling Speed

EMEE MARINA Salleh^a, SIVAKUMAR Ramakrishnan^b
and ZUHAILAWATI Hussain^{c*}

Structural Materials Niche Area, School of Materials and Mineral Resources Engineering,
Engineering Campus, Universiti Sains Malaysia, 14300 Nibong Tebal, Penang, Malaysia.

^aemarina39@yahoo.com, ^bsrsivakumar@usm.my and ^czuhaila@usm.my

Keyword: Mg-Mn alloy; Mechanical alloying; α -Mg phase; Density; Hardness

Abstract. In this work, the effect of the milling speed on the properties of biodegradable Mg-1Mn alloy prepared by mechanical alloying was investigated. The magnesium-based alloy was prepared in solid state route using a high energy planetary mill. A mixture of pure magnesium and manganese powder was mechanically alloyed for 5 hours in argon atmosphere. Milling process was performed at various rotational speeds in order to investigate milling speed effect (i.e., 100, 200, 300 and 400 rpm) on phase formation and bulk properties. The as-milled powder was uniaxially compacted by cold pressing under 400 MPa at room temperature and sintered in argon atmosphere at 500 °C for an hour. X-ray diffraction analysis indicated that a single α -Mg phase was formed in magnesium matrix after sintering process. An increase in milling speed up to 300 rpm resulted in an increase in density and hardness of the binary alloy. The changes of bulk properties of the Mg-Mn alloys were correlated to the formation of solid solution phase and a reduction of porosity which led to an increasing in densification.

Introduction

Magnesium (Mg) alloys are potentially useful as structural materials in the aerospace and automobile industries. Mg has a density of 1.74 g/cm³ which is approximately one-fourth the density of steel and two-thirds that of aluminium. Its specific strength is lower than Ti alloy sheet but relatively higher than steel, aluminium and carbon fiber sheets [1]. Owing to its low density and high specific mechanical properties, Mg-based materials are actively pursued by companies for weight-critical applications. A number of industries are focusing on the development of this special Mg alloys including i. aerospace application in order to minimize emission reduction and fuel efficiency, ii. medical application due to its high biocompatibility and self-degradable in human body and iii. electronic application since it exhibits great improvement in strength, heat transfer, and ability to shield electromagnetic interference and radio frequency interference as compared with current plastic counterparts [2]. The addition of alloying elements in pure Mg helps to alter its properties. Mg is chemically active and can react with other metallic alloying elements to form intermetallic compounds. In this study, Mg was alloyed with manganese (Mn) using mechanical alloying in order to increase its mechanical properties. Mn was chosen as it enables to enhance the saltwater corrosion resistance of Mg as well. The low solubility of Mn in Mg limits the amount of Mn incorporation in Mg. In a previous study, Gu et al. [3] reported that with addition of 1 wt% Mn prepared by conventional casting, its corrosion rate was reduced with a low hydrogen evolution rate. This current work focused on density and hardness of Mg-1wt%Mn that was produced at solid state by powder metallurgy (PM) through mechanical alloying. Generally, powder metallurgy is a useful route to the near net-shape fabrication of engineering components for a variety of applications [4]. It allows consolidation without a melt processing step, which can be advantageous for producing various metallic alloys and composites [5]. Mg alloys were commonly developed

using liquid state processing especially by casting process. However, due to some defects such as inclusions and large pores that usually found in casted alloys, thus mechanical alloying was employed in this study. This present work aims to investigate the effect of milling speed on the structural and properties of binary Mg-Mn alloy developed through mechanical alloying.

Experimental Procedure

A mixture of elemental magnesium powder (97.00 % pure, < 63 μm) and manganese powder (99.00 % pure, < 90 μm) corresponding to Mg-1wt%Mn was mechanically milled at various milling speeds of 100, 200, 300 and 400 rpm. Mechanical alloying was carried at room temperature using a high-energy Fritsch Pulveristte P-5 planetary mill under argon atmosphere. The powder to ball weight ratio of 1:10 was kept constant during the milling process. 20 mm-diameter stainless steel balls were used. 3% n-heptane was added to the powder mixture prior to the milling process to prevent excessive cold welding of the elemental alloy powders. Then, the milled powders were uniaxially cold pressed under 400 MPa at room temperature. In order to form solid bodies, the compacted samples then were sintered at 500 $^{\circ}\text{C}$ for an hour in argon flow. Qualitative X-ray diffraction (XRD) analyses were conducted to identify the presence of any element and phases. Microstructure observation of the bulk Mg-Mn alloys was studied using scanning electron microscopy (SEM). Density of the sintered alloy was measured using pycnometer density equipment according to Archimedes' principle. Vickers microhardness test was carried out by applying an indentation load of 500 gf using diamond pyramid indenter for 10 seconds dwell time. Seven readings were taken from each sintered alloy and the values were then averaged.

Results & Discussion

XRD Analysis

As shown in Fig. 1, XRD pattern of all mechanically alloyed samples produced at different milling speeds showed the presence of one single phase α -Mg after sintering process. In Mg-Mn composition, solubility limit of Mn in Mg phase is 2.2 wt% at eutectic temperature (651 $^{\circ}\text{C}$) but it is very little at room temperature [6]. Therefore, all added Mn element was solid-solved into α -Mg. Therefore, the formed crystal phase in the milled alloy is solid-solution α -Mg. In addition, the peaks of Mg in the sintered alloys were shifted to the left-hand side due to solid solution formation. During formation of solid solution, smaller radius of Mn (127 pm) atoms took place as impurities in the larger Mg (160 pm) lattice. The replacement of Mn in the host site caused a reduction of the lattice. In addition, the shifted angles were also caused by a reduction of crystallite size and/or the accumulation of lattice strain during mechanical alloying [7]. This indicated that the formation of fine crystallite which is due to the increasing number of collisions per unit time during milling process. At low milling speed, the mixture received the least effect from incoming impact energy. Boytsov et al. [8] have noted that increased milling speed or shock energy during mechanical alloying may cause a decrease in crystallite size of pure particles since the higher energy transferred to the powder with increased ball impact energy resulted in greater fracturing of the powder than that caused by cold welding at lower milling intensity.

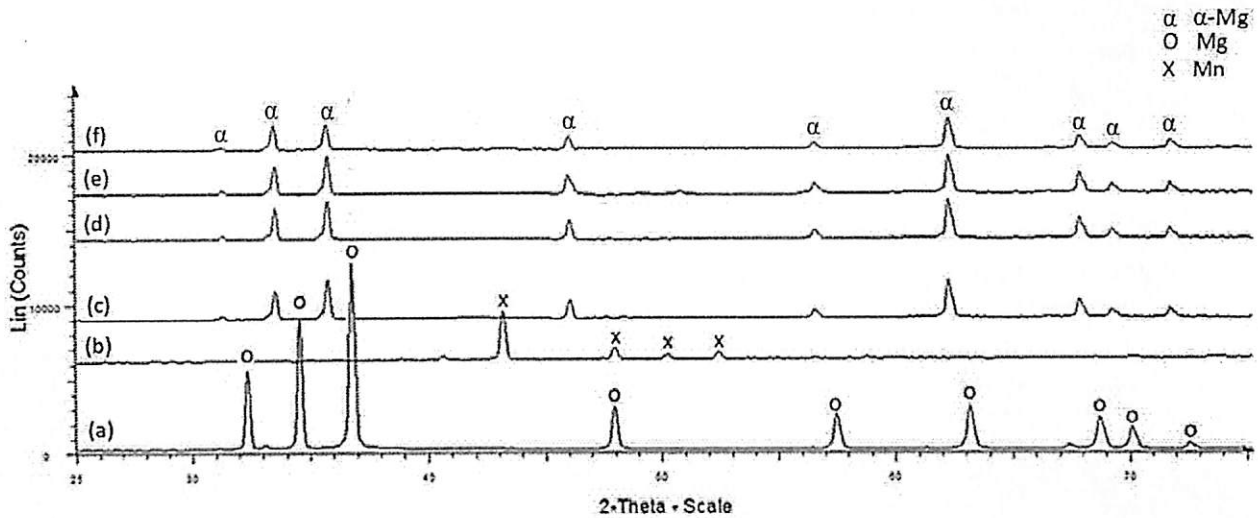


Fig. 1 XRD patterns for (a) as-received pure Mg, (b) as-received pure Mn, sintered Mg-Mn alloys those were mechanically milled at (c) 100, (d) 200, (e) 300 and (f) 400 rpm

Microstructural Investigation

Fig. 2 shows the microstructure of Mg-Mn alloys that were milled at different milling speed. Alloys that were synthesized at low rotational speed (100 rpm) resulted in larger size and higher amount of pores. As the speed was increased up to 300 rpm, compacted microstructure reduced with respect to size and distribution of pores. The reduction of pore size and its distribution at higher speed increased the contact area between grains leading to enhance densification effect, sinterability and its properties afterward. However, too high milling speed resulted in excessive heat generated which caused occurrence of cold welding during mechanical alloying [9]. The increased elimination of pores at 300 rpm compared to that at 100 rpm milling suggested that better densification of the binary Mg-Mn alloy was achieved by mechanical alloying of the Mg-1Mn mixture at 300 rpm milling speed, coupled with appropriate compaction and sintering processes.

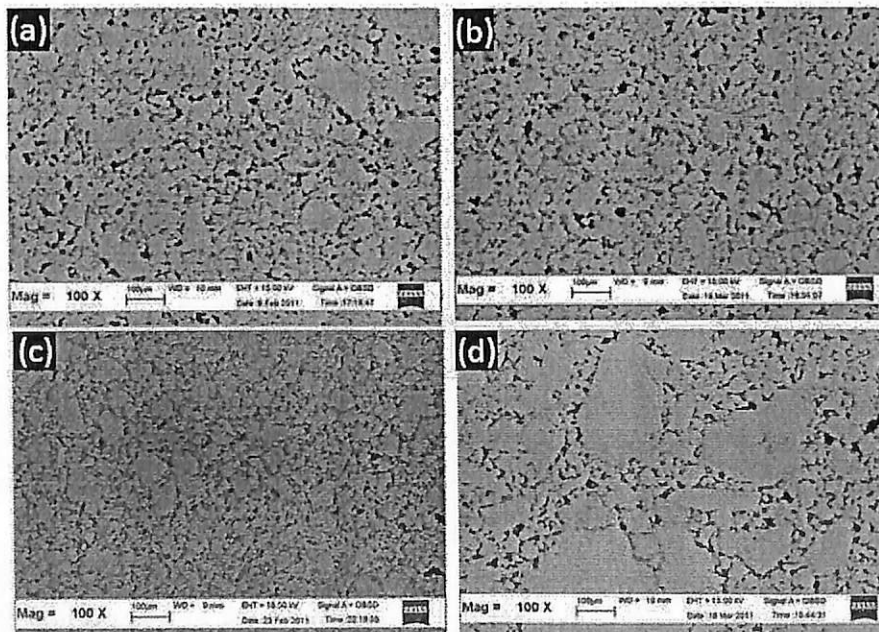


Fig. 2 SEM micrographs for (a) 100 rpm, (b) 200 rpm, (c) 300 rpm and (d) 400 rpm

Density Measurement

As the milling speed increased, the green and sintered densities of the compacted Mg-Mn alloy increased (Fig. 3). The sintered compact exhibited a higher density than that of the green body. This may be due to the presence of pores inside the green body since the pores were not fully

eliminated due to plastic deformation in the powder upon consolidation. During sintering, atom diffusion occurred and reduced the presence of pores. Hence, higher density was attained by the sintered compact. This result can be explained by powder refinement of particles which was caused by higher kneading during mechanical alloying, lowering the distance between particles [10]. As a result, densification during sintering was improved. According to Fig. 3, sintered density of Mg-Mn alloy was increased with increasing in milling speed and reached highest value of 1.7720 g/cm^3 at 300 rpm. A further increase in milling speed up to 400 rpm led to a decrease in the density of the alloy. Reduction of density was mainly affected by the excessive heat generation at higher milling speed and caused the occurrence of cold welding during mechanical alloying [11]. Then, the compressibility of the as milled alloy reduced which resulted in the lowering of its densification effect and its properties afterward.

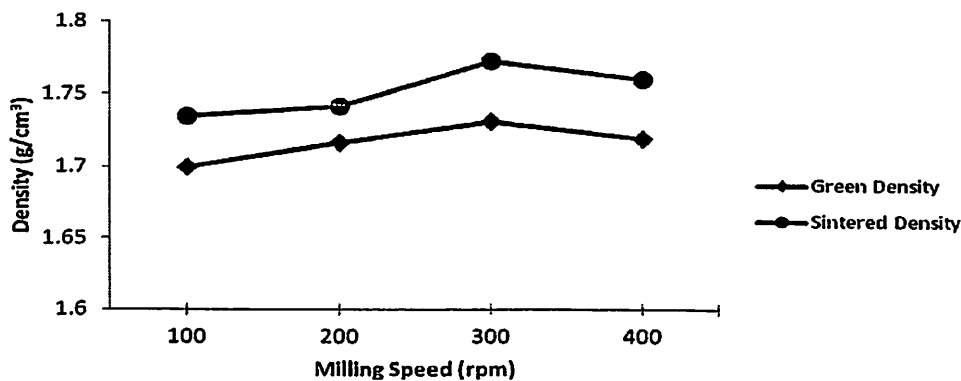


Fig. 3 Green density and sintered density of Mg-Mn compact at different milling speeds

Hardness of Sintered Compact

As shown in Fig. 4, microhardness of Mg-Mn alloy increased from 31.43 HV to 46.16 HV when milling speed was increased from 100 rpm to 300 rpm. The increase in microhardness value of the alloy was mainly attributed to the work hardening mechanism which took place due to severe plastic deformation during uniaxial consolidation [12]. In addition, as milling speed increased, the dispersion of Mn particles in the Mg matrix in order to form a single solid solution phase was also increased during sintering and resulted in stronger bonding between alloying and matrix particles. As a result, densification effect was improved which then enhanced microhardness of the sintered alloys. However, up to 400 rpm of milling speed, hardness was dropped to 41.66 HV. This situation can be explained by the reduction of densification effect due to the low compressibility of as-milled alloy during compaction.

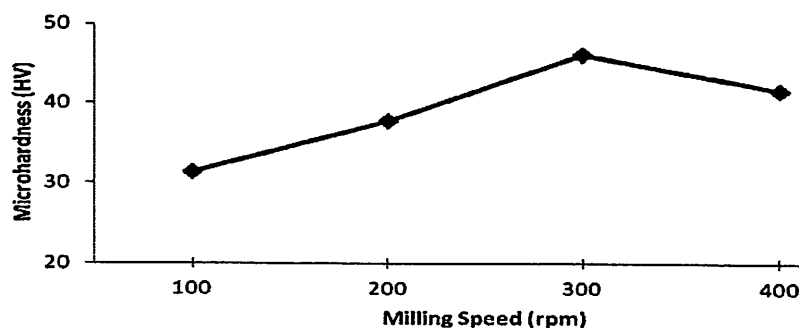


Fig. 4 Hardness of compact sintered Mg-Mn alloy at different milling speeds.

Conclusion

In this paper, Mg-1wt%Mn was prepared in solid state route using mechanical alloying of Mg-Mn powder mixture with a variation of milling speeds. XRD diffraction pattern showed the single phase of α -Mg was formed in the mechanically milled alloy. Alloy prepared at high milling speed

up to 300 rpm showed higher green density, sintered density and microhardness due to refinement of mixture particle size but then reduced at higher milling speed owing to excessive heat generation and lowering in its densification effect. The alloy milled at 300 rpm milling speed provided the highest properties in both density and hardness which were 1.7720 g/cm^3 and 46.16 HV, respectively.

Acknowledgement

The authors would like to thank to Universiti Sains Malaysia RU-PRGS Grant No. 8046026, RU Grant No. 811224 and sponsorship scheme of Malaysian Ministry of Education.

References

- [1] G. Garces, P. Perez, P. Adeva, Mechanical characterization of the alloy Mg-14%Ti-1%Al-0.9%Mn (wt%) synthesized by physical vapour deposition, *J. Alloys & Compds*, 333 (2002) 219-224
- [2] M. Lucaci, A. R. Biris, R.L. Orban, G.B. Sbarcea, V. Tsakiris, Effects of mechanical alloying on the hydrogen storage properties of the $\text{Mg}_{76}\text{Ti}_{12}\text{Fe}_{12-x}\text{Ni}_x$ ($x=4,8$) materials, *J. Alloys & Compds*, 488 (2009) 163-168
- [3] X. Gu, Y. Zheng, Y. Cheng, S. Zhong, T. Xi, In vitro corrosion and biocompatibility of binary magnesium alloy, *Biomaterials* 30 (2009) 484-498
- [4] M. Razavi, M.R.Rahimipour and R. Mansoori, Synthesis of TiC- Al_2O_3 nanocomposite powder from impure Ti chips, Al and carbon black by mechanical alloying, *J. Alloys & Compds*, 450 (2008) 463-467
- [5] J. Patel, K. Morsi, Effect of mechanical alloying on the microstructure and properties of Al-Sn-Mg alloy, *J. Alloys & Compds*, 540 (2012) 100-106
- [6] D.F. Zhang, G.L. Shi, X.B. Zhao and F.G. Qi, Microstructure evolution and mechanical properties of Mg-x%Zn-1%Mn ($x=4,5,6,7,8,9$) wrought alloys, *Trans. Nonferrous Met. Soc China*, 21 (2011) 15-25
- [7] V. Rajkovic, D. Bozic, M.T. Jovanovic, Effects of copper and Al_2O_3 particles on characteristics of Cu- Al_2O_3 composites, *Materials and Design*, 31 (2010) 1962-1970
- [8] O. Boytsov, A.I.Ustinov, E. Gaffet, F. Bernard, Correlation between milling parameters and microstructure characteristics of nanocrystalline copper powder prepared via a high energy planetary ball mill, *J. Alloys & Compds*, 432 (2007) 103-110
- [9] C. Suryanarayana, Mechanical alloying and milling, *Prog. in Materials Science* 46 (2001) 1-184
- [10] M.T. Marques, A.M. Ferraria, J.B. Correia, A.M.B. Rego, R. Vilar, XRD, XPS and SEM characterisation of Cu-NbC nanocomposite produced by mechanical alloying, *Materials Chemistry and Physics*, 109 (2008) 174-180
- [11] E. Botcharova, J. Freudenberger, L. Schultz, Cu-Nb alloys prepared by mechanical alloying and subsequent heat treatment. *Journal of Alloys and Compounds*, 365 (2004) 157-163
- [12] S. Sivasankaran, K. Sivaprasad, R. Narayanasamy and P.V. Satyanarayana, X-ray peak broadening analysis of AA 6061 $_{100-x}$ -x wt.% Al_2O_3 nanocomposite prepared by mechanical alloying, *Materials Characterization*, 62 (2011) 661-672

Design of experiment (DOE) study of biodegradable magnesium alloy synthesized by mechanical alloying using fractional factorial design

Emee Marina Salleh, Sivakumar Ramakrishnan, and Zuhailawati Hussain

Citation: AIP Conference Proceedings **1602**, 1196 (2014); doi: 10.1063/1.4882636

View online: <http://dx.doi.org/10.1063/1.4882636>

View Table of Contents: <http://scitation.aip.org/content/aip/proceeding/aipcp/1602?ver=pdfcov>

Published by the AIP Publishing

Articles you may be interested in

Dynamic mechanical response of magnesium single crystal under compression loading: Experiments, model, and simulations

J. Appl. Phys. **109**, 103514 (2011); 10.1063/1.3585870

Photoluminescence studies of impurity transitions in Mg-doped AlGaIn alloys

Appl. Phys. Lett. **94**, 091903 (2009); 10.1063/1.3094754

Distinguishing between target structure and ionization mechanisms in (e,3e) experiments

AIP Conf. Proc. **604**, 102 (2002); 10.1063/1.1449321

In situ x-ray photoelectron spectroscopy study of evaporated magnesium on chemically synthesized polypyrrole films

J. Vac. Sci. Technol. A **19**, 2680 (2001); 10.1116/1.1399319

Reduction mechanism of surface oxide in aluminum alloy powders containing magnesium studied by x-ray photoelectron spectroscopy using synchrotron radiation

Appl. Phys. Lett. **70**, 3615 (1997); 10.1063/1.119250

Design of Experiment (DOE) Study of Biodegradable Magnesium Alloy Synthesized by Mechanical Alloying Using Fractional Factorial Design

Emee Marina Salleh, Sivakumar Ramakrishnan and Zuhailawati Hussain*

*School of Materials and Mineral Resources Engineering,
Engineering Campus, Universiti Sains Malaysia,
14300 Nibong Tebal, Penang, Malaysia*

Abstract. The biodegradable nature of magnesium (Mg) makes it a most highlighted and attractive to be used as implant materials. However, rapid corrosion rate of Mg alloys especially in electrolytic aqueous environment limits its performance. In this study, Mg alloy was mechanically milled by incorporating manganese (Mn) as alloying element. An attempt was made to study both effect of mechanical alloying and subsequent consolidation processes on the bulk properties of Mg-Mn alloys. 2^{k-2} factorial design was employed to determine the significant factors in producing Mg alloy which has properties closes to that of human bones. The design considered six factors (i.e. milling time, milling speed, weight percentage of Mn, compaction pressure, sintering temperature and sintering time). Density and hardness were chosen as the responses for assessing the most significant parameters that affected the bulk properties of Mg-Mn alloys. The experimental variables were evaluated using ANOVA and regression model. The main parameter investigated was compaction pressure.

Keywords: Mg-Mn alloys; Mechanical alloying, Hardness; Density; 2^{k-2} factorial design.
PACS: 81.20.Ev, 87.85.J

INTRODUCTION

Magnesium alloys have been suggested for biomedical application due to their potentials to serve as biodegradable metallic implants since they can be gradually dissolved, absorbed, consumed or excreted in human body and then disappear after bone tissues heal [1, 2]. In comparison with stainless steel and titanium alloys, biodegradable magnesium alloys are identified as revolutionizing biometals. Magnesium implants demonstrate higher biological activity than conventional metals but its ability is limited by high degradation rate in human bio-environment [3, 4]. Elastic modulus of magnesium is about 40-45 GPa which is very close to that human bone (10-40 GPa). So it can reduce the chance of stress shielding effects observed in the case of higher modulus materials such as titanium [5, 6]. There have been several different types of alloying elements used in Mg based materials but a number of them will cause negative effect to human body. For example, excessive copper amounts have been linked to neurodegenerative diseases like Alzheimer's and in high doses of aluminium has been shown to increase estrogen-related gene expression in human breast cancer cell when cultured in a laboratory setting [7]. Mn is a co-factor in the formation of bone cartilage and bone collagen. Mn is beneficial to the normal skeletal growth and development as well [2]. Thus, in this study, Mg-Mn was produced by mechanical alloying (MA) method since it is an effective tool to produce metallic alloys with fine microstructure [8]. MA i.e. high-energy ball milling enables high energy impact on the charged powder by collision between the grinding media and powder particles, which causes severe plastic deformation, repeated fracturing and cold welding of the particles leading to nanocrystalline materials formation [9, 10, 11]. Generally, however, little information is available regarding the production and bulk properties of Mg alloy prepared by MA technique. Hence, further investigation need to be performed in order to produce Mg-Mn alloys with the desired properties. In this present study, density and hardness were investigated in order to ensure the alloys produced have ranges close to that of human bones.

EXPERIMENTAL CONDITION

Materials Preparation

A mixture of elemental magnesium powder (99.99 % pure, < 63 μm) and manganese powder (99.99 % pure, < 90 μm) was mechanically milled at room temperature using a high-energy Fritsch Pulveristte P-5 planetary mill under argon atmosphere. The powder to ball weight ratio of 1:10 was kept constant during the milling process. 20 mm-diameter stainless steel balls were used. 3% n-heptane was added to the powder mixture prior to the milling process to prevent excessive cold welding of the elemental alloy powders. Then, the milled powders were uniaxially cold pressed and sintered in order to form solid bodies. Qualitative X-ray diffraction (XRD) analyses were conducted to identify the presence of any element and phases. Morphology of the bulk Mg-Mn alloys was studied using scanning electron microscopy (SEM). Density of the sintered alloys was measured using pycnometer density equipment according to Archimedes' principle. The sample with the 10 mm² surface area was placed under the diamond indenter. Hardness test was performed under 500 gf of indentation load with 10 seconds of dwell time. Ten readings were taken for each sample.

Statistical Design

The experimental procedure was performed according to fractional factorial design, which is basically a series of experiments involving k factors, each of which has two levels ('low' – and 'high' +). Six factors studied were divided into two stages of experimental work with the objective of learning how each factor affects the density and hardness. Three factors of mechanical alloying (i.e milling time, milling speed and percentage of Mn) and three factors of consolidation process (i.e compaction pressure, sintering temperature and sintering time). 16-run two-level fractional factorial design was used as shown in Table 1.

TABLE (1). Factors and levels evaluated in the experiments

Factor	Code	Unit	Level	
			-1	+1
Milling Time	A	h	2	10
Milling Speed	B	rpm	100	400
Percentage of Mn	C	wt%	0.25	1.00
Compaction Pressure	D	MPa	100	400
Sintering Temperature	E	°C	300	500
Sintering Time	F	h	1	3

RESULTS AND DISCUSSION

Structural Analysis

XRD pattern of all mechanically alloyed samples produced according to the model showed the presence of one single phase α -Mg as shown in Figure 1. In this alloy composition, solubility limit of Mn in Mg phase is 2.2 wt% at eutectic temperature but it is very little at room temperature. Therefore, all added Mn element solid-solved into α -Mg, the formed crystal phase in the powder milled is super solid-solution α -Mg. However, the peaks of sintered alloys were shifted to the left-hand side due to reduction of crystallite size and/or the accumulation of lattice strain during mechanical alloying. This indicated that the formation of fine crystallite which is due to the increasing number of collisions per unit time during milling process.

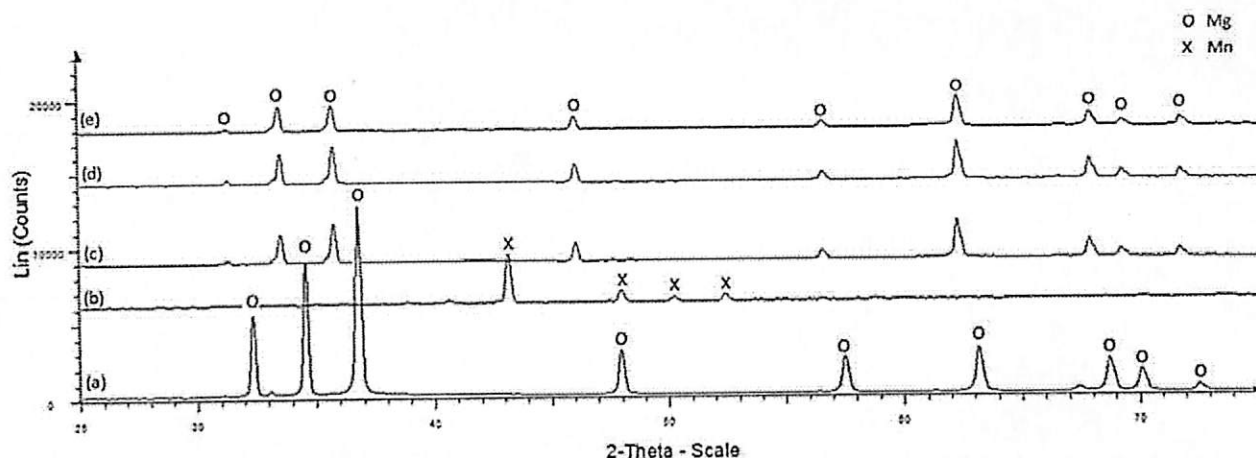


FIGURE 1. XRD patterns for (a) as-received pure Mg, (b) as-received pure Mn, (c) #1, (d) #9 and (e) #14

Figure 2 shows the microstructure of Mg-Mn alloys that were compacted under different pressure. Alloys that were compacted under low pressure (100 MPa) resulted in larger size and higher amount of pores. As the pressure was increased up to 400 MPa, compacted microstructure reduced with respect to size and distribution of pores. The reduction of pore size and its distribution at higher pressure increased the contact area between grains leading to enhance densification effect, sinterability and its properties afterward. Under backscattered mode, grey areas and fine white spot regions were detected which corresponded to Mg-rich constituency and high weight fraction of Mn respectively. Mn particles were uniformly distributed as they diffused through the Mg matrix during MA.

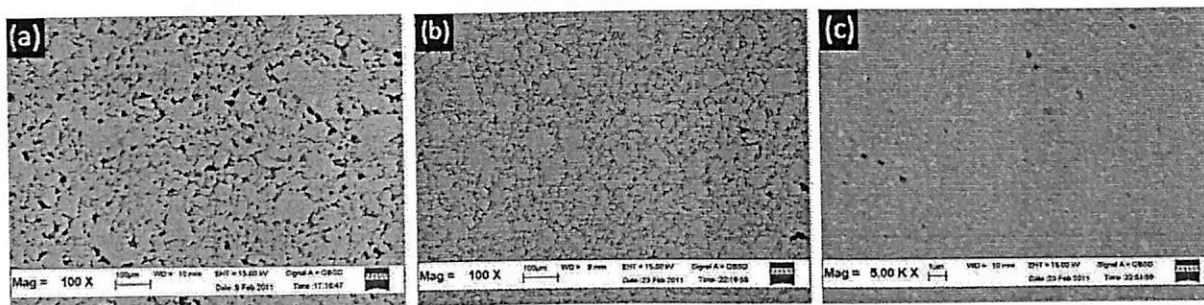


FIGURE 2. SEM micrographs for (a) 100 MPa, (b) 400 MPa and (c) backscattered image of sample #9

Analysis of the Model

Statistical effect of variables was calculated within 95% confidence interval. Table 2 shows the lowest density and hardness were obtained from run 4 and run 5 respectively, while the highest density and hardness were achieved at their highest levels (run 14). Final density was predicted to be in range of 1.70 g/cm^3 to 7.20 g/cm^3 since original density of Mg and Mn are 1.738 g/cm^3 and 7.210 g/cm^3 respectively. However, the obtained data showed density values mostly less than 1.800 g/cm^3 . It indicated that the density was not only dependent on starting materials but it was slightly affected by the variables studied in the model. This range of density obtained was considerably accepted to be used as implant materials since the density of natural bone is between 1.70 to 2.10 g/cm^3 .

TABLE (2). Two-level-fractional-factorial design for mechanically milled Mg-Mn alloys

Run (#)	A	B	C	D	E=ABC	F=BCD	Y ₁ Density (g/cm ³)	Y ₂ Hardness (Hv)
1	-	-	-	-	-	-	1.5302	23.22
2	+	-	-	-	+	-	1.5928	23.64
3	-	+	-	-	+	+	1.5600	23.06
4	+	+	-	-	-	+	1.5186	40.82
5	-	-	+	-	+	+	1.5944	19.20
6	+	-	+	-	-	+	1.5912	25.28
7	-	+	+	-	-	-	1.5838	41.64
8	+	+	+	-	+	-	1.5772	21.90
9	-	-	-	+	-	+	1.7828	52.56
10	+	-	-	+	+	+	1.7628	49.50
11	-	+	-	+	+	-	1.7512	54.56
12	+	+	-	+	-	-	1.7514	49.40
13	-	-	+	+	+	-	1.7808	48.40
14	+	-	+	+	-	-	1.8006	54.94
15	-	+	+	+	-	+	1.7644	47.94
16	+	+	+	+	+	+	1.7750	52.32

A normal probability of the standardized effect of factors studied at alpha =0.05 was plotted. Analysis of the effect of principal factors showed that in the considered range of parameters, compaction pressure is the most significant variable in achieving desired biomaterial alloy. As applied pressure was increased, the density of compacted alloys increased due to enhancement of densification effect [13, 14]. In other words, the compaction pressure increased the density. Theoretically, incorporating of Mn in Mg matrix reduced the original hardness of Mg (26 Hv) since Mn has lower hardness which is 19.6 Hv. However, according to this model, hardness of the most of samples was increased. As compaction pressure was increased, the diffusivity of Mn particles to the Mg matrix was increased during sintering. Thus, it caused the formation of stronger bonding between those particles. As shown in Table 2, Mg-Mn alloys which were compacted under 400 MPa provided a larger range of hardness (48.40 to 54.94 Hv) than samples which were compacted under 100 MPa (i.e 19.20 to 41.64 Hv). The hardness obtained was considerably accepted since the hardness of natural bone is laid on 20 to 60 Hv. Figure 4 and Figure 5 present the normal probability plots of the residuals for both density and hardness. The data shows a consistent distribution the points which lie close to a straight line. This plot appears satisfactory since it is approximately normally distributed.

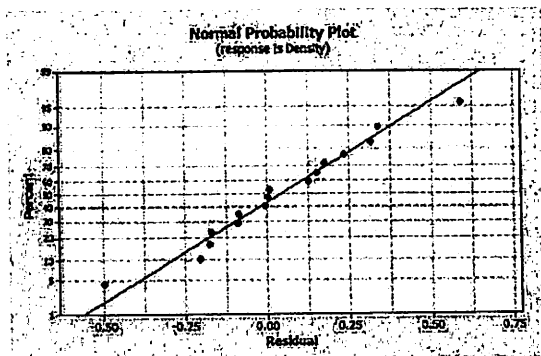


FIGURE 3. Normal probability plot of residuals (Y₁)

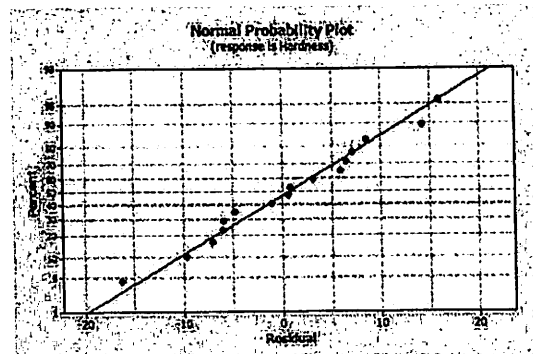


FIGURE 4. Normal probability plot of residuals (Y₂)

The factorial design can cover the main and interaction effects of the parameters within the whole range of selected parameter. According to the sparsity-of-effects principle in factorial design, it is most likely that main (single factor) effects and two-factor interactions are the most significant effect. In other words, higher order interactions such as three-factor interactions are very rare. Table 3 shows an idea about linear and interaction effects of the parameters. In general, the smaller p-value, the more significant the terms observed. From this table, it was found that the variable with largest effect on both density and hardness was compaction pressure (main effect) with p-value of 0.017 and 0.038, respectively. Other factors gave least effects which could be considered insignificant to

this model. The interactions of AB (milling time-milling speed) and AD (milling time-compaction) considered to have a significant effect on both responses. Other interactions were very low and were neglected. Thus, this implies that the model was influenced by main effect rather than low-order interaction effect.

TABLE (3). Effects and regression coefficients for density and hardness

Variable	Density			Hardness		
	Regression Coefficient	Estimated Effect	p-value	Regression Coefficient	Estimated Effect	p-value
Overall Average	1.65108		0.00	37.961		0.00
A	0.01738	-0.03475	0.045	0.861	-1.722	0.056
B	-0.02837	-0.05675	0.168	-0.994	1.987	0.083
C	0.03235	0.06470	0.125	0.866	1.733	0.210
D	0.08255	0.16510	0.017	10.616	21.232	0.038
E	0.02320	0.04640	0.140	-1.389	-2.778	0.303
F	0.01757	0.03515	0.246	0.874	1.748	0.408
AB + CE	-0.02478	-0.04955	0.036	-1.984	-3.968	0.044
AC + BE	0.01995	0.03990	0.397	0.394	0.788	0.912
AD + EF	-0.01880	-0.03760	0.042	-1.426	-2.852	0.049
AE + BC + DF	0.02005	0.04010	0.395	1.129	2.258	0.755
AF + DE	0.01062	0.02125	0.627	4.006	8.012	0.333
BD + CF	-0.01975	-0.03950	0.401	-3.516	-7.033	0.382
BF + CD	0.01422	0.02845	0.526	1.206	2.413	0.739
ABD	-0.01135	-0.02270	-	-0.924	-1.847	-
ABF	0.02383	0.04765	-	4.374	8.748	-

Regression equation (1) and (2) generated from the experimental data can be used to predict the properties of the Mg-Mn alloys for both density and hardness respectively. The regression analysis of the experimental data suggested that the relationship between all the responses of Mg-Mn alloys and the factors was best fitted with a linear model. The model equations for all responses which described this relationship in terms of coded factors were as follows:

$$\text{Density} = 1.651 + 0.018A - 0.028B + 0.032C + 0.083D + 0.023E + 0.017F - 0.025AB + 0.020AC - 0.019AD + 0.020AE + 0.011AF - 0.020BD + 0.014BF - 0.011ABD + 0.024ABF \quad (1)$$

$$\text{Hardness} = 37.961 + 1.722A - 1.987B + 1.733C + 21.232D - 2.778E + 1.748F - 1.984AB + 0.394AC - 1.426AD + 1.129AE + 4.006AF - 3.516BD + 1.206BF - 0.924ABD + 4.374ABF \quad (2)$$

Fit quality of the above models can be checked through R^2 test and analysis of variance (ANOVA). These tests are the most accepted and convenient methods which allow a researcher to examine the fitted model to ensure that it provides an adequate approximation to the true system and verify that none of the least squares regression assumptions are violated [15]. R^2 value gives a correlation between the experimental response and the predicted response and should be high for a particular model to be significant. R^2 for both density and hardness were 94.64% and 88.15%, respectively. According to R^2 , it shows a good agreement between the model and the experiment data.

CONCLUSION

Statistically designed experiments were conducted and the parameters which influence the density and hardness of Mg-Mn alloys were established. Density and hardness obtained showed ranges that approximately close to bone properties which were 1.5186 to 1.8006 g/cm³ and 19.20 to 54.94 Hv, respectively. The statistical analysis demonstrated that compaction pressure was the most significant factor for both density and hardness.

ACKNOWLEDGMENT

The authors would like to thank to Universiti Sains Malaysia RU-PRGS Grant No. 8046026, RU Grant No. 811224 and sponsorship scheme of Ministry of Higher Education (Malaysia).

REFERENCES

1. W. Li, S. Guan, J. Chen, J. Hu and S. Chen, *Materials Characterization* **62**, 1158-1165 (2011).
2. X. Gu, Y. Zheng, Y. Cheng, S. Zhong and T. Xi, *Biomaterials* **30**, 484-498 (2009).
3. E. Zhang and L. Yang, *Materials Science and Engineering A* **497**, 111-118 (2008).
4. D.S Yin, E. Zhang and S.Y Zeng, *Transactions of Nonferrous Metals Society of China* **18**, 763-768 (2008).
5. M.K. Datta, D.T Chou, D. Hong, P. Saha, S.J. Chung, B. Lee, A. Sirinterlikci, M. Ramanathan, A. Roy and P.N. Kumta, *Materials Science and Engineering B* **176**, 1637-1643 (2011).
6. X. Zhao, L.L. Shi and J. Xu, *Journal of Mechanical Behavior of Biomedical Materials* **18**, 181-190 (2013).
7. P.S. Dharam, A. McGoron, *Journal of Biomimetics, Biomaterials, and Tissue Engineering* **12**, 1-24 (2011).
8. J. Gubicza, M. Kassem, G. Ribarik and T. Ungar, *Materials Science and Engineering A* **372**, 115-122 (2004).
9. S. Sivasankaran, K. Sivaprasad, R. Narayanasamy and P.V. Satyanarayana, *Materials Characterization* **62**, 661-672 (2011).
10. X. Sauvage, F. Wetscher and P. Pareige, *Acta Materialia* **53**, 2127-2135 (2005).
11. Y.S. Kwon, K.B. Gerasimov and S.K. Yoon, *Journal of Alloys and Compounds* **346**, 276-281 (2002).
12. M. Azimi and G.H. Akbari, *Journal of Alloys and Compounds* **509**, 27-32 (2011).
13. I. Lahiri and S. Bhargava, *Powder Technology* **189**, 433-438 (2009).
14. M.T. Marques, A.M. Ferraria, J.B. Correia, R.D. Botelho and R. Vilar, *Materials Chemistry and Physics* **109**, 174-180 (2008).
15. V. Sridhar, A. M. Shanmugharaj, J. K. Kim, and D. K. Tripathy, *Polymer Science* **30(6)**, 691-701 (2009).

Hydroxyapatite-Coated Magnesium-Based Biodegradable Alloy: Cold Spray Deposition and Simulated Body Fluid Studies

Abdullah C.W. Noorakma, Hussain Zuhailawati, V. Aishvarya, and B.K. Dhindaw

(Submitted April 17, 2013; in revised form April 17, 2013; published online May 18, 2013)

A simple modified cold spray process in which the substrate of AZ51 alloys were preheated to 400 °C and sprayed with hydroxyapatite (HAP) using high pressure cold air nozzle spray was designed to get biocompatible coatings of the order of 20–30 μm thickness. The coatings had an average modulus of 9 GPa. The biodegradation behavior of HAP-coated samples was tested by studying with simulated body fluid (SBF). The coating was characterized by FESEM microanalysis. ICPOES analysis was carried out for the SBF solution to know the change in ion concentrations. Control samples showed no aluminum corrosion but heavy Mg corrosion. On the HAP-coated alloy samples, HAP coatings started dissolving after 1 day but showed signs of regeneration after 10 days of holding. All through the testing period while the HAP coating got eroded, the surface of the sample got deposited with different apatite-like compounds and the phase changed with course from DCPD to β-TCP and β-TCMP. The HAP-coated samples clearly improved the biodegradability of Mg alloy, attributed to the dissolution and re-precipitation of apatite showed by the coatings as compared to the control samples.

Keywords bioactivity, biodegradability, cold spray deposition, hydroxyapatite, magnesium alloy, SBF study

1. Introduction

In the commonly used implant materials such as Ti-6Al-4V, stainless steel, and Co-Cr alloys, release of toxic metal ions into the body and their adverse effects on the host over a period of time is well documented (Ref 1). Increased concern over the toxicity of metallic implants led to development of biodegradable implants and biocompatible coatings on implant materials.

The biodegradable implants can gradually be dissolved, absorbed, consumed, or excreted. Magnesium has been suggested as an alternative biomaterial recently due to its easy degradability and near equivalent mechanical properties to that of bone. The strong points in favor of using magnesium as implant are strongly fortified by their attractive biological

performances (Ref 2, 3): (1) metal magnesium is biodegradable in body fluid by corrosion; (2) Mg²⁺ is an essential element to the human body (the daily intake of Mg²⁺ for a normal adult is 300–400 mg) and hence harmless; (3) Magnesium can accelerate the growth of new bones tissues; (4) Density, elastic modulus, and yield strength of magnesium are closer to the bone tissue than that of the conventional implants (Ref 2, 3).

Despite its excellent properties magnesium-based alloys have not seen tangible applications in biomedical implant industry (Ref 4). To date magnesium and its alloys have been studied in the development of cardiovascular stents, bone fixation material, and porous scaffolds for bone repair (Ref 4–6). Nevertheless, the main limitation to the medical application is their corrosion behavior. Corrosion occurs rapidly even for a biodegradable material and additionally, it is not homogenous due to the tendency for localized corrosion (Ref 7). Another issue raised is related to the formation of hydrogen during corrosion. In the case of high evolution of hydrogen gas, magnesium cannot be absorbed in the body and a balloon effect takes place. In addition, an alkaline pH shift in the vicinity of corroding surface that is also a concern for medical applications. Therefore, it is necessary to carry out surface treatment or form coatings (Ref 8). The coatings enable biodegradation at controlled rate, and hence they offer a limited barrier function.

In order to control the degradation rate that can be extremely rapid to Mg alloy, it is useful to coat with hydroxyapatite (HAP). The HAP [Ca₁₀(PO₄)₆OH₂] is a form of calcium apatite and is the major component that is composed of same ions responsible to construct the mineral part of bone and teeth. HAP is bioactive with bone bonding ability, clinically used as bone spacers and fillers. The lack of cytotoxic effect makes HAP biocompatible with hard tissue and soft tissue (Ref 9). HAP helps to improve the biodegradation rate of magnesium alloys.

Abdullah C.W. Noorakma, School of Materials and Mineral Resources Engineering, Universiti Sains Malaysia, 14300 Nibong Tebal, Pulau Pinang, Malaysia, and now Faculty of Design and Engineering Technology, Universiti Sultan Zainal Abidin, 21300 Kuala Terengganu, Malaysia; Hussain Zuhailawati, School of Materials and Mineral Resources Engineering, Universiti Sains Malaysia, 14300 Nibong Tebal, Pulau Pinang, Malaysia; V. Aishvarya, Surface Engineering Department, Institute of Minerals and Materials Technology, Council of Scientific & Industrial Research (CSIR), Bhubaneswar 751013, India; and B.K. Dhindaw, Indian Institute of Technology, Bhubaneswar, 604, A Block, Toshali Bhawan, Satyanagar, Bhubaneswar 750015, India; Contact e-mails: wan_noorakma@yahoo.com, zuhaila@eng.usm.my, aishvarya@immt.res.in, dhindaw@metal.iitkgp.ernet.in.

Recently, some research works were performed to slow down the biodegradation rate of magnesium alloys, including sol gel (Ref 1) electrodeposition (Ref 2). Among them, plasma spraying of magnesium alloys has not been widely investigated possibly due to the low melting temperature of magnesium. Additionally, when HAP is plasma sprayed, it may be converted into other calcium phosphate phases such as α - or β -tricalcium phosphate, tetracalcium phosphate (TTCP), or calcium oxide (CaO) and the crystallinity of HAP may also be lowered due to rapid solidification. These alterations in chemistry and crystallinity often interfere with the novel bioactive properties of HAP as well as its adhesion to the implant (Ref 9, 10).

In this study, we demonstrate a novel approach to coat the HAP on AZ51 magnesium alloy by the modified cold spray (CS) deposition technique. AZ51 was chosen as experimental alloy to investigate the biodegradation of magnesium coated with HAP. Since the coated samples were meant for specific applications where time bound healing should start before the whole implant dissolves, regeneration of HAP from the SBF solution was studied in particular to examine the bioactivity of the coating.

To investigate the effect of HAP coating by the above technique, dissolution study was conducted to find the bioactivity when subjected to the physiological medium. The biodegradation rate of AZ51 coated with HAP by cold-sprayed coating technique was evaluated in the simulated body fluid (SBF).

2. Materials and Methods

2.1 Materials

The substrate material was AZ51 (5% Al, 1% Zn) magnesium alloy plate. The alloy was obtained from GKSS research center, Germany. The specimens were cut into small pieces with 15 mm \times 15 mm \times 4 mm. The specimens surface were ground with 1000 grit SiC paper to ensure the same surface roughness. Then the specimens were ultrasonically cleaned in acetone for 5 min. HAP, $\text{Ca}_5\text{OH}(\text{PO}_4)_3$ (purum p.a., $\geq 90\%$) powder supplied by Sigma Aldrich were used as spray-dried materials. The average particle size of powder was 4 μm . The as-received HAP powder was characterized with Bruker AXS D8 XRD unit using a monochromatic $\text{Cu K}\alpha$ radiation at a scan rate of 0.04 degree/s in the range of 20°-60° angle. XRD result of the as-received HAP powder indicated the characteristic peaks of pure HAP (Fig. 1). The crystallographic structure of

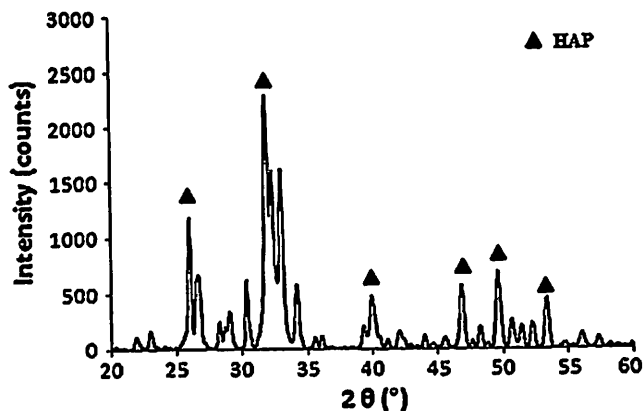


Fig. 1 XRD pattern of as-received HAP powder

HAP was hexagonal with $P63/m$ space group. The lattice constant was, $a = 9.424 \text{ \AA}$ and matched with the reference pattern file no. 01-074-0565 (ICDD).

2.2 Preparation of HAP Coatings

In conventional CS technique hot gases at temperatures 500-700 °C is used as carriers of the sprayed powders while the substrate remains at room temperature. In the present study, the CS technique was modified by using ambient air at room temperature as the spraying medium and heating the substrate to 400 °C. This modification helped in retaining the HAP properties which usually show phase changes at high temperature deposition. HAP coating was prepared by placing the AZ51 substrate inside a furnace where it was preheated to a temperature of 400 °C for 1 h. After the substrate was heated for 1 h, the HAP powder was sprayed using the modified CS deposition system. In this process the HAP powder was deposited on preheated substrate by high pressure powder feeder through an air spraying nozzle. The nozzle was kept 40 mm from the preheated substrate. The spraying HAP powder was accelerated to a high velocity and deposited on the heated AZ51 substrate. The air pressure was 10 bars and was controlled at room temperature.

2.2.1 Characterization of HAP Coatings and SBF Solution. The surface morphology, deposit thickness, and the composition of as-deposited coating and test samples were studied by field emission scanning electron microscopy Zeiss SUPRA 35VP (FESEM) from Germany, equipped with energy dispersion x-ray spectrometry (EDX). EDX was carried out at a voltage of 15 kV and a working distance of 10 mm, while morphology was studied at 5 mm working distance and 5 kV. Surface topography of coatings was examined by atomic force microscope (AFM). The AFM model was NanoNavi SII from Japan.

The hardness and elastic modulus of the coating were evaluated by the Nanoindentation test. Nanoindentation was performed using Nano Test Instrument (Micro Materials Ltd Wrexham, UK). Three different loads were used: 10, 100, and 300 mN. The indentations were conducted using the load control mode, where the load is applied and then released after the set peak. An initial load of 0.05 mN was used for locating the surface with Berkovich indenter. After this a loading rate of 10% of the load was applied. A dwell time of 5 s was applied at the maximum load.

The calcium, phosphorous, and magnesium ions concentration in the solution were analyzed immediately after the specimens were removed from SBF solution using the Perkin Elmer 8300 inductively coupled plasma optical emission spectroscopy (ICPOES), USA. All the SBF test solutions were appropriately diluted in de-ionized water and subjected to ICPOES analysis.

2.3 Studies with SBF

SBF was prepared as described by Kakubo et al. (Ref 11) by dissolving reagent grade NaCl, NaHCO_3 , KCl, $\text{K}_2\text{HPO}_4 \cdot 3\text{H}_2\text{O}$, $\text{MgCl}_2 \cdot 6\text{H}_2\text{O}$, CaCl_2 , Na_2SO_4 , in ion exchanged and distilled water. The synthesized solution was buffered at $\text{pH } 7.30 \pm 0.05$ with Tris-hydroxymethyl aminomethane, $(\text{HOCH}_2)_3\text{CNH}_2$, and 1 M HCl. All chemicals used in this study were of analytical reagent grade obtained from Sigma Aldrich, USA.

The volume of the SBF solution for soaking the specimen was determined by the formula $V_s = S_a/10$ where the V_s is the volume of the SBF (ml) and S_a is the apparent surface area of

the specimen (mm^2) (Ref 11). The calculated volume of SBF was put into plastic container and was heated at 36.5°C . The specimens were placed in the SBF after the solution attained a temperature of 36.5°C . Uncoated AZ51 specimens were used as control sample henceforth mentioned as 'Control', to check the biodegradation effect of SBF on pure alloy.

The control and coated AZ51 specimens were soaked in the SBF solution for various periods of 1, 4, 10, and 14 days. The solution pH was monitored during the immersion period using a 3-point calibrated pH electrode (SYSTRONICS 362). After reaching the immersion time, the specimens were taken out for analysis from SBF solution and gently rinsed with pure water. The experiments were carried out at 37°C in the water bath. The test tubes were sealed to remain sterile. The specimens were dried in desiccators without heating. In the same test tube it was not possible to place several samples, as the change in the chemistry of the solution due to each sample would interfere with the dissolution characteristics of the other samples. Thus one sample could only be placed in one test tube.

3. Result and Discussion

3.1 Surface Morphologies and Chemical Analysis of HAP Coatings

Figure 2(a) and (b) shows the SEM micrograph depicting the surface morphology and the structure of HAP coating on the samples. SEM micrograph clearly showed that a dense HAP coating was deposited on AZ51 plate. Based on this

microstructure, the HAP particles were found to be bonded well to each other during the CS process. Possibly higher impact velocity of HAP particles in conjunction with the heat from AZ51 substrate might have caused the particles to bond with each other. Figure 2(c) shows the cross-sectional view of the coating. The film thickness ranged $20\text{--}30\ \mu\text{m}$ with an average value of $25\ \mu\text{m}$ and was nearly uniform. The SEM microanalysis with EDX spectra on the coating surface showed that the main elements in the coating were Ca, P, and O with a weight percentage in the range of HAP composition. At the interface with the substrate Ca, P, O, and Mg were observed. Some dark voids were seen at the interface zone. These may have formed due to the deposition process. Since the aim of this study was not to allow dissolution of the complete coating till the interface, the characterization of the interface was not pursued further.

XRD pattern of the coatings showed similar peak as placed in Fig. 1 (not shown). This result indicated that the modified CS technique did not change the character of the HAP phase in the coating deposited on the heated AZ51 substrate.

3.2 Surface Topography of HAP Coatings

Surface topography of the HAP coating surface was visualized by the AFM. Figure 3 shows the AFM image of coating. From this figure it is seen that the coating roughness was uniform and the size of the smallest HAP particle in the agglomerate was about $40\text{--}60\ \text{nm}$. Agglomeration can be seen in some areas of the topography image. The variation in color in different regions is due to variation in signal with depth

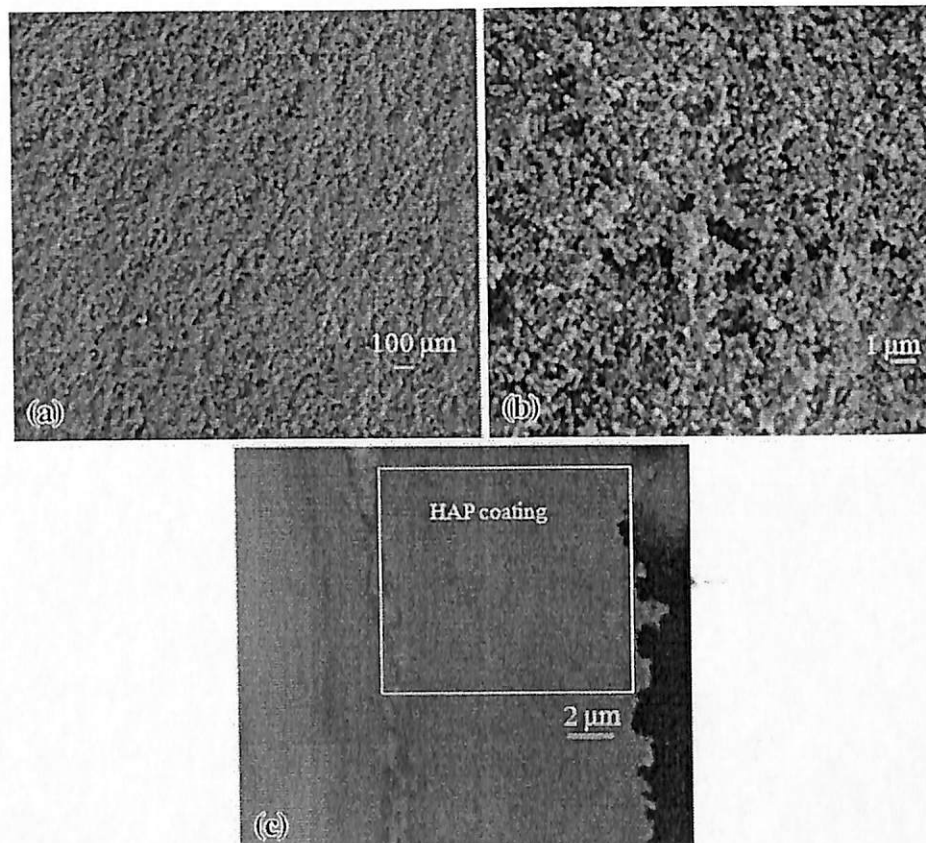


Fig. 2 SEM micrograph of HAP coating on the sample (a) low magnification, (b) high magnification, (c) cross-sectional view

which corresponds to the height difference or roughness of sample.

3.3 Hardness and Elastic Modulus of Coatings

The hardness of the coating using nano indenter was determined at four points. Three different loads were applied in these tests: 10, 100, and 300 mN. The average hardness values obtained were calculated and plotted against load as presented in Fig. 4(a).

Average hardness of HAP coating obtained was 0.1 GPa for the minimum load of 10 mN. The applied load 10 mN caused the penetration depth of 2275 nm (Fig. 4b). As the load increased to 100 mN with penetration of 9346 nm, the hardness obtained was comparable to that obtained under 10 mN applied load. At 300 mN with maximum depth of 12,460 nm, the hardness obtained was 0.09 GPa. Based on these readings, it can be concluded that the hardness was more or less uniform within the HAP coating. However, within the HAP coating, the hardness slightly increased towards the surface of the coating. Similar observations, in different system, were also reported by Samandari et al. (Ref 12) using plasma spray process to coat HAP on the Ti substrate. The hardness increased from the substrate to the surface (Ref 12).

The average elastic modulus of HAP coating was in the range of 9 GPa as seen in Fig. 4(c). A gradual increase of elastic modulus reading within the coating towards the surface was observed. At the lowest load applied for indentation coating showed the highest elastic modulus value. The elastic modulus of HAP coating was found to be greater than polymeric material like polystyrene but little lower than lead (Ref 13). These values are also similar to hardness of the cold compacted iron powder (Ref 14).

3.4 Biodegradable Behaviors of HAP-Coated Samples

In the SBF studies, dissolution and mineralization of the coating are the two main processes that occur. It was observed in the present experiments that the dissolution and mineralization in the HAP coating varied with the soaking time, as well as the changing ion concentration in SBF.

Figure 5 shows the SEM micrograph of the control sample at different time after immersion in SBF. From the morphology of control sample it is seen that cracks were visible after day 1 (Fig. 5a) with tiny pits formation which grew deeper with time (Fig. 5b, c) towards the end of experiment. The control sample

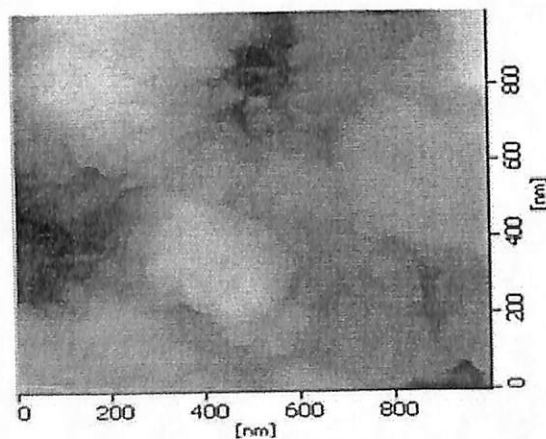


Fig. 3 Two-dimensional AFM image of coated AZ51

showed significant corrosion in the SBF as expected. Table 1 shows the magnesium content on the surfaces of the control samples. Dissolution of Mg into the SBF in the control sample is evident from the decreasing weight percentage (94 to 52.9%) of Mg on the sample surface. Other than magnesium the elements present in the surface were O, Cl, P, Ca in varying proportions. This could mean that Mg was precipitated as magnesium hydroxide or magnesium chloride on the surface. Magnesium hydroxide acts as a passive protective layer under alkaline conditions which is why the Mg does not completely dissolve into SBF (Ref 15). The corrosion could therefore be due to $MgCl_2$ formation which causes pit nucleation on the surface as reported by Hornberger et al. (Ref 15).

Figure 6 shows the change in morphology of HAP-coated test samples at different time after immersion in SBF. Figure 6(a) shows that the HAP coating on the test samples started dissolving after the first day of immersion. The EDX analysis of the coated test samples and the ICP analysis of the SBF solution after immersion are given in Tables 2 and 3,

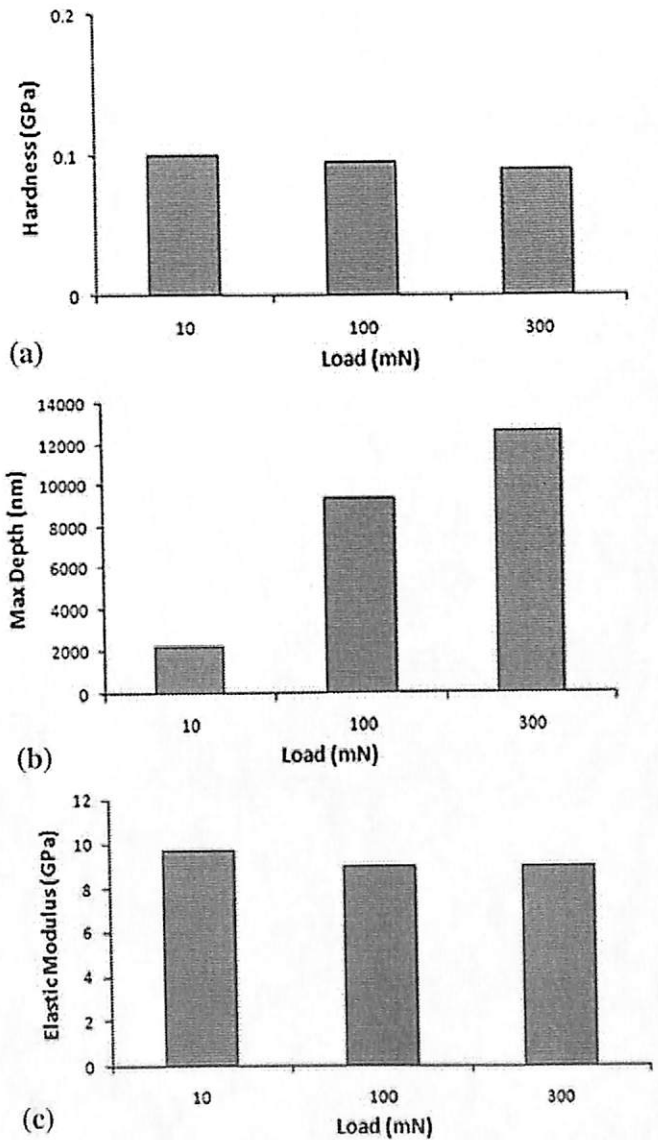


Fig. 4 (a) Hardness of HAP coating at different applied loads, (b) maximum depth of penetration vs. applied load, (c) elastic modulus of HAP coating

respectively. Table 2 shows that there is a general decrease in Mg and fluctuations in the weight percentage of Ca and P elements. The ICP analysis of the SBF solution showed a corresponding increase in Mg and fluctuating Ca and P contents (Table 3). Aluminum did not corrode into SBF and was not detected in ICP analysis. This is beneficial as aluminum corrosion is reported as adverse for bone growth (Ref 3, 4) and the AZ51 alloy shows stability with aluminum. The surface of the coated samples became rough with some loose particles dispersed over the surface. A similar phenomenon was reported for HAP/Ti alloy composite coating deposited by plasma spray on Ti-6Al-4V substrate after soaking in the SBF solution by Gu et al. (Ref 16). It was proposed that this increase in surface roughness of the coating provided nucleation sites and lowered interface energy for bone apatite to anchor (Ref 16).

After 4 days of immersion, the ICP analysis of the solution (Table 3) and the surface morphology of the sample showed significant changes (Fig. 6b). The surface appeared porous and the structure was different from initially seen loose particles on the surface. ICP analysis of SBF showed that there was 10 times reduction in P content with marginal decrease in Ca compared to the first day immersion data. This point out that apatite nucleated on the substrate from solution, probably not noticeable in the SEM image (Fig. 6b), even when corrosion reaction took place.

Figure 6(c) shows the surface morphology of the coating after 10 days of immersion. It was seen that the surface of coated sample was covered by some newly formed layer consisting of small granular agglomerates. The EDX analysis of

the agglomerates on the coating showed the presence of Ca, P, O, and Mg, indicating that the granular agglomerate is apatite. However, the weight of Ca element was low on surface and correspondingly high in SBF solution indicating that only little amount of apatite has formed. Chemical analysis of the solution at this stage by ICP showed that Mg content increased over day 4 while P decreased marginally (Table 3). However the small increase in Ca in SBF does not totally preclude the formation of apatite in isolated areas in the film. This confirms that the coating is bioactive, inducing apatite formation.

At the end of 14 days of immersion in SBF, the microanalysis of the coating showed an increase in Ca (Table 2). ICP analysis of the SBF solution complemented this result showing considerable reduction in Ca and a very marginal increase in P (Table 3). Possibly isolated precipitation of apatite on the surface coating might be forming with dissolution still continuing in some other areas. This is also visible in the SEM micrograph as precipitated zone (Fig. 6d). There was a significant reduction in the magnesium content in the SBF (Table 3) meaning dissolution rate slowed down, but was still faster than rate of apatite formation. The SEM micrograph of

Table 1 Change of magnesium concentration on control sample surface during the period of immersion in SBF solution (based on EDX data)

Immersion time, days	0	1	4	10	14
Magnesium on surface, wt.%	94	52.9	52.6	61.2	52.6

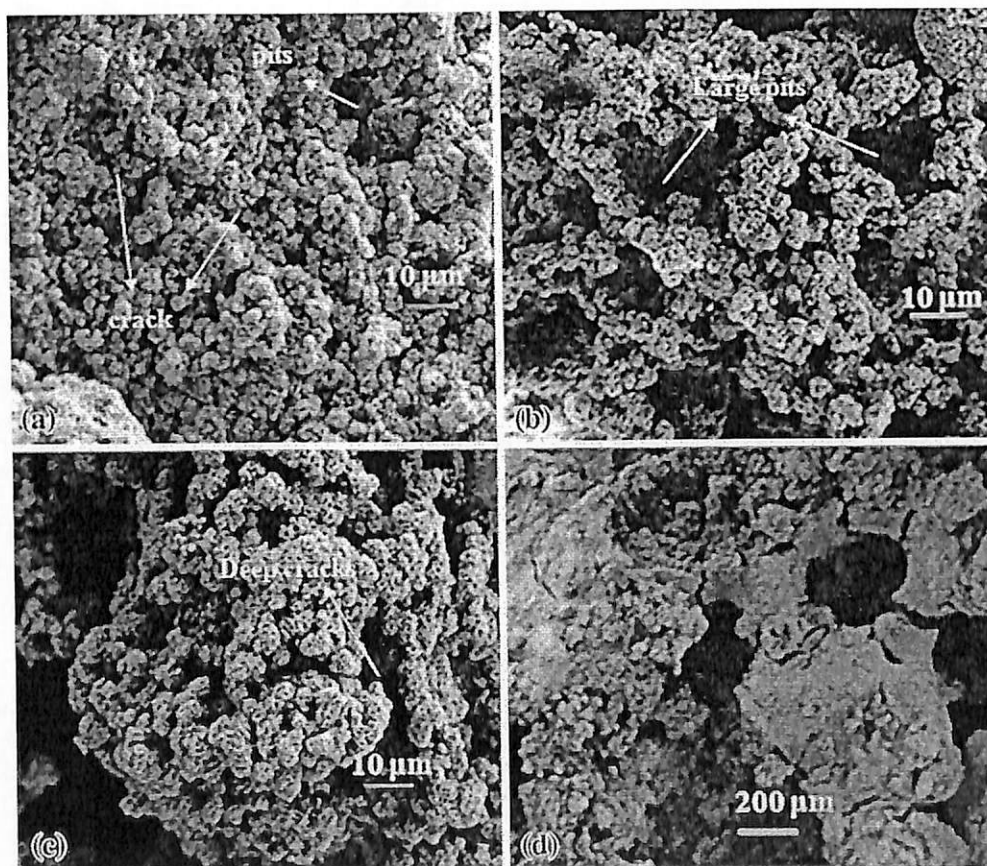


Fig. 5 Surface morphology of control sample showing pit formation (a) after 1 day, (b) after 4 days, (c) after 10 days, and (d) after 14 days of immersion in SBF during in vitro test

the surface after 14 days shows the existence of large size pores and microcracks. It is speculated that the degradation process started happening at the end that caused the damage to the surface structure of the coating. The EDX analysis also showed that 1.2 wt.% Cl was present on the surface at this stage. This indicated that magnesium chloride formation could have initiated.

The pH curve (Fig. 7) shows that the final pH was 8.96 at the end of the incubation period. In the test sample, the pH increase is slower as compared to control sample till day 4. Control sample reaches maximum pH (8.96) after first day of immersion thereafter remains stable. Based on the conditions that prevailed, it is possible to estimate what phase of calcium orthophosphate could have precipitated on the surface, from EDX, ICPOES, and pH data (Ref 17-19). As reported earlier the mechanical properties of the CS coatings were not high enough to make them amenable to analytical procedures including making thin films for TEM micro-diffraction analysis, that involved intense abrasion and cutting procedures. Thus results of EDX analysis along with results from ICPOES were used to semi-quantitatively evaluate the behavior of the precipitating products on the surface. Comparison with similar other works available in the literature were invoked to further substantiate the analysis. To evaluate the dissolution and re-precipitation of apatite, ICPOES data (Table 3) and EDX data (Table 2) are rationalized by calculating the Mg/Ca and Ca/P ratios respectively. The phase of re-precipitated apatite changed through the course of the

Table 2 Change of elemental composition in HAP-coated test samples during the period of immersion (based on EDX data)

Time, days	Ca, wt.%	P, wt.%	Mg on surface, wt.%	Molar Ca/P on substrate
1	0.58	2.05	64.26	0.212
4	0.82	1.89	58.73	0.325
10	0.34	3.45	51.16	0.0739
14	1.16	0.91	54.0	0.956

Table 3 ICPOES analysis of SBF solution after immersion of HAP-coated AZ51 test samples

Immersion time, days	Ion concentration in SBF solution, mg/L			Molar Mg/Ca in solution
	Mg	Ca	P	
0	50.9	158.6	35.1	0.535
1	55.3	162.2	44.6	0.568
4	3906	158.7	4.4	41.02
10	4471	182.8	3.6	40.76
14	3369	149.3	4.2	37.61

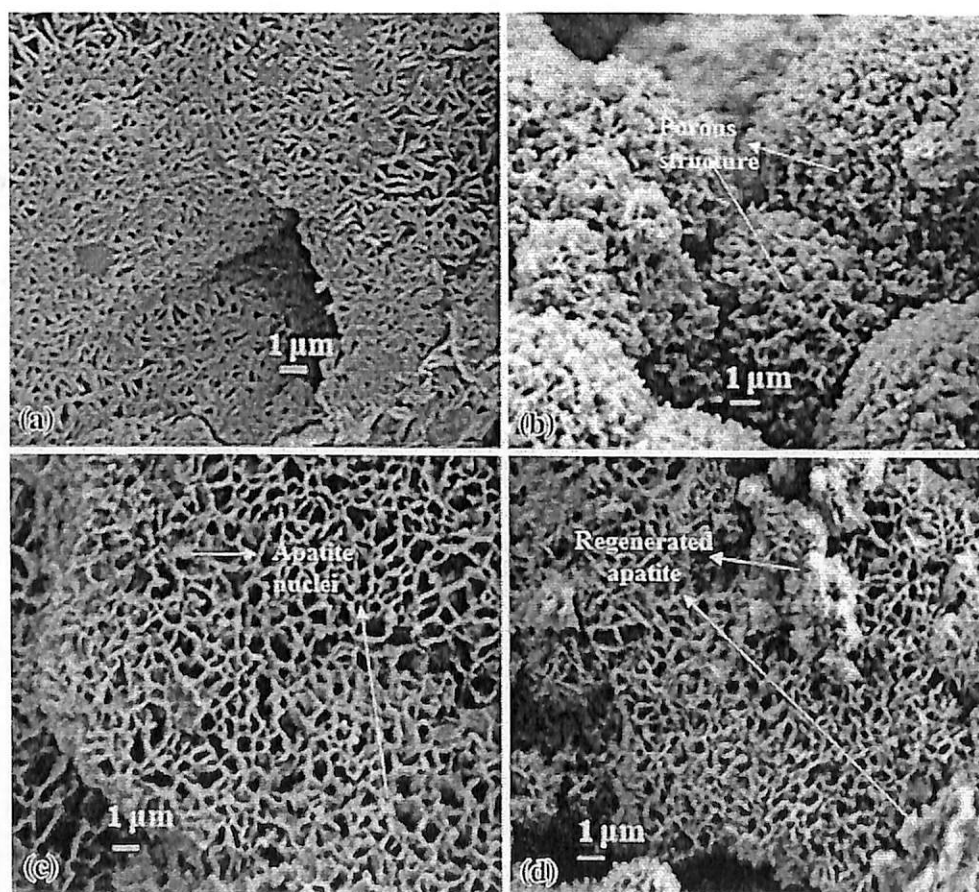


Fig. 6 Surface morphology of HAP-coated samples (a) after 1 day, (b) after 4 days, (c) after 10 days, and (d) after 14 days of immersion in SBF. Initial degradation (a, b) and isolated re-precipitation (c, d) of apatite is visible

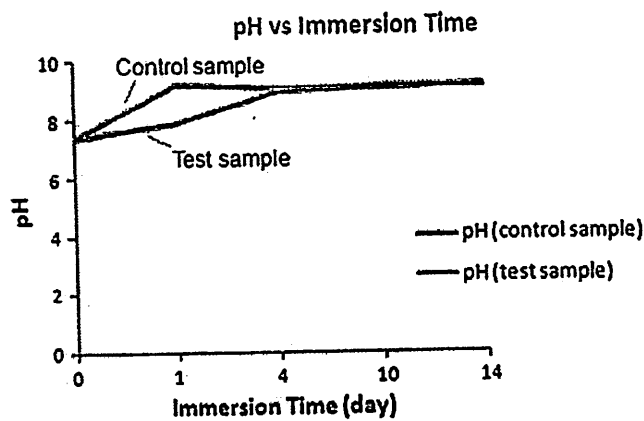


Fig. 7 pH trend of control and test samples during the in vitro experiment

experiment. The molar Ca/P ratio of original SBF solution before the beginning of the experiment is 1.514 (not mentioned in table). From the final molar Ca/P value of 0.956 on day 14 (Table 2), it can be said that the regenerated phase is possibly dicalcium phosphate dihydrate (DCPD). But pH conditions favor β -TCP or β -TCMP formation, which is ideally precipitated in pH range of 5-9 and temperature range of 25-95 °C. Under the same conditions, presence of Mg^{2+} ions in the solution above a ratio of 0.4 with respect to Ca^{2+} , allows biologic or synthetic Mg-substituted TCP formation (Ref 17). The molar Ca/P value and the Mg/Ca values as shown in Tables 2 and 3, respectively, are 0.956 and 37.6 at a pH of 8.96. These values match the conditions said by LeGeros et al. (Ref 18). Hence considering the influence of mildly alkaline pH along with the molar ratios, β -TCMP or Mg-TCP is the most probable phase formed (Ref 17, 18). The stability of both β -TCMP and Mg-TCP in body conditions is little low compared to HAP under physiologic conditions (Ref 19-21), but they act as precursor to the biologic apatite (which is associated with minor but important component such as CO_3 and Mg) as they easily substitute Ca and PO_4 and form calcium-deficient apatite (the naturally occurring apatite) (Ref 17, 22). Due to their faster degradability compared to HAP, β -TCP itself is being used as bone graft substitute and in dental applications allowing faster natural bone growth, a problem encountered with HAP causing prolonged bone growth periods (Ref 18, 21). The re-precipitated phase in the present study is possibly a suitable bioactive material for implant purpose. This is one of the key observations of the present work. Hence with the present rate of biodegradation and bioactivity, the material is suitable for any biodegradable implant application including stents and bone implants. Further in vitro studies of the HAP-coated AZ51 alloy with cell lines can confirm this potential application.

4. Conclusion

A simple and effective CS processing route has been used to prepare HAP coatings on magnesium alloy samples. The coating characterization by SEM confirmed the presence of compact HAP coating on the sample without any phase change during the modified processing. The average thickness of the

coating was 25 μm . The smallest aggregates in the coating observed were in the size range of 40-60 nm. Hardness and elastic modulus measured by nano-indentation were found to be around 0.1 and 9 GPa, respectively, indicating that the inter-molecular forces in the coatings are in the high end range of polymers and slightly below metallic lead. SBF tests carried out using SBF solution showed that the HAP coating started dissolving after 1 day of holding and showed signs of regeneration after 10 days. The phase of re-precipitated apatite changed through the course of experiment due to the influence of pH, molar Ca/P and Mg/Ca ratios in solution. At the end of the experiment the apatite re-precipitated as β -TCMP due to increase in pH and favorable change in molar Ca/P and Mg/Ca ratios. The uncoated control samples showed considerable degradation from the very first day onwards of the immersion period. These findings show that the coated alloy is both biodegradable and bioactive, suitable for possible use as biodegradable orthopedic implants.

References

1. S. Shadanbaz and G.J. Dias, Calcium Phosphate Coatings on Magnesium Alloys for Biomedical Applications: A Review, *Acta Biomater.*, 2012, 8, p 20-30
2. Y.W. Song, D.Y. San, and E.H. Han, Electrodeposition of HAP Coating on AZ91D Magnesium Alloy for Biomaterial Application, *Mater. Lett.*, 2008, 62, p 3276-3279
3. G.L. Song, Recent Progress in Corrosion and Protection of Magnesium Alloy, *Adv. Eng. Mater.*, 2005, 7, p 563-586
4. F. Witte, N. Hort, C. Vogt, S. Cohen, K.U. Kainer, R. Willumeit, and F. Feyerabend, Degradable Biomaterials Based on Magnesium Corrosion, *Curr. Opin. Solid State Mater. Sci.*, 2008, 12, p 63-72
5. R. Zeng, W. Dietzel, F. Witte, N. Hort, and C. Blawert, Progress and Challenge for Magnesium Alloys as Biomaterials, *Adv. Eng. Mater.*, 2008, 10, p B3-B14
6. F. Witte, The History of Biodegradable Magnesium Implants: A Review, *Acta Biomater.*, 2010, 6, p 1680-1692
7. S. Hiromoto and M. Tomozawa, HAP Coating of AZ31 Magnesium Alloy by a Solution Treatment and Its Corrosion Behavior in NaCl Solution, *Surf. Coat. Technol.*, 2011, 205, p 4711-4719
8. J.E. Gray and B. Luan, Protective Coatings on Magnesium and Its Alloys—A Critical Review, *J. Alloys Compd.*, 2002, 336, p 88-113
9. A. Choudhuri and P.S. Mohanty, Bioceramic Composite Coating by Cold Spray Technology, *Proceedings of the International Thermal Spray Conference*, 2009, p 391-396
10. J. Weng, Q. Liu, J.G.C. Wolke, X. Zhang, and K.D. Groot, Formation and Characteristics of the Apatite Layer on Plasma-Sprayed HAP Coatings in Simulated Body Fluid, *Biomaterials*, 1997, 18, p 1027-1035
11. T. Kokubo and H. Takadama, How Useful is SBF in Predicting In Vivo Bioactivity?, *Biomaterials*, 2006, 27, p 2907-2915
12. S.S. Samandari and K.A. Gross, Nanoindentation Reveals Mechanical Properties Within Thermally Sprayed HAP Coatings, *Surf. Coat. Technol.*, 2008, 203, p 1660-1664
13. B.J. Briscoey, L. Fiori, and E. Pelillo, Nano-indentation of Polymeric Surfaces, *J. Phys. D: Appl. Phys.*, 1998, 31, p 2395-2405
14. D. Poquillon, V. Baco-Charles, P. Tailhades, and E. Andrieu, Cold Compaction of Iron Powders-Relations Between Powder Morphology and Mechanical Properties, Part II. Bending Tests: Result and Analysis, *Powder Technol.*, 2002, 126, p 75-84
15. H. Hornberger, S. Virtanen, and A.R. Boccaccini, Biomedical Coatings on Magnesium Alloys—A Review, *Acta Biomater.*, 2012, 8, p 2442-2455
16. Y.W. Gu, K.A. Khor, and P. Cheang, In Vitro Studies of Plasma-Sprayed HAP/Ti-6Al-4V Composite Coatings in Simulated Body Fluid (SBF), *Biomaterials*, 2002, 24, p 1603-1611

17. R.Z. LeGeros, Calcium Phosphates in Oral Biology and Medicine, *Monographs in Oral Sciences*, Vol 15, H. Myers, Ed., Karger, Basel, 1991,
18. R.Z. LeGeros, A.M. Gatti, R. Kijkowska, D.Q. Mijares, and J.P. LeGeros, Mg-Substitutes Tricalcium Phosphates: Formation and Properties, *Key Eng. Mater.*, 2004, 254–256, p 127–130
19. J.C. Elliott, *Structure and Chemistry of Apatites and Other Calcium Orthophosphates*, Elsevier, Amsterdam, 1994, p 137–138
20. L. Cleries, J.M. FernalHdez-Pradas, and J.L. Morenza, Behavior in Simulated Body Fluid of Calcium Phosphate Coatings Obtained by Laser Ablation, *Biomaterials*, 2000, 21, p 1861–1865
21. A. Priya, S. Nath, K. Biswas, and B. Basu, In Vitro Dissolution of Calcium Phosphate-Mullite Composite in Simulated Body Fluid, *J. Mater. Sci. Mater. Med.*, 2010, 21, p 1817–1828
22. R.Z. LeGeros, Apatites in Biological Systems, *Prog. Cryst. Growth*, 1981, 4, p 1–45

THE 3rd INTERNATIONAL CONFERENCE ON MATHEMATICAL SCIENCES (ICMS3)

Putra World Trade Centre (PWTC), Kuala Lumpur
December 17 - 19, 2013



15 November 2013

Dear Eme Marina Salleh, Zuhailawati Hussain and Sivakumar Ramakrishnan
School of Materials and Mineral Resources Engineering,
Engineering Campus, Universiti Sains Malaysia,
14300 Nibong Tebal, Penang, Malaysia

Congratulations. We are pleased to announce that your reviewed paper entitled "**Design of Experiment (DOE) Study of Biodegradable Magnesium Alloy Synthesized by Mechanical Alloying Using Fractional Factorial Design**" has been accepted for a presentation at the 3rd International Conference on Mathematical Sciences (ICMS3). If you have not registered or paid, we kindly request that you register and pay for the fees before **November 18, 2013**.

The conference registration fees are as follows:

		Early Bird Registration (before 6 Sept 2013)	Normal Registration (after 6 Sept 2013)
Local Participant	Professional	RM1,000	RM1,100
	Student	RM800	RM850
International Participant	Professional	USD400	USD450
	Student	USD350	USD400
Member of PERSAMA	Professional	RM1,000	RM1,000
	Student	RM800	RM800

All payments should be made via bank draft/ money order/ cheque payable to "Persatuan Sains Matematik Malaysia". Details of the conference can be found at <http://www.ukm.my/confukm/index.php/ICMS/ICMS3>.

Thank you very much for your interest in the 3rd International Conference on Mathematical Sciences (ICMS3) and looking forward to see you in Putra World Trade Centre, Kuala Lumpur on 17 – 19 December 2013.

Yours sincerely,

PROF. DR. ANUAR MOHD. ISHAK
Conference Chair ICMS3 2013

Secretariat of ICMS3, School of Mathematical Sciences, Faculty of Science and Technology, Universiti Kebangsaan Malaysia,
43600 UKM Bangi, Selangor DarulEhsan

Tel: 03-8921 3929/5712 | Fax: 03-8925 4519 | Website: <http://www.ukm.my/confukm/index.php/ICMS/ICMS3> | E-mail: icms3ukm@gmail.com

showed that sodium acetate have higher deposition rate up to 12 µm/h, whereas sodium citrate provided better surface morphology with lower surface roughness.
Keyword: Electroless Ni-P Coating; Complexing Agent; Deposition Rate; Surface Morphology; Surface Roughness.

ICOFM2014-117: Effect of Aluminium and Silicon to IMC Formation in Low Ag-SAC Solder

*Maslinda Kamarudin¹, Anasyida Abu Seman¹ and Nurulakmal Mohd. Sharif¹
¹Structural Materials Niche Area, School of Materials and Mineral Resources Engineering, Universiti Sains Malaysia.
 *Email: mas.linda122@gmail.com

Abstract: The effect of Al and Si addition on IMC formation at the solder and Cu substrate interface was investigated. The Al and Si with 1.0 wt.% Al, 2.0 wt.% Al and 2.0 wt.% Al with 2.0 wt.% Si were added to Sn-0.3 wt.% Ag-0.5 wt.% Cu (SAC0305) solder alloy. Solder alloys were prepared by casting process. Melting temperature of each solder alloys was determined using DSC. Reflow process of the solder alloys were carried out at 260 °C on Cu substrate. Morphology of the intermetallic compound (IMC) formed at the solder joint was observed using Fe-SEM equipped with EDX. The addition of Al and Si reduced the thickness of IMC layer formed at the solder joint. The addition of 1.0 wt.% Al formed planar shape of IMC while the addition of 2.0 wt.% Al and the combination of 2.0 wt.% Al and 2.0 wt.% Si formed scallop shape of IMC. This is due to Cu-Al IMC and Ag-Al IMC scattered near the interface that act as diffusion barrier to Sn diffusion. This suggests that the addition of right amount of Al and Si could form thinner IMC layer that could lead to increase of reliability of solder interconnect.
Keyword: Intermetallic Compound (IMC); Microstructure; Diffusion; Solder Interconnect.

ICOFM2014-128: Effects of Surface Treatment on Titanium Alloys Substrate by Acid Etching for Dental Implant

*A. Jemat¹, M. J. Ghazali², M. Razali² and Y. Otsuka³
¹Department of Mechanical & Materials Engineering, Faculty of Engineering and Built Environment, 43600 UKM Bangi Selangor Darul Ehsan, Malaysia
²Faculty of Dentistry, Department of Periodontology, National University of Malaysia, Jalan Raja Muda Abdul Aziz, 50300 Kuala Lumpur, Malaysia
³Department of System Safety, Nagasaki University of Technology, 1603-1 Kamijimokko-cho Nagaoka-shi, Nagasaki 940-2188, Japan
 *Email: pida.jemat@yahoo.com

Abstract: Many studies were carried out to investigate the ability of titanium alloys for dental implant. Surface treatment is one of the famous methods to increase the titanium surface properties. The purpose of this paper is to investigate the effects of acid etching on the surface topography and roughness of titanium alloys (Ti-6Al-4V ASTM 1472-99). Acid etchings were carried out by using different type of acids with same time exposures. All etched surface were characterized by using an X-ray diffraction (XRD), a scanning electron microscope (SEM) and a roughness tester. Acid etched and pure surface were comparatively analysed. Results obtained show that the type of acids influenced the surface topography as well as roughness properties. The microstructure of the surface is highly modified after acid etching. Further we can confirm that, the experimental etched titanium alloys had features of a roughened surface with micro-roughness. In general, the experimental surface (0.137 µm - 3.986 µm) was significantly rougher than control surface (0.124 µm).
Keyword: Titanium Alloy; Acid Etched; Roughness; Surface Topography.

ICOFM2014-18: Microstructure and Compressive Strength of Magnesium-Zinc Alloy Reinforced with Different Percentage of Bio-Glass Content

*Mohd Amin Farhan Zafudla¹ and Shamsul Baharia Jamaludin¹
¹Sustainable Engineering Research Cluster, School of Materials Engineering, Universiti Malaysia Perlis, No. 66-68, Blok B, Taman Pertiwi Indah, Seriab, Perlis, Malaysia.
 *Email: aminzafudin90@yahoo.com

Abstract: The objective of this work is to fabricate composite Mg-Zn filled with 45S5 bio-glass (5, 10, and 15 wt. %) via powder metallurgy. The microstructure of the sintered composite was investigated using optical microscope and scanning electron microscope. The densities of the composites were also evaluated. The densities of the compacts are increasing with increasing bio-glass content. Compression test was done by the Instron machine. The result showed that bio-glass was dispersed in the Mg-Zn matrix. Compressive strength was decreased as the amount of bio-glass increased. However, the results are still comparable to natural bone, which is important to reduce the stress shielding effect.
Keyword: Magnesium-Zinc Alloys; Bio-Glass; Microstructure; Compressive Strength.

ICOFM2014-17: The Effect of Zn Concentration on The Corrosion Behavior of The Composite Magnesium-10wt.% Bio-Glass

*Siti Aishah Buyong¹, Shamsul Baharia Jamaludin¹ and Rohaya Abdul Malek¹
¹Cluster of Sustainable Engineering, School of Materials Engineering, University Malaysia Perlis, Blok B, No. 66-68 (First Floor), Taman Pertiwi Indah, Jalan, Jalan Kangar-Alor Setar, Seriab, 01000 Kangar, Perlis, Malaysia
 *Email: aishahbuyong@gmail.com

Abstract: This paper presents the corrosion behavior of the composite Mg-10wt.% bio-glass (45S5) with different concentration of Zn addition. Bio-glass (BG) was added to

the composite in order to improve bioactivity behavior of magnesium. The composite was fabricated by mixing, compacting followed by sintering. Composites was compacted at 550 MPa and sintered at 450°C under an argon atmosphere. Corrosion behavior was investigated by the immersion test. Sintered samples were immersed in 0.9 % NaCl solution and monitored by hydrogen evolution and XRD analysis. The results showed that hydrogen evolution rate decreased with addition of Zn content. The microstructure and phase analysis were observed by optical microscope, scanning electron microscope and x-ray diffraction.
Keyword: Composite; Mg; Zn; 0.9% NaCl Solution; Hydrogen Evolution.

ICOFM2014-109: Design of Experiment (DOE) Study of Hydroxyapatite-Coated Magnesium by Cold Spray Deposition

*Md Razi Hasniyati¹, Hussain Zuhailawati¹, Sivakumar Ramakrishnan¹, Brij Kumar Dhiladaw² and Siti Noor Fazliab Mohd Noor³
¹Structural Materials Niche Area Group, School of Materials and Mineral Resources Engineering, Engineering Campus, Universiti Sains Malaysia, 14300 Nibong Tebal, Penang, Malaysia
²School of Metallurgical Materials and Mineral Engineering, IIT Bhubaneswar, India
³Paediatric Dentistry Unit, Advanced Medical and Dental Institute, Universiti Sains Malaysia, 18-1, Persiaran Seksyen 4/9, IPPT Lot 13, Bandar Putra Bertam, 13200 Kepala Batas, Pulau Pinang, Malaysia
 *Email: hasniyatirazi@gmail.com

Abstract: In this study, hydroxyapatite powder was sprayed onto pure magnesium plate using a simple modified cold spray process. The effects of process parameters (i.e. standoff distance, surface roughness, substrate, substrate heating temperature and number of spray) were studied using 2^{k-1} factorial design. Analysis of variant (ANOVA) were used to determine the significant of process parameters on the coating which has properties closes to that of human bones. Thickness of coating, nanohardness and elastic modulus were chosen as the responses for assessing the most significant parameters that affected the hydroxyapatite coated onto pure magnesium plate. HAP particles have found to be bonded well in sample of run 11 while sample of run 4 show poor bonding between HAP particles and magnesium substrate. The effect of individual variables on the response was briefly discussed.
Keyword: ANOVA; Hardness; (2^{k-1}) Fractional Design; Cold Spray; Design of Experiment.

ICOFM2014-47: Effect of Cooling Rate on the Corrosion Behaviour of Zn-Al and Zn-Al-Mg alloy

*H. T. Low, *E. Hamzah, S. Farahany, H.R. Baksheshi-Rad and M. H. Cho¹
¹Faculty of Mechanical Engineering, Universiti Teknologi Malaysia, 81310 UTM Johor Bahru, Johor, Malaysia
²Kiswire Sdn Bhd, Research & Development Centre, S.E. Asia Regional H.Q.
 *Email: esah@fkm.utm.my

Abstract: Zinc and its alloy is non-ferrous metal often used as anodic material for the corrosion control in industries. The aim of this research is to determine the corrosion behavior of Zn alloy with different cooling rate during casting process. The three zinc alloys used were Zn-0.5Al, Zn-0.5Al-0.1Mg and Zn-0.5Al-0.3Mg. The cooling rates were varied by pouring the melt into the ceramic and steel moulds. Thermal analysis test was conducted to identify phase reaction and quantify the cooling rate data. Material characterization and electrochemical test were performed on the cast samples by using standard equipment. The results show that the Zn-0.5Al-0.3Mg cast with fast cooling rate had the lowest corrosion rate compare to others. This indicates that the magnesium addition can improve the corrosion resistance of Zn-Al alloy.
Keyword: Zinc Alloy; Corrosion; Cooling Rate.

ICOFM2014-151: SiC-Reinforced Aluminum-Silicon Composite via Pressureless Infiltration Using Polystyrene as External Binder

*Nurul Nadia Mohd Salim¹, H.Zuhailawati¹, H.Mohamad¹, A.S.Anasyida¹
¹School of Materials & Mineral Resources Engineering, Engineering Campus, Universiti Sains Malaysia, Nibong Tebal, Malaysia
 *Email: nadiasalim90@gmail.com

Abstract: SiC-reinforced aluminum composite was developed by pressureless infiltration technique using polystyrene as external binder. The metal matrix composites obtained were characterized for phase composition, microstructure, density, porosity, hardness and thermal expansion. The SiC particles were uniformly distributed within the Al-Si matrix with the help of polystyrene as external binder. The variation in the density of the composites was found to be linear with volume fraction in the usual manner. The hardness increased with increasing SiC content and highest hardness was 64.52 HV achieved with 20 vol.% of SiC. Thermal conductivity of the composites increased with increasing of SiC volume fraction up to 27.34 W/mK.
Keyword: Al-Si Alloy; Pressureless Infiltration; Thermal Conductivity; SiC.